MATHEMATICAL MODELLING OF THE PLUNGER PUMP OPERATION WITH NUMERICAL METHODS FOR SIMULATING THE FLOW ACROSS THE VALVE

By

Tian Chen

Faculty of Science, University of Ontario Institute of Technology

December 12, 2011

A thesis submitted to the
University of Ontario Institute of Technology
in accordance with the requirements of the degree
of Master of Science in the Faculty of Science

Abstract

Plunger pumps are needed for heavy duty sludge pumping at wastewater treatment facilities. America's leading pump manufacturer Wastecorp Inc. brought their plunger pump problem to us in late 2009. It was found that when the flow rate reaches a critical value, the plunger pump starts to generate a clicking noise.

A one-dimensional model was built for studying the flow of a typical plunger pump operation. The velocities and pressures are calculated at certain interesting locations. Pressure jumps have been found while opening or closing the valves. The valve motion is then modeled with considerations to its geometry. The results show that as the plunger speed reaches a critical value, the valve moves more rapidly and more likely to hit the wall and generates a noise. We also provide a methodology to study the flow across the valve in higher resolution. A finite-difference approach to the Navier-Stokes equations are presented with the immersed boundary method.

Acknowledgements

First of all, I would like to express my gratitude to my supervisor Dr. C. Sean Bohun, who has patiently guided and passionately inspired me throughout the course of my graduate studies. Working with him has been a privilege and a great joy.

I would also like to give special thanks to Prof. Huaxiong Huang at York University for his ideas in modelling, as well as his expertise in computational fluid dynamics. Other professors in applied mathematics at UOIT also assisted me with their knowledge. Especially, I have discussed with Dr. Lennaert van Veen and Dr. Greg Lewis about numerical methods for fluid flow in general.

Many of my colleagues have inspired me. Especially, I would like to thank Dr. Nicolas Périnet for his speciality in fluid simulation and experience in related numerical issues. Also I have discussed with Kevin Green and Gavin Lobo about parallel computing. Dongdong He at York University helped me with some technicalities of the immersed boundary method.

We appreciate MITACS and Wastecorp Inc. for bringing us this industrial problem as a seed.

Last but not least, I thank my parents for all of their support during the hard times.

Author's Declaration

I declare that this work was carried out in accordance with the regulations of the University of Ontario Institute of Technology. The work is original except where indicated by special reference in the text and no part of this document has been submitted for any other degree. Any views expressed in the dissertation are those of the author and in no way represent those of the University of Ontario Institute of Technology. This document has not been presented to any other University for examination either in Canada or overseas.

Tian Chen

Date: December 12, 2011

Contents

List of Figures

Chapter 1

Introduction

1.1 Motivation and Literature Review

A particular industrial problem was the motivation of this thesis. America's leading pump manufacturer Wastecorp brought their plunger pump problem to a workshop on industrial mathematics in late 2009. Their plunger pumps work well in general. However, it has been found that when the resistance to the pump reaches a critical value, the plunger pump, which is driven by an AC motor, starts to generate a clicking noise in a periodic fashion. A preliminary model was set up during the workshop in order to model the flow and hopefully identify the factors that might be responsible for the vibration. We continued with careful studies in this thesis, to gain a better understanding of the fluid dynamics involved during the plunger pump operation.

Plunger pumps are reciprocating pumps which require a system of suction and discharge valves to ensure that the fluid moves in a particular direction. One line of Wastecorp's plunger pumps are engineered for heavy duty sludge pumping applications at municipal and industrial wastewater treatment facilities. A typical plunger pump consists of a cylinder with a reciprocating plunger, shown in Figure 1.1. The suction and discharge valves are placed on each side of the cylinder. The valves are made of iron balls which sit on a ring while closed. In the suction stroke the plunger retracts and the suction

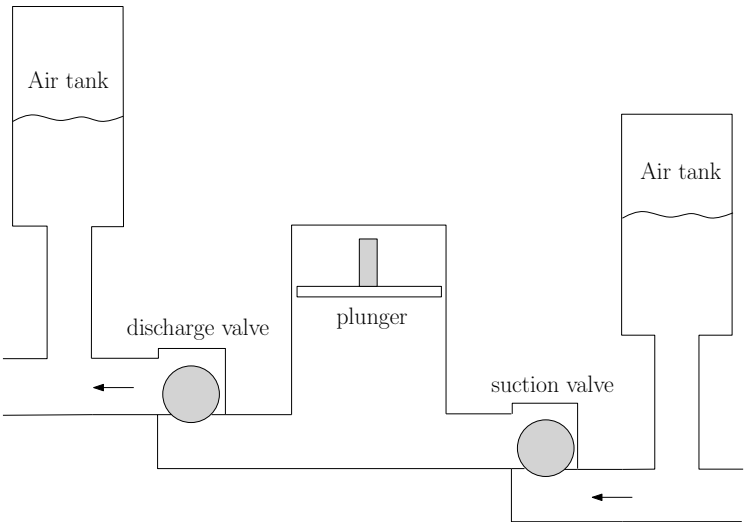

Figure 1.1: A cross-sectional view of a typical plunger pump.

valve opens causing suction of fluid into the cylinder; in the forward stroke the plunger pushes the liquid out of the discharge valve. The valve motion is only driven by the flow. As the valves close and open, the air tanks on both sides, known as compensators, reduce the effects of sudden changes of flow directions. During the pump operation, the air tanks are sealed.

Ideally, the valves should open and close at a precise instant to facilitate the suction or discharge stroke. It is known that the smooth and quiet operation of a pump is primarily a reflection of the dynamics of the valve operations (Henshaw, 2009). However, inertia causes the valves to be slightly delayed with respect to the strokes of the piston. (Price et al., 1995) explains how pressure spikes and possible cavitations can form due to the late-opening valves. Cavitations will create damage on the system components. (Henshaw, 2009) explains how hydraulic shocks can result due to the late-closing valves. These hydraulic shocks cause excessive pump noise and vibration, and shortens the lives of the pumps.

Efforts have been made to understand the valve dynamics with plunger pump operation. (Lyashkov, 1972) presents a numerical model for simulating the operation of high pressure cryogenic pumps and the valve motion is carefully considered according to the geometry. The pressure in the plunger

cylinder is modeled with compressible fluids and pressure spikes are clearly seen in the simulation results. However, the model is not connected with inlet or outlet flow effects. (Johnston, 1991) gives a detailed mathematical description of reciprocating pumps with the model of valve motion embedded within the inlet and outlet flow. The positions of the valve are categorized into three phases, i.e., fully closed, partially open, or fully open. In each situation, the net forces are carefully considered and the cavitation effects are also included with the pressure equations. However, the inlet pressure is assumed to be constant and the effects of pipeline system is not considered. (Shu et al., 1997) suggests that the pipeline pressure pulsation produced by reciprocating pumps are a significant source of noise and vibration. Thus, the model of pipeline system is connected to the existing model in (Johnston, 1991) to allow simulations of pressure pulsation. One drawback of this last model is that the flow equations valid within the pipelines are treated rather simply.

1.2 Thesis Outline

In this thesis, we present careful mathematical derivations for the flow model that describes the fluid dynamics in the plunger pump system. The first model consists of a full geometry of the plunger pump and studies the flow at certain interesting locations. The flow properties in the pipelines are derived from the Navier-Stokes equations. Although assumptions are made to simplify the model into ideal fluids, viscous effects can be simply added to adapt different Reynolds numbers. The dynamics of the air tanks are also included. However, the valve motion has not been resolved in the first model, so the second model studies the valve motion in detail.

In an effort to make the thesis self contained, the fundamental equations of fluid dynamics are developed in the Appendix. Chapter 2 presents the first one-dimensional model with simulation results. The geometry of the valves has been simplified to open or closed gates, and pressure jumps have been

found in the simulations. However, the motions of the valves have not been resolved. Thus Chapter 3 presents a refined one-dimensional model concerning the motions of the valves. Following this, Chapter 4 discusses, at some length, the behavior of the flow in a vicinity of the valve and the formulation of an immersed boundary method to study the fluid-valve interactions. Much of this material is expanded upon in the appendix.

Chapter 2

The One-dimensional Flow Model

In this chapter, we will derive a one-dimensional flow model for the plunger pump. The model consists of the plunger, the air tanks, the pipes, and the valves in which the system forms a closed circulation. The equations of motion of the fluid in the model are derived from the Navier-Stokes equations. We will analyze the differential equations of the model and some of the numerical results.

2.1 The Geometry of the Model

In order to study the motion of fluids in a plunger pump, we would like to understand the pressures and velocities of flow at certain interesting locations. We can consider a closed system in a laboratory setting, shown in Figure 2.1. The fluid circulates through the pump within an outer pipe, so that the fluid leaves the discharge valve, travels through the outer pipe and eventually comes back to the suction valve. The geometry of the valves is simplified to open or closed gates. It is important to note that in this model, both valves are assumed to be either fully closed or completely open.

The plunger is located at the center with an air tank on either side. Both

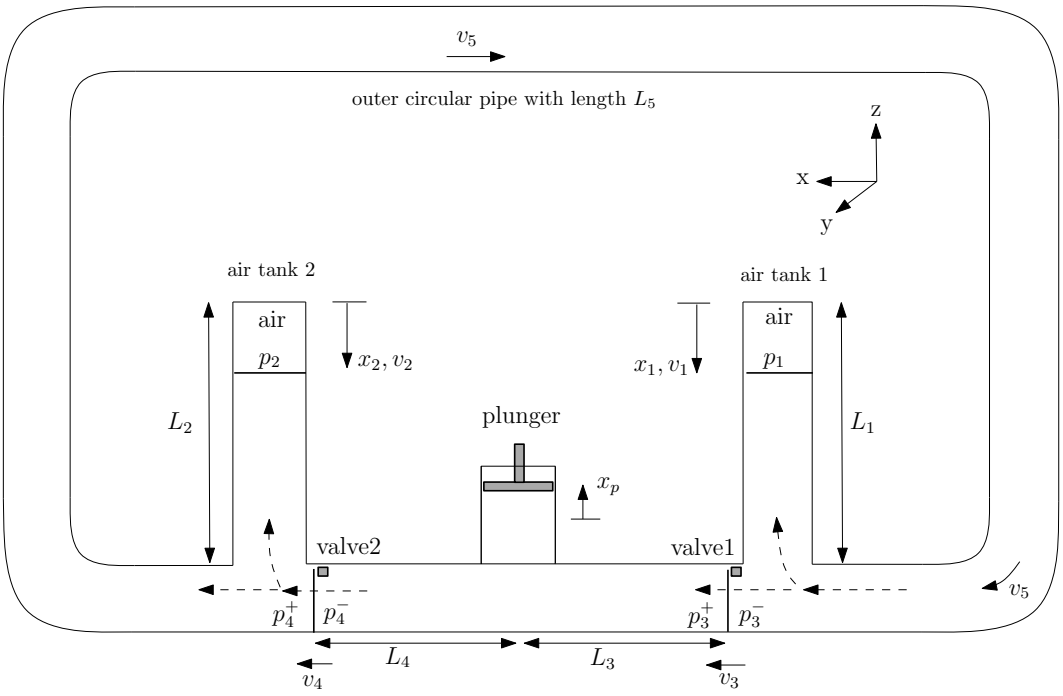

Figure 2.1: The Geometry of the One-dimensional Model.

of the valves only open to the left. L_1 and L_2 denote the heights of the air tank 1 and air tank 2, respectively, L_3 denotes the length of the pipe from valve 1 to the center of the plunger and L_4 denotes the length of the pipe from the center of the plunger to valve 2. The outer circular pipe is of length L_5. The position of the air/liquid interface in air tank 1 is x_1, measured from the top of air tank 1. Similarly for x_2. The position of the plunger is denoted by x_p from a local coordinate along the z-direction. The average flow velocities in air tank 1 and 2 are v_1 and v_2 respectively, measured along the negative z-axis. The average velocity passing through valve 1 is v_3 and the average velocity passing through valve 2 is v_4, measured along the x-axis. The average velocity in the outer circulation is v_5. The pressure of the air inside air tank 1 is p_1. Similarly for p_2. p_p denotes the liquid pressure under the plunger. p_3^- is the flow pressure before entering through valve 1 and p_3^+ is the flow pressure after entering through valve 1. Similarly for p_4^- and p_4^+.

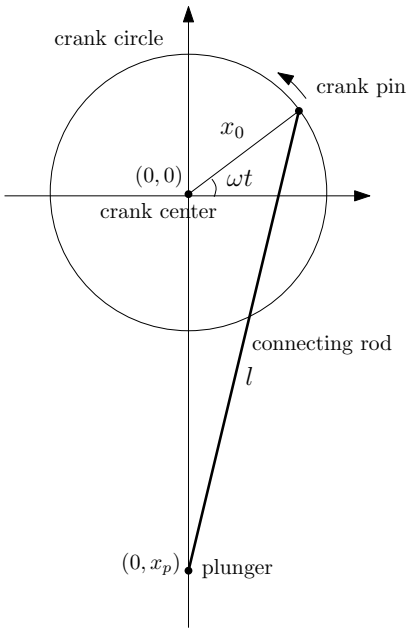

Figure 2.2: The geometry of the motion of the plunger.

2.1.1 The Plunger Motion

The plunger is connected to a rotating crank through a connecting rod, shown in Figure 2.2. The crank is centered at $(0,0)$ and the connecting rod is pinned on the crank with a distance x_0 to its center. As the crank rotates, the plunger moves up or down along the vertical axis.

The position of the plunger can be written as

$$(0, x_p) = x_0(\cos\omega t, \sin\omega t) + l(d_1, d_2), \tag{2.1.1}$$

where ω is the angular frequency of the rotating crank, l is the length of the connecting rod, (d_1, d_2) is a unit vector along l and

$$d_1^2 + d_2^2 = 1. \tag{2.1.2}$$

Thus, by solving (2.1.1) and (2.1.2) simultaneously, we get

$$x_p = x_0 \sin\omega t \pm \sqrt{l^2 - x_0^2 \cos^2\omega t}. \tag{2.1.3}$$

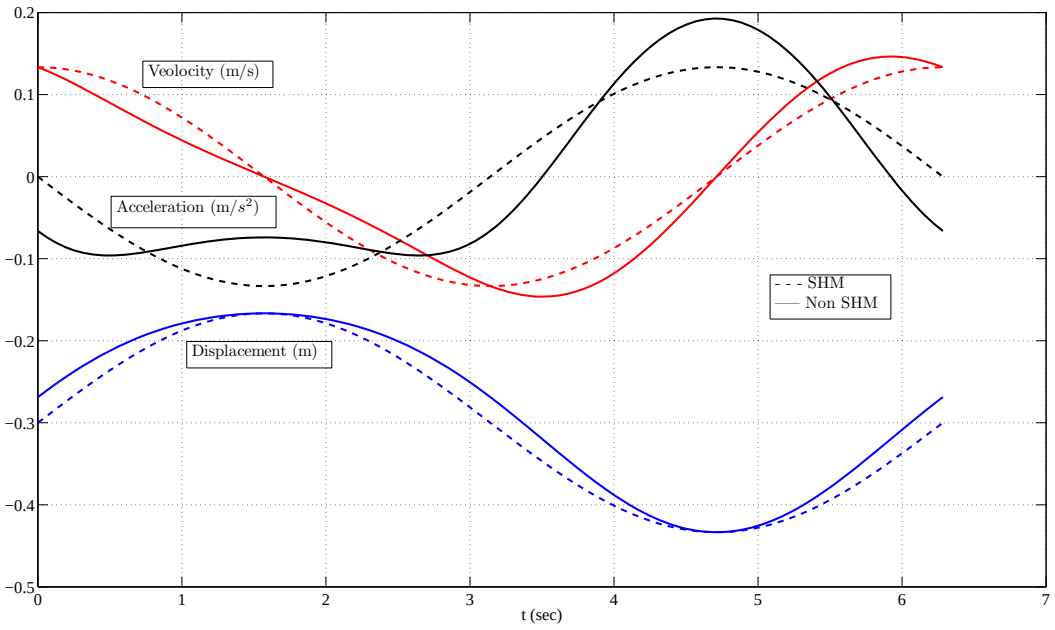

Figure 2.3: An example of displacement, velocity and acceleration of the plunger. The dashed line indicates the simple harmonic motion and the solid line shows the plunger motion as described in (2.1.4).

When $\omega t = -\pi/2$, $x_p = -x_0 - l$. Thus, we take the minus sign on the right-hand side of (2.1.3) and it gives

$$x_p = x_0 \sin \omega t - \sqrt{l^2 - x_0^2 \cos^2 \omega t}. \tag{2.1.4}$$

The velocity and acceleration of the plunger can be calculated by taking the first and second derivatives with respect to t of (2.1.4), i.e.,

$$\dot{x}_p = x_0 \omega \cos \omega t - \frac{x_0^2 \omega \cos \omega t \sin \omega t}{\sqrt{l^2 - x_0^2 \cos^2 \omega t}}, \tag{2.1.5}$$

$$\ddot{x}_p = -x_0 \omega^2 \sin \omega t + \frac{x_0^4 \cos^2 \omega t \sin^2 \omega t}{\left(l^2 - x_0^2 \cos^2 \omega t\right)^{3/2}} + \frac{\omega^2 x_0^2 \left(\sin^2 \omega t - \cos^2 \omega t\right)}{\sqrt{l^2 - x_0^2 \cos^2 \omega t}}. \tag{2.1.6}$$

An example of the plunger motion is illustrated with $l = 0.3$ m, $x_0 = 0.13$ m and $\omega = 1$ rad/sec. The displacement, velocity and acceleration of the plunger is shown in Figure 2.3 with solid lines. If $x_0 \ll l$, (2.1.4) can be approximated

as

$$x_p = x_0 \sin \omega t - l. \tag{2.1.7}$$

The above equation represents a simple harmonic motion and it can be understood as having a connecting rod hanging vertically downwards from the crank pin at all times and the plunger is attached to the end of the connecting rod. The plunger is not only allowed to move up or down, but also left and right with the rotation of the crank pin. In Figure 2.3, we compare the displacement of the plunger described by (2.1.4) with the simple harmonic motion described by (2.1.7) by using the same parameters.

In (2.1.7), we start rotating the crank anti-clockwise from the horizontal axis, so x_p is described as a sine function. If we start rotating at $(0, x_0)$ and shift the displacement of the plunger upwards by l, then

$$x_p = x_0 \cos \omega t, \tag{2.1.8}$$

and consequently

$$\dot{x}_p = x_0 \omega \sin \omega t, \tag{2.1.9}$$

$$\ddot{x}_p = -x_0 \omega^2 \cos \omega t. \tag{2.1.10}$$

For simplicity, we will use (2.1.8) to (2.1.10) for our numerical simulations. Expression (2.1.4) will include higher order harmonic effects in the solution.

2.1.2 Control Volumes

In order to analyze the flow in the closed system described above, we shall divide the system into several compartments. Each compartment is a *control volume* which we will analyze in detail.

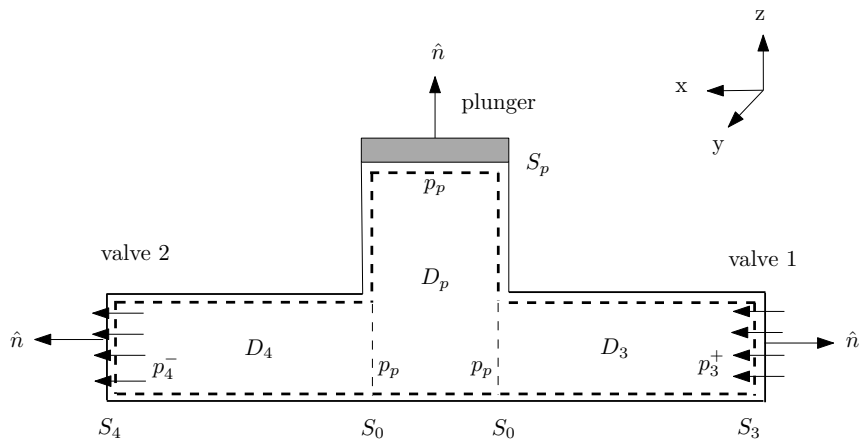

Figure 2.4: A cross-sectional view of control volume CV_1.

The first control volume, namely CV_1, encloses the fluid region underneath the plunger and between both valves, shown in Figure 2.4. It is bounded by the pipe walls, the plunger, and the valves. The boundary of CV_1 is known as its *control surface*, denoted by CS_1. We have unit normal vectors pointing outward from the control surface. The cross-sectional area of the pipe at valve 1 is S_3 and the cross-sectional area at valve 2 is S_4. S_p denotes the cross-sectional area of the plunger.

For further analysis, we also divide CV_1 into three regions. The pipe between both valves is cut into D_3 and D_4. D_p is the region below the plunger. S_0 denotes the cross-sectional area of the pipe of D_3 and D_4 near the plunger.

The second control volume, CV_2, shown in Figure 2.5, consists of the fluid region in the outer circular pipe, air tank 1, and the region D_3 defined previously in CV_1. Its control surface is denoted by CS_2. We let D_5 be the fluid region in the outer circular pipe and D_1 be the liquid region in air tank 1. The unit normal vectors are pointing outward everywhere from this control surface. S_1 is the cross-sectional area of air tank 1. S_4 denotes the cross sectional area of the pipe L_5 near valve 2.

The last control volume CV_3 is similar to CV_2 and is shown in Figure 2.6.

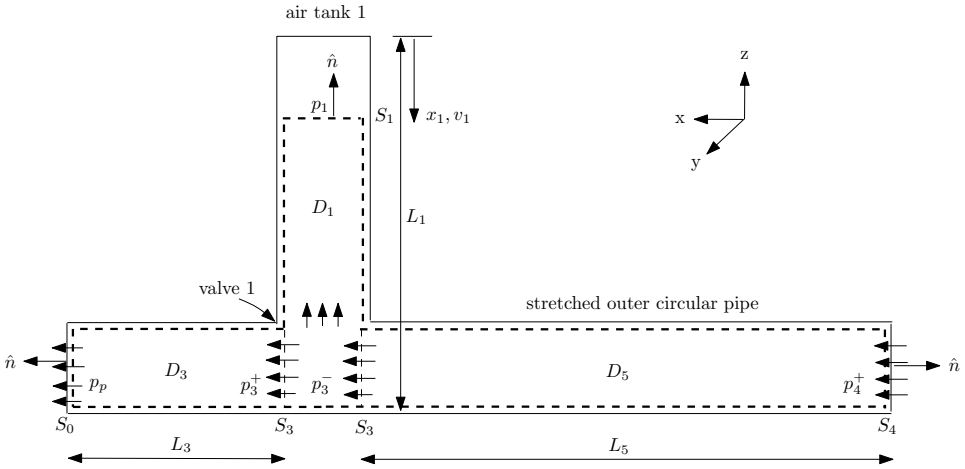

Figure 2.5: A cross-sectional view of control volume CV_2.

2.2 Derivation of the Model

2.2.1 Assumptions

The applications of Wastecorp's plunger pumps include raw and digested sewage sludge, industrial and chemical waste and slurries, pulp and paper stock, oil refinery sludge etc. These sludge fluids can exhibit non-Newtonian behavior where the shear rate and shear stress do not vary proportionally as for a Newtonian fluid such as water (Slatter, 1997). Depending on the sludge type and concentration, different viscosity models can be used to describe the non-linear relationship between shear rate and shear stress. However, in our first model, we would like to simply assume that the sludge concentration is low and the fluid is mostly water. Thus the fluid behaves as a Newtonian fluid and it is incompressible.

Recall the Navier-Stokes equations derived in the Appendix:

$$\frac{\partial \vec{v}}{\partial t} + \vec{v} \cdot \nabla \vec{v} = -\frac{1}{\rho} \nabla p + \nu \nabla^2 \vec{v} + \vec{g}, \tag{2.2.1}$$

where ρ is the fluid density, $\vec{v}$ is the flow velocity, p is the pressure, ν is the kinematic viscosity, and $\vec{g}$ represents the acceleration due to gravity. Since we

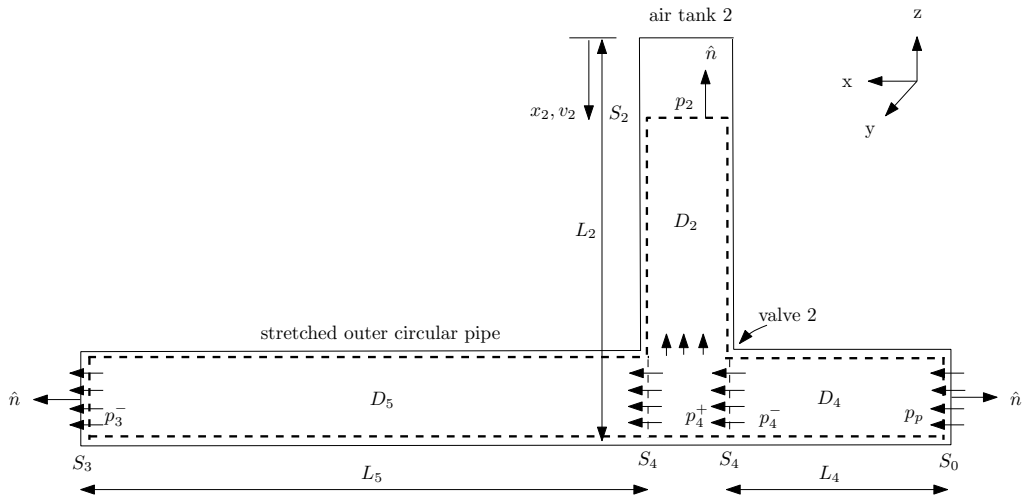

Figure 2.6: A cross-sectional view of control volume CV_3.

assume that the fluid is mostly water, the continuity equation gives us

$$\nabla \cdot \vec{v} = 0. \tag{2.2.2}$$

For non-dimensionalization, we set

$$\vec{v} = V\vec{v}^*, \qquad \vec{x} = L\vec{x}^*, \qquad t = Tt^*, \qquad p = Pp^*, \qquad \vec{g} = G\vec{g}^*,$$

where V is a reference velocity, L is a reference length, $P = \rho V^2$, $T = L/V$, $G = V/T = V^2/L$. The choice for P comes from the Bernoulli's equation and the choices for T and G come from a consistency in units. Substituting these variables back into (2.2.1) and (2.2.2) and dropping the stars, the incompressible Navier-Stokes equations in non-dimensionalized form read

$$\frac{\partial \vec{v}}{\partial t} + \vec{v} \cdot \nabla \vec{v} = -\nabla p + \frac{1}{Re}\nabla^2 \vec{v} + \vec{g}, \tag{2.2.3}$$

$$\nabla \cdot \vec{v} = 0, \tag{2.2.4}$$

where $Re = VL/\nu$ is the *Reynolds number*.

To estimate the Reynolds number, we look at Model PE-61A plunger pumps, for example. The radius of the pipe is about 0.1 m, and the maximum capacity is known as 40 gallons per minute. We divide the volumetric flow rate by cross-sectional area of the pipes to get

$$40 \text{ gpm} = 40 \times \frac{6.3 \times 10^{-5} \text{ m}^3/\text{s}}{\pi \times 0.051^2 \text{ m}^2} \approx 0.3 \text{ m/s}.$$

The kinematic viscosity of water at 20°C is about 1×10^{-6} m^2/s, thus

$$Re = \frac{LV}{\nu} \approx \frac{0.1 \text{ m} \times 0.3 \text{ m/s}}{1 \times 10^{-6} \text{ m}^2/\text{s}} = 3000.$$

In reality, the viscosity has a higher value and the above is the maximum Reynolds number expected.

To derive our model, we use the dimensional form of the Navier-Stokes equations (2.2.1) and the continuity equation (2.2.2). To simplify the geometry, we first assume that the pipes, the plunger and the air tanks all have the same cross-sectional area. For simplicity, we ignore the gravitational effects, hence,

$$\vec{g} = 0. \tag{2.2.5}$$

Note that the gravitational term can be added, however, the dynamics of the solution will not change by gravitational effects.

Since we are aiming to derive a one-dimensional model, we also assume that there are no viscous effects so that the flow velocities are uniform along the cross-section of the pipes and

$$\nu \nabla^2 \vec{v} = 0. \tag{2.2.6}$$

This means that instead of the no-slip condition, the velocities at the pipe

walls are parallel to the walls. Also,

$$\vec{v} \cdot \hat{n} = 0 \tag{2.2.7}$$

at any wall.

If we add viscous effects, the viscous term has to be included in the Navier-Stokes equations. Depending on the profile of the flow, we are able to simplify the model to one-dimension by using average velocities along cross-sections. An extra viscous term which includes the average flow velocity and the Reynolds number will appear. Thus the average velocity can be solved with any given Reynolds number. In the viscous flow case, the no-slip condition is satisfied. As the viscosity tends to zero, the viscous term vanishes and we get back to the case of an ideal fluid.

We consider further the directions of flow. In CV_1, for example, if the plunger is pushed downwards, we shall assume that the flow being pushed by the plunger will change its direction from vertical to horizontal abruptly while it enters the pipe region D_3 and D_4, shown in Figure 2.7. Similarly for the pulling case. The velocities are also assumed to be uniform in D_3, D_4 and D_p respectively. This assumption generalizes to all control volumes, so we have

$$\vec{v} \cdot \nabla \vec{v} = 0. \tag{2.2.8}$$

Thus, the Navier-Stokes equations are simplified to

$$\rho \left(\frac{\partial \vec{v}}{\partial t} \right) = -\nabla p \tag{2.2.9}$$

with the continuity equation

$$\nabla \cdot \vec{v} = 0. \tag{2.2.10}$$

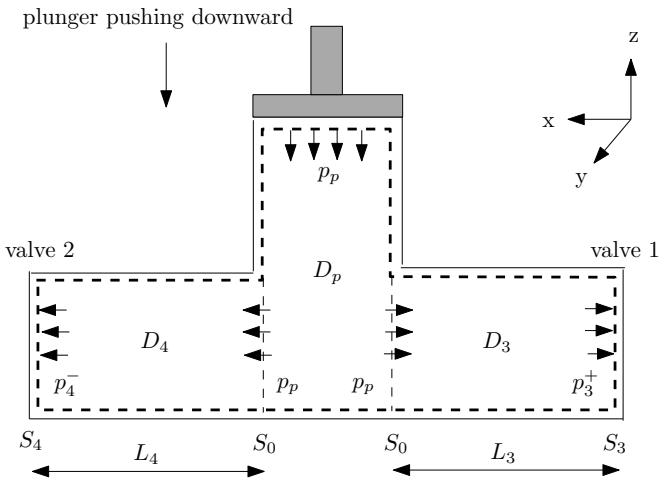

Figure 2.7: Homogenous flow in D_3, D_4 and D_p.

2.2.2 Analysis with the Navier-Stokes Equations

Each control volume shall be analyzed. We start with CV_1 and consider the continuity equation (2.2.10). Integrating (2.2.10) over CV_1, we get

$$\iiint_{CV_1} \nabla \cdot \vec{v}\, dV = 0.$$

By the divergence theorem, this implies

$$\iint_{CS_1} \vec{v} \cdot \hat{n}\, dS = \iint_{S_3+S_4+S_p} \vec{v} \cdot \hat{n}\, dS + \iint_{\text{pipe walls}} \vec{v} \cdot \hat{n}\, dS = 0.$$

From assumption (2.2.7), we deduce that the second term in the above equation vanishes so

$$\iint_{S_3+S_4+S_p} \vec{v} \cdot \hat{n}\, dS = 0.$$

At a particular time t,

$$\iint_{S_3+S_4+S_p} \vec{v} \cdot \hat{n}\, dS \Big|_t = -v_3 S_3 \Big|_t + v_4 S_4 \Big|_t + \dot{x}_p S_p \Big|_t = 0 \tag{2.2.11}$$

where $\dot{x}_p$ is the plunger velocity. Similarly at time $t + \Delta t$ where Δt is small,

$$\iint\limits_{S_3+S_4+S_p} \vec{v} \cdot \hat{n}\, dS\Big|_{t+\Delta t} = -v_3 S_3\Big|_{t+\Delta t} + v_4 S_4\Big|_{t+\Delta t} + \dot{x}_p S_p\Big|_{t+\Delta t} = 0. \tag{2.2.12}$$

Subtracting (2.2.11) from (2.2.12), taking the limit as $\Delta t \to 0$ and using the assumption that $S_3 = S_4 = S_p$, we get

$$-\frac{\partial v_3}{\partial t} + \frac{\partial v_4}{\partial t} + \frac{\partial \dot{x}_p}{\partial t} = 0.$$

From assumption (2.2.8), we arrive at

$$-\dot{v}_3 + \dot{v}_4 + \ddot{x}_p = 0 \tag{2.2.13}$$

where $\dot{v}_i = \frac{d}{dt} v_i$, $i = 3, 4$.

Now consider the momentum equation (2.2.9). Taking the volume integral of (2.2.9) over D_4,

$$\rho \iiint\limits_{D_4} \frac{\partial \vec{v}}{\partial t}\, dV = \iiint\limits_{D_4} -\nabla p\, dV. \tag{2.2.14}$$

By an alternative form of the divergence theorem, the right-hand side of (2.2.14) can be calculated as

$$\begin{aligned} \iiint\limits_{D_4} -\nabla p\, dV &= -\iint\limits_{\partial D_4} p\hat{n}\, dS \\ &= -\left(\iint\limits_{S_0} p\hat{n}\, dS + \iint\limits_{S_4} p\hat{n}\, dS + \iint\limits_{\text{pipe walls}} p\hat{n}\, dS \right) \end{aligned}$$

where ∂D_4 is the surface boundary of D_4, $\hat{n}$ is the unit normal vector pointing outward from ∂D_4. Since the surface integral of $p\hat{n}$ over the pipe walls is

canceled out to be zero, we have

$$-\iint_{\partial D_4} p\hat{n}\, dS = -\left(\iint_{S_0} p\hat{n}\, dS + \iint_{S_4} p\hat{n}\, dS\right)$$
$$= \left(p_p S_0 - p_4^- S_4\right)\hat{e}_x$$

where $\hat{e}_x$ is the unit vector along the x-axis.

For the left-hand side of equation (2.2.14), we have assumed that $\vec{v}$ is homogenous in D_4, so

$$\rho \iiint_{D_4} \frac{\partial \vec{v}}{\partial t}\, dV = \rho \frac{\partial \vec{v}_4}{\partial t} S_4 L_4$$

where $\vec{v}_4$ is the uniform flow velocity in D_4. Equating both sides of (2.2.14) and using the assumption that S_0 is equal to S_4, we have

$$\rho \frac{\partial \vec{v}_4}{\partial t} = \frac{p_p - p_4^-}{L_4}\hat{e}_x.$$

Since $\vec{v}_4 = v_4 \hat{e}_x$, and v_4 is independent of space variables, we arrive at

$$\dot{v}_4 = \frac{1}{\rho}\frac{p_p - p_4^-}{L_4}. \tag{2.2.15}$$

A similar analysis can be carried out with the momentum equation (2.2.9) in D_3, the result gives

$$\dot{v}_3 = \frac{1}{\rho}\frac{p_3^+ - p_p}{L_3}. \tag{2.2.16}$$

Finally, by substituting (2.2.15) and (2.2.16) back into (2.2.13), we obtain the following relation:

$$\frac{p_3^+ - p_p}{L_3} + \frac{p_4^- - p_p}{L_4} = \rho \ddot{x}_p. \tag{2.2.17}$$

This finishes our analysis of CV_1.

Let us continue by analyzing CV_2. First, integrating the continuity equation (2.2.10) over CV_2 and use the divergence theorem, we get

$$\iiint_{CV_2} \nabla \cdot \vec{v} dV = \iint_{CS_2} \vec{v} \cdot \hat{n} dS = 0.$$

Assumption (2.2.7) gives

$$\iint_{S_4+S_1+S_0} \vec{v} \cdot \hat{n} dS = 0. \tag{2.2.18}$$

At a particular time t,

$$\iint_{S_4+S_1+S_0} \vec{v} \cdot \hat{n} dS \Big|_t = -v_5 S_4 \Big|_t - v_1 S_1 \Big|_t + v_3 S_0 \Big|_t = 0 \tag{2.2.19}$$

and at time $t + \Delta t$,

$$\iint_{S_4+S_1+S_0} \vec{v} \cdot \hat{n} dS \Big|_{t+\Delta t} = -v_5 S_4 \Big|_{t+\Delta t} - v_1 S_1 \Big|_{t+\Delta t} + v_3 S_0 \Big|_{t+\Delta t} = 0. \tag{2.2.20}$$

Subtracting (2.2.19) from (2.2.20), taking the limit as $\Delta t \to 0$, and using the assumption that $S_0 = S_1 = S_4$, we have

$$-\frac{\partial v_5}{\partial t} - \frac{\partial v_1}{\partial t} + \frac{\partial v_3}{\partial t} = 0.$$

Since assumption (2.2.8), we arrive at

$$-\dot{v}_5 - \dot{v}_1 + \dot{v}_3 = 0. \tag{2.2.21}$$

Next, consider the momentum equation (2.2.9). Integrating (2.2.9) over D_3

gives us (2.2.16) again and integrating over D_1 results in

$$\dot{v}_1 = \frac{1}{\rho}\frac{p_1 - p_3^-}{L_1 - x_1}. \tag{2.2.22}$$

Integrating (2.2.9) over D_5 results in

$$\dot{v}_5 = \frac{1}{\rho}\frac{p_4^+ - p_3^-}{L_5}. \tag{2.2.23}$$

We finish our analysis in CV_2 by substituting (2.2.16), (2.2.22) and (2.2.23) back to equation (2.2.21), we obtain:

$$\frac{p_3^- - p_4^+}{L_5} = \frac{p_1 - p_3^-}{L_1 - x_1} + \frac{p_p - p_3^+}{L_3}. \tag{2.2.24}$$

Last for CV_3, we follow the same analysis from previous. By integrating the continuity equation (2.2.10), we get

$$-\dot{v}_4 + \dot{v}_5 - \dot{v}_2 = 0. \tag{2.2.25}$$

Integrating the momentum equation (2.2.9) over D_2 gives

$$\dot{v}_2 = \frac{1}{\rho}\frac{p_2 - p_4^+}{L_2 - x_2}. \tag{2.2.26}$$

Integrating (2.2.9) over D_5 gives (2.2.23) again and integrating over D_4 gives (2.2.15) again. Finally, by substitution we get

$$\frac{p_3^- - p_4^+}{L_5} = \frac{p_4^+ - p_2}{L_2 - x_2} + \frac{p_4^- - p_p}{L_4}. \tag{2.2.27}$$

To summarize, we have the following set of ordinary differential equations:

$$\dot{x}_1 = v_1, \qquad \dot{x}_2 = v_2, \tag{2.2.28}$$

$$\dot{v}_1 = \frac{1}{\rho}\frac{p_1 - p_3^-}{L_1 - x_1}, \qquad \dot{v}_2 = \frac{1}{\rho}\frac{p_2 - p_4^+}{L_2 - x_2}, \qquad \dot{v}_3 = \frac{1}{\rho}\frac{p_3^+ - p_p}{L_3}, \tag{2.2.29}$$

$$\dot{v}_4 = \frac{1}{\rho}\frac{p_p - p_4^-}{L_4}, \qquad \dot{v}_5 = \frac{1}{\rho}\frac{p_4^+ - p_3^-}{L_5}, \tag{2.2.30}$$

as well as the pressure relations:

$$\frac{p_3^- - p_4^+}{L_5} = \frac{p_1 - p_3^-}{L_1 - x_1} + \frac{p_p - p_3^+}{L_3}, \tag{2.2.31}$$

$$\frac{p_3^- - p_4^+}{L_5} = \frac{p_4^+ - p_2}{L_2 - x_2} + \frac{p_4^- - p_p}{L_4}, \tag{2.2.32}$$

$$\rho\ddot{x}_p = \frac{p_3^+ - p_p}{L_3} + \frac{p_4^- - p_p}{L_4}. \tag{2.2.33}$$

To close the system of equations we require an equation of state for the gas in the compensators. The question of existence and uniqueness reduces to the standard linear ODE theory depending on the state of the valves. Provided $x_1 \neq L_1$, $x_2 \neq L_2$, $L_3 \neq 0$, $L_4 \neq 0$, $L_5 \neq 0$ and at least one valve is open, there exists a unique local solution to the system of ordinary differential equations. See Section 2.3.2 for more details.

2.2.3 Equations of State

Now we make a connection between the positions of the air/liquid interface and the pressures in the air tanks. If we assume that there is no heat transfer between the gas and its surroundings while it is compressed (or expanded), we can use the adiabatic equation of state (Illner et al., 2000)

$$PV^\gamma = \text{constant}, \tag{2.2.34}$$

where γ is a parameter assumed to be constant during the process ($\gamma = 1.4$ for air). In air tank 1, for example, the air volume is measured as $V_1 = S_1 x_1$ and

the air pressure is p_1. If we denote the initial pressure as p_{10} and the initial air/liquid interface position as x_{10}, then

$$p_1 S_1^\gamma x_1^\gamma = p_{10} S_1^\gamma x_{10}^\gamma.$$

Therefore in air tank 1,

$$p_1 = p_{10} \left(\frac{x_{10}}{x_1} \right)^\gamma. \tag{2.2.35}$$

Similarly for air tank 2,

$$p_2 = p_{20} \left(\frac{x_{20}}{x_2} \right)^\gamma. \tag{2.2.36}$$

2.2.4 Flow at Open or Closed Valves

We discuss what happens with the pressures and velocities at open or closed valves.

First consider the pressures. If valve 1 is closed, then we assume that the fluid is static in D_3 and the pressure is the same everywhere in D_3. So we have $p_3^+ = p_p$. If valve 1 is open, the pressures before and after entering through valve 1 are assumed to be identical, i.e., $p_3^+ = p_3^-$. Similarly for valve 2. Thus,

$$\begin{aligned} p_3^+ &= p_p, \quad \text{if valve 1 is closed,} \\ p_3^+ &= p_3^-, \quad \text{if valve 1 is open.} \end{aligned} \tag{2.2.37}$$

$$\begin{aligned} p_4^+ &= p_p, \quad \text{if valve 2 is closed,} \\ p_4^+ &= p_4^-, \quad \text{if valve 2 is open.} \end{aligned} \tag{2.2.38}$$

Now consider the flow velocities. If valve 1 is closed, then there is no flow coming into the plunger through valve 1 and $v_3 = 0$. Similarly if valve 2 is closed, then $v_4 = 0$.

2.2.5 Conditions to Open or Close the Valves

There are two situations we need to consider:

1. How a closed valve can be popped open;
2. How an open valve can be pushed closed.

Let us consider the first case. Assume valve 1 is closed, then $v_3 = 0$ and $p_3^+ = p_p$. To open valve 1, we need $p_3^- > p_3^+ + \Delta p$, where Δp is a positive number to overcome the inertia of the valve. Once valve 1 is open, we would have $p_3^+ = p_3^-$.

For the second case, suppose valve 1 is open and $p_3^+ = p_3^-$. Suppose v_3 is changing from positive to negative, this means that the flow is driving the valve back to its closed position. We use the condition $v_3 < 0$ to close valve 1. Once valve 1 is closed, we set $p_3^+ = p_p$ and v_3 should be zero.

The same conditions apply to valve 2. See Table 2.1 for all cases.

At time $t^{(n)}$		Conditions	At time $t^{(n+1)}$	
valve 1 is closed	$p_3^+ = p_p$ $v_3 = 0$	$p_3^- > p_3^+ + \Delta p$ otherwise	valve 1 opens valve 1 stays closed	$p_3^+ = p_3^-$ $p_3^+ = p_p$, $v_3 = 0$
valve 1 is open	$p_3^+ = p_3^-$	$v_3 < 0$ otherwise	valve 1 closes valve 1 stays open	$p_3^+ = p_p$, $v_3 = 0$ $p_3^+ = p_3^-$
valve 2 is closed	$p_4^+ = p_p$ $v_4 = 0$	$p_4^- > p_4^+ + \Delta p$ otherwise	valve 2 opens valve 2 stays closed	$p_4^+ = p_4^-$ $p_4^+ = p_p$, $v_4 = 0$
valve 2 is open	$p_4^+ = p_4^-$	$v_4 < 0$ otherwise	valve 2 closes valve 2 stays open	$p_4^+ = p_p$, $v_4 = 0$ $p_4^+ = p_4^-$

Table 2.1: Conditions to open or close a valve.

2.3 Numerical Algorithm and Remarks on Simulation Issues

We derived from the previous section the set of differential equations for $x_1, x_2, v_1, ..., v_5$:

$$\begin{aligned} \dot{x}_1 &= v_1, & \dot{x}_2 &= v_2, & & \\ \dot{v}_1 &= \frac{1}{\rho}\frac{p_1 - p_3^-}{L_1 - x_1}, & \dot{v}_2 &= \frac{1}{\rho}\frac{p_2 - p_4^+}{L_2 - x_2}, & \dot{v}_3 &= \frac{1}{\rho}\frac{p_3^+ - p_p}{L_3}, \\ \dot{v}_4 &= \frac{1}{\rho}\frac{p_p - p_4^-}{L_4}, & \dot{v}_5 &= \frac{1}{\rho}\frac{p_4^+ - p_3^-}{L_5}, & & \end{aligned} \tag{2.3.1}$$

as well as the algebraic relations for $p_3^+, p_3^-, p_4^+, p_4^-, p_p$:

$$\begin{aligned} p_3^+ &= p_p, \quad \text{if valve 1 is closed,} \\ p_3^+ &= p_3^-, \quad \text{if valve 1 is open,} \end{aligned} \tag{2.3.2}$$

$$\begin{aligned} p_4^+ &= p_p, \quad \text{if valve 2 is closed,} \\ p_4^+ &= p_4^-, \quad \text{if valve 2 is open,} \end{aligned} \tag{2.3.3}$$

and the continuity relations:

$$\frac{p_3^- - p_4^+}{L_5} = \frac{p_1 - p_3^-}{L_1 - x_1} + \frac{p_p - p_3^+}{L_3},$$

$$\frac{p_3^- - p_4^+}{L_5} = \frac{p_4^+ - p_2}{L_2 - x_2} + \frac{p_4^- - p_p}{L_4}, \tag{2.3.4}$$

$$\rho\ddot{x}_p = \frac{p_3^+ - p_p}{L_3} + \frac{p_4^- - p_p}{L_4}, \tag{2.3.5}$$

where the pressures p_1, p_2 are related with x_1, x_2 according to:

$$p_1 = p_{10}\left(\frac{x_{10}}{x_1}\right)^\gamma, \qquad p_2 = p_{20}\left(\frac{x_{20}}{x_2}\right)^\gamma. \tag{2.3.6}$$

Expressions (2.3.1)-(2.3.6) is a system of differential algebraic equations which consists of 14 equations for 14 unknowns. Our aim is to solve the unknown vari-

ables $x_1, x_2, v_1, ..., v_5, p_3^{\pm}, p_4^{\pm}, p_p, p_1, p_2$ with a set of initial conditions x_{10},...,v_{50}. Notice that the linear system (2.3.2)-(2.3.4) is singular when both valves are closed, and has a unique solution otherwise. Below we present a direct numerical approach to solve the above differential algebraic equations.

2.3.1 The Algorithm

We divide the time interval $[0, t_{\text{end}}]$ into N equal subintervals with size Δt, i.e.,

$$t^{(n+1)} = t^{(n)} + \Delta t$$

where $n = 0, ..., N-1$. Here, $t^{(0)} = 0$ and $t^{(N)} = t_{\text{end}}$.

Step 1: Initialization.
At $t = 0$, we give initial guesses for the pressures $p_i^{(0)} = p_{i0}, i = 1, 2$, the positions of the air/liquid interface $x_i^{(0)} = x_{i0}, i = 1, 2$, and the initial velocities $v_i^{(0)} = v_{i0}, i = 1, ..., 5$. Since $x_p = x_0 \cos \omega t$, the plunger is about to push down at $t = 0$. Thus we also assume that valve 1 is closed and valve 2 is open.

For $t = t^{(0)}, ..., t^{(N-1)}$, repeat Step 2 to Step 7:
Step 2: Assign corresponding pressure equations using (2.3.2) and (2.3.3), according to whether a particular valve is open or closed.
Step 3: Calculate the plunger acceleration $\ddot{x}_p$, then solve the linear system of equations (2.3.2)-(2.3.4) (e.g. by Gaussian Elimination) for $p_3^{\pm}$, $p_4^{\pm}$ and p_p.
Step 4: Update x_1, x_2, v_1, ..., v_5 from (2.3.1) by a numerical integration scheme. For example, a first order Euler scheme can be used. First, we update

the velocities by

$$v_1^{(n+1)} = v_1^{(n)} + \frac{\Delta t}{\rho}\frac{p_1^{(n)} - p_3^{-(n)}}{L_1 - x_1^{(n)}}, \qquad v_2^{(n+1)} = v_2^{(n)} + \frac{\Delta t}{\rho}\frac{p_2^{(n)} - p_4^{+(n)}}{L_2 - x_2^{(n)}},$$
$$v_3^{(n+1)} = v_3^{(n)} + \frac{\Delta t}{\rho}\frac{p_3^{+(n)} - p_p^{(n)}}{L_3}, \qquad v_4^{(n+1)} = v_4^{(n)} + \frac{\Delta t}{\rho}\frac{p_p^{(n)} - p_4^{-(n)}}{L_4},$$
$$v_5^{(n+1)} = v_5^{(n)} + \frac{\Delta t}{\rho}\frac{p_4^{+(n)} - p_3^{-(n)}}{L_5}.$$

Then x_1 and x_2 can be calculated by using the updated values of v_1 and v_2, i.e.,

$$x_1^{(n+1)} = x_1^{(n)} + \Delta t\ v_1^{(n+1)}, \qquad x_2^{(n+1)} = x_2^{(n)} + \Delta t\ v_2^{(n+1)}.$$

Step 5: Update p_1 and p_2 from (2.3.6), i.e.,

$$p_1^{(n+1)} = p_1^{(n)}\left(\frac{x_1^{(n)}}{x_1^{(n+1)}}\right)^{\gamma}, \qquad p_2^{(n+1)} = p_2^{(n)}\left(\frac{x_2^{(n)}}{x_2^{(n+1)}}\right)^{\gamma}.$$

Step 6: Set $t^{(n+1)} = t^{(n)} + \Delta t$.

Step 7: Check if valves change states according to Table 2.1 and go back to Step 2.

2.3.2 Remarks on Changing the States of the Valves

The condition $v_i < 0$, $i = 3, 4$, for closing a valve needs some extra care. By computing v_i at each fixed time step and say we have $v_i > 0$ at $t^{(n)}$ and $v_i < 0$ at $t^{(n+1)}$. Since the valve is closed as soon as a negative velocity is detected, we need to adjust the time step to ensure that at some t^* where $t^{(n)} < t^* < t^{(n+1)}$, $v_i(t^*) = 0$, $i = 3, 4$. Since we know the values of v_i at each $t^{(n)}$ and $t^{(n+1)}$, t^* can be found by a root-finding algorithm. For example, the secant method can be used and only one iteration is needed to find the exact value of t^* since we have used a first order Euler scheme to update the velocities.

From (2.3.2) and (2.3.3), we see that there are four distinct situations

concerning open or closed valves, i.e.,

1. valve 1 is open, valve 2 is closed;
2. valve 1 is closed, valve 2 is open;
3. both valves are closed;
4. both valves are open.

For each of the four situation, we have a different set of linear equations (2.3.2)-(2.3.4). For situations 1, 2 and 4, the linear system has a unique solution since the determinant is non-zero. However, challenges arise while both valves are closed. The linear system (2.3.2)-(2.3.4) for $p_3^{\pm}$, $p_4^{\pm}$ and p_p reads

$$\begin{pmatrix} 0 & 1 & 0 & 0 & -1 \\ 0 & 0 & 1 & 0 & -1 \\ \frac{1}{L_5}+\frac{1}{L_1-x_1} & \frac{1}{L_3} & 0 & -\frac{1}{L_5} & -\frac{1}{L_3} \\ \frac{1}{L_5} & 0 & -\frac{1}{L_4} & -\frac{1}{L_5}-\frac{1}{L_2-x_2} & \frac{1}{L_4} \\ 0 & \frac{1}{L_3} & \frac{1}{L_4} & 0 & -\frac{1}{L_3}-\frac{1}{L_4} \end{pmatrix} \begin{pmatrix} p_3^- \\ p_3^+ \\ p_4^- \\ p_4^+ \\ p_p \end{pmatrix} = \begin{pmatrix} 0 \\ 0 \\ \frac{p_1}{L_1-x_1} \\ -\frac{p_2}{L_2-x_2} \\ \rho\ddot{x}_p \end{pmatrix}. \tag{2.3.7}$$

The row echelon form of the augmented matrix gives

$$\begin{pmatrix} \frac{L_1-x_1+L_5}{L_5(L_1-x_1)} & \frac{1}{L_3} & 0 & -\frac{1}{L_5} & -\frac{1}{L_3} & \frac{p_1}{L_1-x_1} \\ 0 & 1 & 0 & 0 & -1 & 0 \\ 0 & 0 & 1 & 0 & -1 & 0 \\ 0 & 0 & 0 & -\frac{L_5+L_1-x_1+L_2-x_2}{(L_2-x_2)(L_1-x_1+L_5)} & 0 & -\frac{(L_2-x_2)p_1+(L_1-x_1+L_5)p_2}{(L_2-x_2)(L_1-x_1+L_5)} \\ 0 & 0 & 0 & 0 & 0 & \rho\ddot{x}_p \end{pmatrix}. \tag{2.3.8}$$

We see the linear system is singular as a consequence of the conservation of mass and the assumption of incompressibility. Thus, it has infinitely many solutions while $\ddot{x}_p = 0$, and no solution while $\ddot{x}_p \neq 0$. Since we use $x_p = x_0 \cos\omega t$, $\ddot{x}_p = 0$ if and only if $x_p = 0$. However, when $x_p = 0$, we are in either situation 1 or 2, i.e., one valve is open and the other one is closed. Therefore, we must avoid this singularity. One way to avoid this is to artificially force the original closed valve to open. This special treatment is shown in Table 2.2.

2.4 Results

A Matlab program is coded to simulate the motion of Model PE-61A plunger pumps, in which the parameters and initial conditions are given in Table 2.3. Figures 2.10 to 2.9 show a typical simulation of 5 strokes, with $L_5 = 200$ m. We first give qualitative explanations to the results. Further quantitative analysis will be presented later in this chapter.

2.4.1 Qualitative Behaviors

Let us look at the first stroke. Figure 2.8 shows that as the plunger is pushed downwards, $v_3 = 0$ and $v_4 > 0$. This means that valve 1 is closed and valve 2 is open during the first downward stroke. Next, when the plunger is pulled upwards, valve 1 is open and valve 2 is closed. We confirm the states of the valves by examining Figure 2.9. During the first downward stroke, $p_3^+ > p_3^-$ and $p_4^+ = p_4^-$ which is consistent with the fact that valve 1 is closed and valve 2 is open. In the pulling case, $p_3^+ = p_3^-$ and $p_4^+ > p_4^-$ which verifies that valve 1 is open and valve 2 is closed.

From Figure 2.10 and 2.11, we see that the air volumes and pressures in both of the air tanks undergo opposite variations. During the downward plunger movement, since valve 2 is open, some liquid flows into air tank 2 and some flows through L_5 and comes back to air tank 1. So in both air tanks, the air is compressed as we see in Figure 2.10. Consequently, the pressures p_1 and p_2 are both increased, as shown in Figure 2.11. The opposite happens for the upward plunger movement.

At time $t^{(n)}$	At time $t^{(n+1)}$	Adjusted at time $t^{(n+1)}$
valve 1 is closed valve 2 is open	both valves are closed	valve 1 opens valve 2 stays closed
valve 1 is open valve 2 is closed	both valves are closed	valve 1 stays closed valve 2 opens

Table 2.2: Changing valve states at both valves are closed.

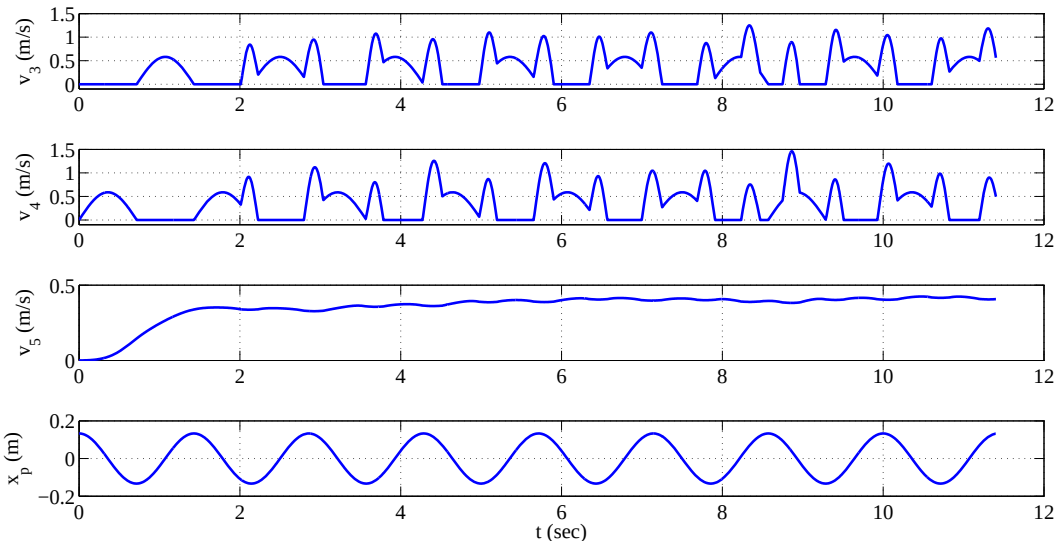

Figure 2.8: v_3, v_4, v_5 when $L_5 = 200$ m.

By looking at the second stroke and afterwards, we notice that the solution goes into a different regime. From Figure 2.8, it can be seen that as we start the second downward stroke, valve 1 closes and valve 2 opens. And as seen in Figure 2.9, p_3^- gradually becomes larger than p_3^+. As $p_3^- > p_3^+ + \Delta p$, valve 1 is popped open, according to Table 2.1. Thus we get a sudden increase for v_3 and v_4 since both valves are now opened, as shown in Figure 2.8. Then as the plunger is pulled up again, v_4 goes from positive to negative, valve 2 is then closed and valve 1 remains open, and now we see that in Figure 2.9, p_4^- gradually becomes larger than p_4^+. As $p_4^- > p_4^+ + \Delta p$, valve 2 is popped open at the end of the second stroke. This behavior then continues periodically with the strokes.

If we look at v_5 in Figure 2.8, it increases from zero to about 0.3 m/s during the first stroke, and gradually increases to about 0.4 m/s after the fifth stroke. This can be compared with the maximum capacity of Model PE-61A plunger pumps which is known about 0.3 m/s. This validates our model qualitatively. With the addition of viscosity, the velocity v_5 will not change with the same plunger velocity. However, extra power is needed to overcome the frictional effects.

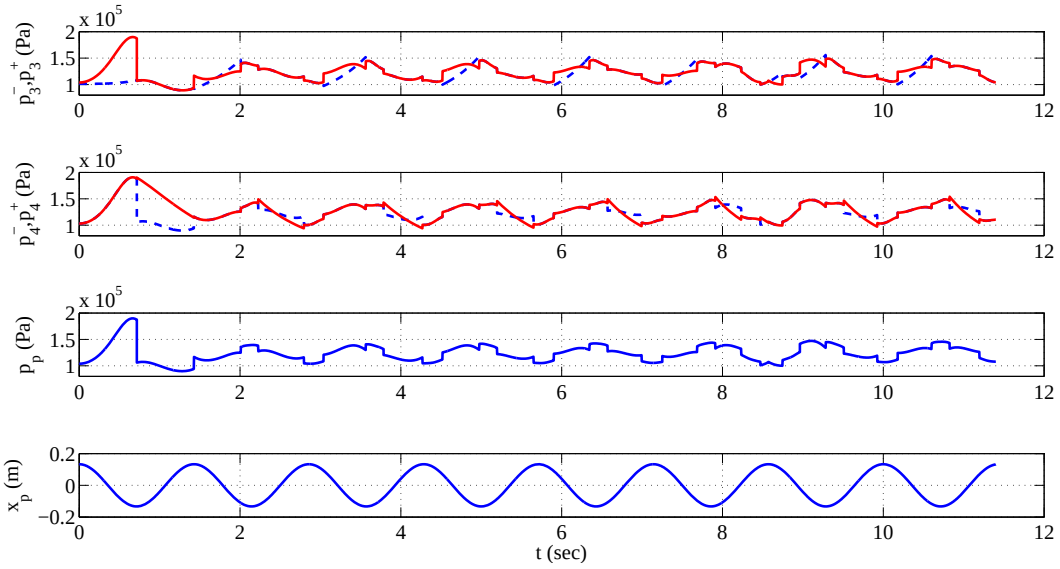

Figure 2.9: $p_3^{\pm}$, $p_4^{\pm}$, p_p when $L_5 = 200$ m. The dashed line shows p_i^-, $i = 3, 4$, and the solid line indicates p_i^+, $i = 3, 4$.

2.4.2 Variation of L_5

We found previously that the solution contains two different regimes. The first regime only contains the situations where one valve is open and the other one is closed. The second regime allows both valves to be open for some times. This phase change of the solutions might be caused by the fact that we have a closed loop. The fluid that being pumped out from the discharge valve circulates back and pops up the suction valve. We ran the program by varying the length of L_5 while other parameters were kept fixed. It is interesting to find that the duration of the first regime depends upon L_5. This indicates some natural oscillation of the solutions due to the closed loop system. The levels of the air/liquid interface and air pressures in both of the air tanks oscillate due to the connecting outer loop.

Simulation results for $L_5 = 800$ m are shown in Figures 2.12 to 2.14 and $L_5 = 3200$ m are shown in Figures 2.15 to 2.17. By comparing with the case of $L_5 = 200$ m, we see that the first regime of the solution remains longer as we increase L_5. In particular, when $L_5 = 200$ m, it only takes one stroke for the solution to get into the second regime; when $L_5 = 800$ m, it takes about two

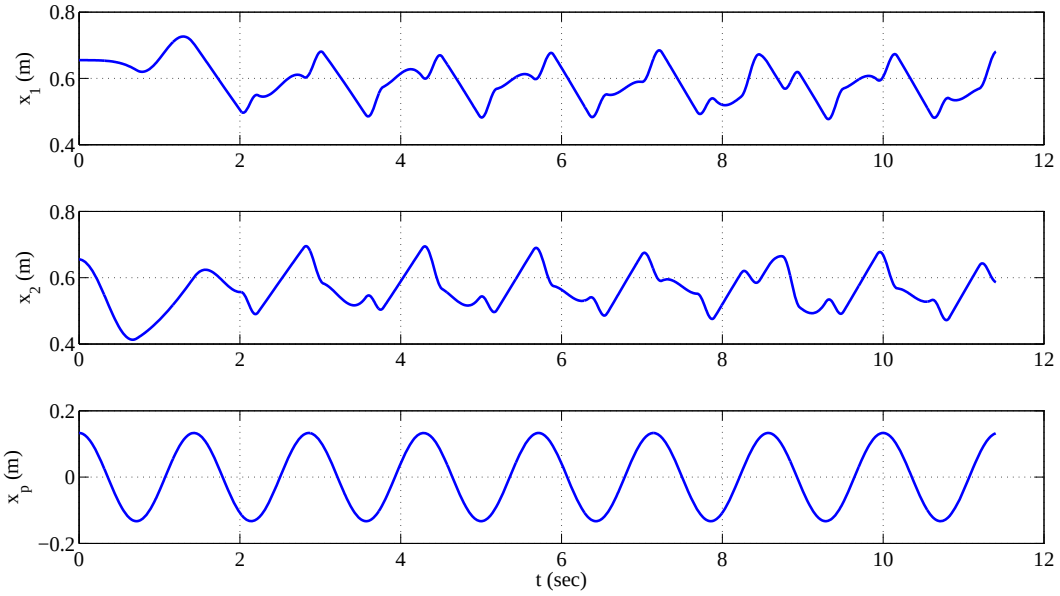

Figure 2.10: x_1, x_2 when $L_5 = 200$ m.

strokes for the solution to develop into the second regime; when $L_5 = 3200$ m, it takes about four strokes. Thus, as the length of L_5 quadruples, the duration of the first regime doubles.

We see that in Figures 2.14 and 2.17, x_1 and x_2 also vary on a larger scale in the first regime of the solution. This suggests another possible oscillation other than the strokes of the plunger. We shall analyze these observations in the next section.

2.5 Further Analysis

As mentioned in the previous section, the solution oscillates with a frequency different from the stroke frequency, as seen in the first regime. In order to understand the oscillatory behaviors better, we carry out some asymptotic analysis. As discussed before, we have four different situations:

1. valve 1 is open, valve 2 is closed;
2. valve 1 is closed, valve 2 is open;
3. both valves are closed;

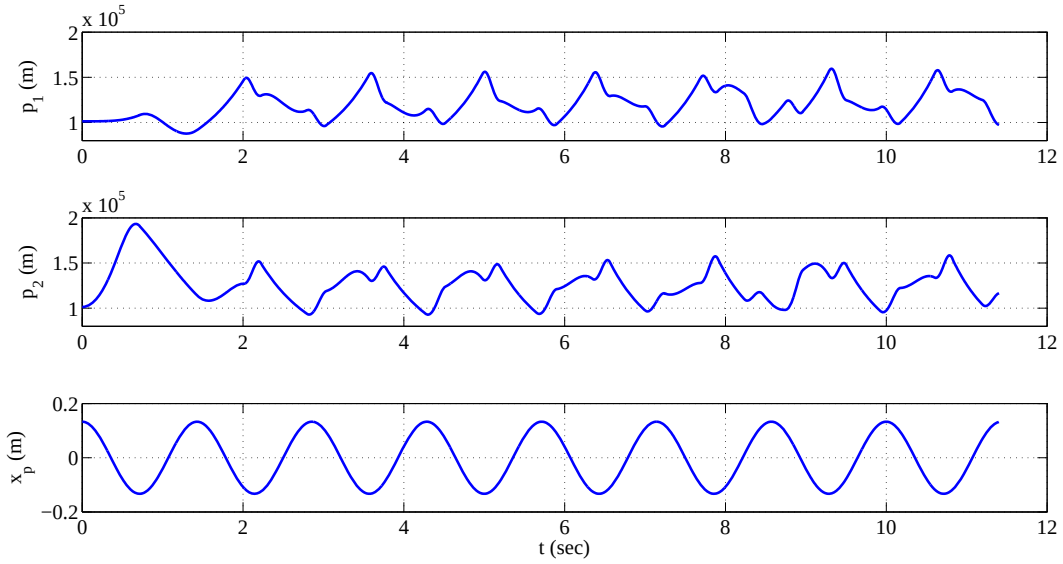

Figure 2.11: p_1, p_2 when $L_5 = 200$ m.

4. both valves are open.

For each of the above cases, we can solve the linear system (2.3.2)-(2.3.4) symbolically and then substitute the pressure solutions $p_3^{\pm}$, $p_4^{\pm}$ and p_p back to (2.3.1). Below we give the resulting ordinary differential equations for each situation.

Situation 1: valve 1 is open, valve 2 is closed. System (2.3.2)-(2.3.4) has a unique solution, and substitution gives

$$\dot{v}_1 = \frac{1}{\rho}\frac{p_1 - p_2 + \rho\ddot{x}_p\,(L_5 + L_2 - x_2)}{L_5 + L_2 - x_2 + L_1 - x_1}, \tag{2.5.1}$$

$$\dot{v}_2 = \frac{1}{\rho}\frac{p_2 - p_1 + \rho\ddot{x}_p\,(L_1 - x_1)}{L_5 + L_2 - x_2 + L_1 - x_1}, \tag{2.5.2}$$

$$\dot{v}_3 = \ddot{x}_p, \quad \dot{v}_4 = 0, \quad \dot{v}_5 = \frac{1}{\rho}\frac{p_2 - p_1 + \rho\ddot{x}_p\,(L_1 - x_1)}{L_5 + L_2 - x_2 + L_1 - x_1}. \tag{2.5.3}$$

Situation 2: valve 1 is closed, valve 2 is open. System (2.3.2)-(2.3.4) has a

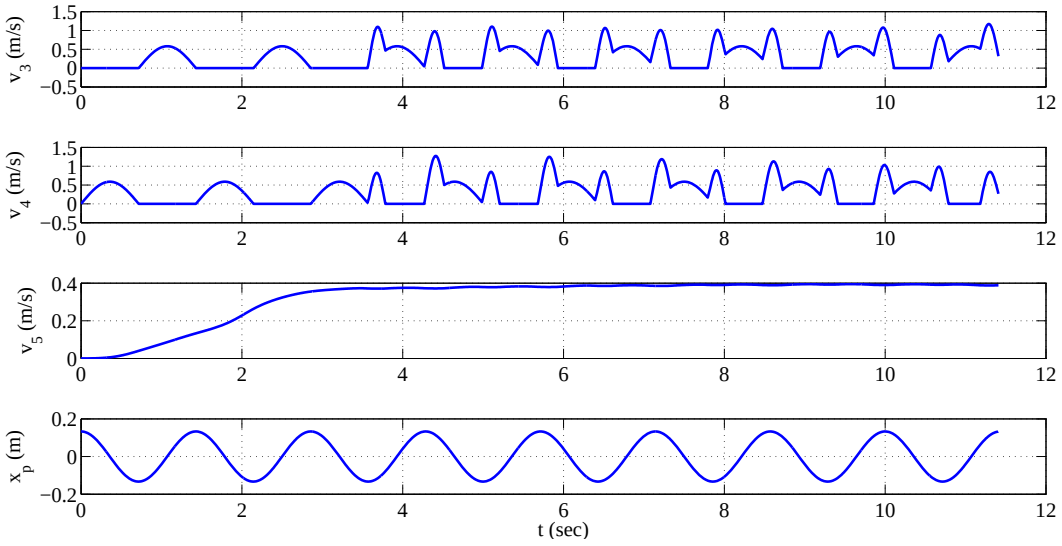

Figure 2.12: v_3, v_4, v_5 when $L_5 = 800$ m.

unique solution, and substitution yields

$$\dot{v}_1 = \frac{1}{\rho}\frac{p_1 - p_2 + \rho\ddot{x}_p\,(L_2 - x_2)}{L_5 + L_2 - x_2 + L_1 - x_1}, \tag{2.5.4}$$

$$\dot{v}_2 = \frac{1}{\rho}\frac{p_2 - p_1 + \rho\ddot{x}_p\,(L_5 + L_1 - x_1)}{L_5 + L_2 - x_2 + L_1 - x_1}, \tag{2.5.5}$$

$$\dot{v}_3 = 0, \quad \dot{v}_4 = -\ddot{x}_p, \quad \dot{v}_5 = \frac{1}{\rho}\frac{p_2 - p_1 - \rho\ddot{x}_p\,(L_2 - x_2)}{L_5 + L_2 - x_2 + L_1 - x_1}. \tag{2.5.6}$$

Situation 3: both valves are closed. Pressure solutions exist if and only if $\ddot{x}_p = 0$. When $\ddot{x}_p = 0$, we have infinitely many solutions, i.e.,

$$p_3^- = \frac{(L_1 - x_1)p_2 + (L_5 + L_2 - x_2)p_1}{L_5 + L_1 - x_1 + L_2 - x_2},$$
$$p_4^+ = \frac{(L_2 - x_2)p_1 + (L_5 + L_2 - x_2)p_1}{L_5 + L_1 - x_1 + L_2 - x_2},$$
$$p_3^+ = p_4^- = p_p = s$$

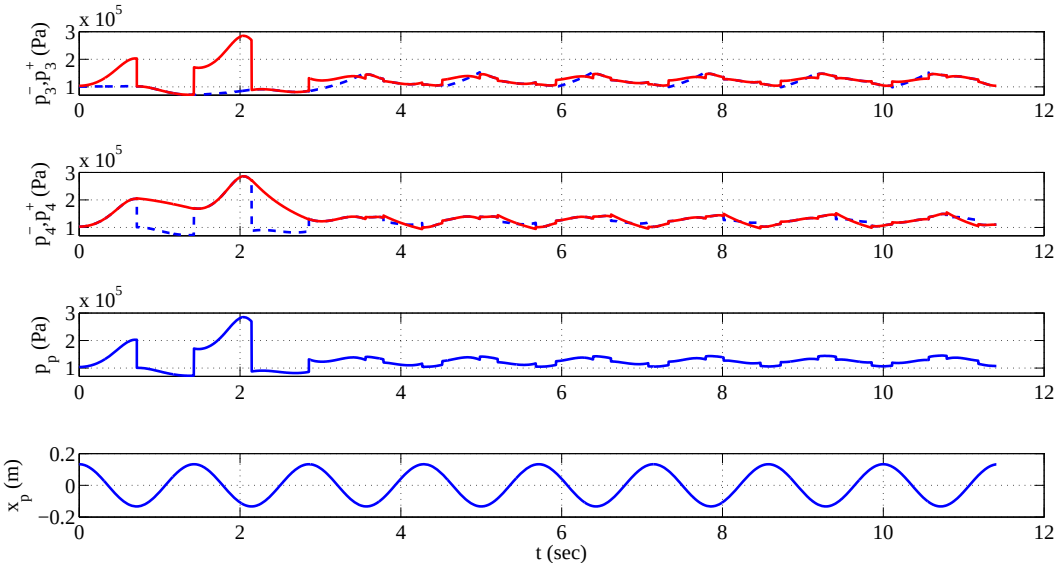

Figure 2.13: $p_3^{\pm}$, $p_4^{\pm}$, p_p when $L_5 = 800$ m. The dashed line shows p_i^-, $i = 3, 4$, and the solid line indicates p_i^+, $i = 3, 4$.

where s is an arbitrary real number. Substitution yields

$$\dot{v}_1 = \frac{1}{\rho}\frac{p_1 - p_2}{L_5 + L_2 - x_2 + L_1 - x_1},$$
$$\dot{v}_2 = \frac{1}{\rho}\frac{p_2 - p_1}{L_5 + L_2 - x_2 + L_1 - x_1},$$
$$\dot{v}_3 = 0, \quad \dot{v}_4 = 0, \quad \dot{v}_5 = \frac{1}{\rho}\frac{p_2 - p_1}{L_5 + L_2 - x_2 + L_1 - x_1}.$$

Situation 4: both valves are open. Pressure solution is unique and substitution gives

$$\dot{v}_1 = \frac{1}{\rho}\frac{(p_1 - p_2)(L_3 + L_4 + L_5) + \rho\ddot{x}_p\left[(L_4 + L_2 - x_2)L_5 + (L_3 + L_4)(L_2 - x_2)\right]}{(L_1 + L_2 + L_3 + L_4 - x_1 - x_2)L_5 + (L_3 + L_4)(L_1 - x_1 + L_2 - x_2)},$$
$$\dot{v}_2 = \frac{1}{\rho}\frac{(p_2 - p_1)(L_3 + L_4 + L_5) + \rho\ddot{x}_p\left[(L_3 + L_1 - x_1)L_5 + (L_3 + L_4)(L_1 - x_1)\right]}{(L_1 + L_2 + L_3 + L_4 - x_1 - x_2)L_5 + (L_3 + L_4)(L_1 - x_1 + L_2 - x_2)},$$
$$\dot{v}_3 = \frac{1}{\rho}\frac{(p_2 - p_1)L_5 + \rho\ddot{x}_p\left[(L_4 + L_2 - x_2)L_5 + L_4(L_1 - x_1 + L_2 - x_2)\right]}{(L_1 + L_2 + L_3 + L_4 - x_1 - x_2)L_5 + (L_3 + L_4)(L_1 - x_1 + L_2 - x_2)},$$
$$\dot{v}_4 = \frac{1}{\rho}\frac{(p_1 - p_2)L_5 - \rho\ddot{x}_p\left[(L_3 + L_1 - x_1)L_5 + L_3(L_1 - x_1 + L_2 - x_2)\right]}{(L_1 + L_2 + L_3 + L_4 - x_1 - x_2)L_5 + (L_3 + L_4)(L_1 - x_1 + L_2 - x_2)},$$
$$\dot{v}_5 = \frac{1}{\rho}\frac{(p_2 - p_1)(L_3 + L_4) + \rho\ddot{x}_p\left[(L_1 - x_1)L_4 - (L_2 - x_2)L_3\right]}{(L_1 + L_2 + L_3 + L_4 - x_1 - x_2)L_5 + (L_3 + L_4)(L_1 - x_1 + L_2 - x_2)}.$$

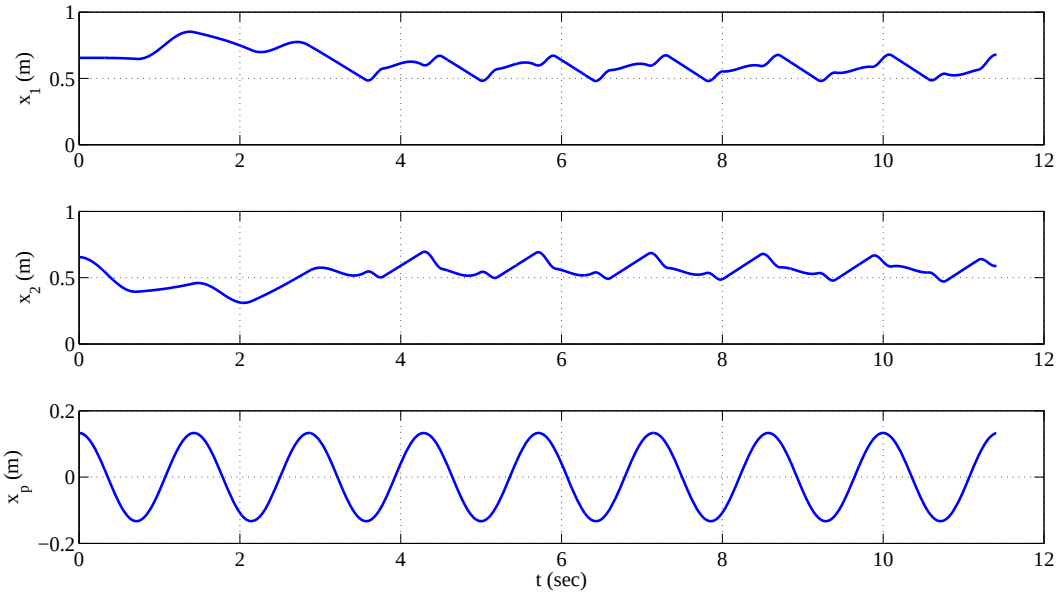

Figure 2.14: x_1, x_2 when $L_5 = 800$ m.

2.5.1 Linearization

Let us consider situation 1. We re-write (2.5.1) as

$$\ddot{x}_1 = \frac{1}{\rho}\frac{p_1 - p_2}{L_5 + L_2 - x_2 + L_1 - x_1} + \frac{\ddot{x}_p(L_5 + L_2 - x_2)}{L_5 + L_2 - x_2 + L_1 - x_1}. \tag{2.5.7}$$

The second term on the right-hand side of (2.5.7) represents the oscillations of the plunger motion. The first term on the right-hand side of (2.5.7) represents some natural oscillation. The contribution from the plunger oscillations can be obviously seen in Figures 2.10, 2.14 and 2.17. In order to understand the natural oscillation, we can expand the first term on the right-hand side in powers of $1/L_5$ to get

$$\ddot{x}_1 = \frac{1}{\rho}(p_1 - p_2)\,\epsilon + \frac{1}{\rho}(p_2 - p_1)(L_1 - x_1 + L_2 - x_2)\,\epsilon^2 + O\left(\epsilon^3\right) \tag{2.5.8}$$

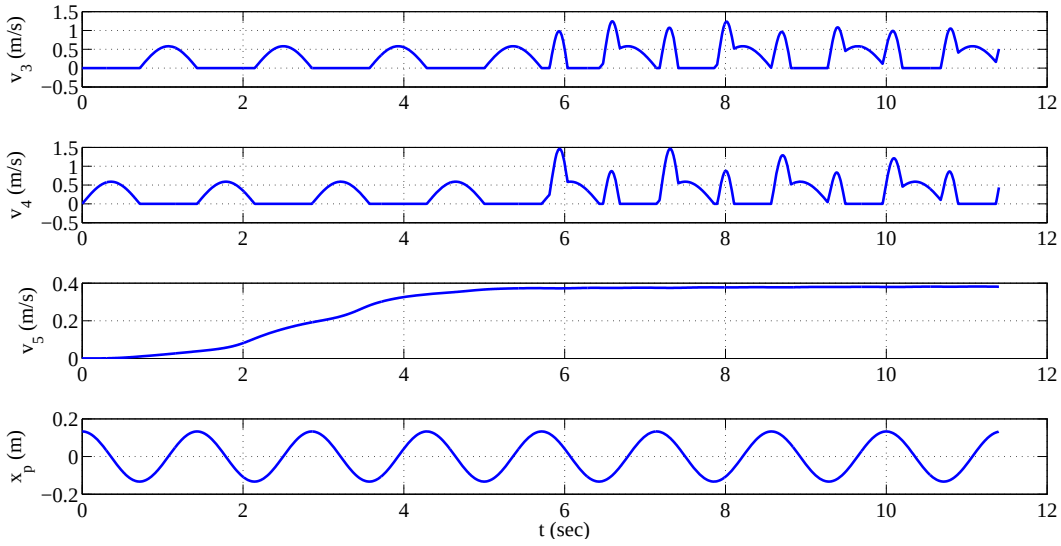

Figure 2.15: v_3, v_4, v_5 when $L_5 = 3200$ m.

where $\epsilon = 1/L_5$. For simplicity, Let us consider the case of $\gamma = 1$ (isothermal), so

$$p_1 = \frac{p_{10}x_{10}}{x_1},$$
$$p_2 = \frac{p_{20}x_{20}}{x_2},$$

where p_{i0}, $i = 1, 2$, are the initial pressures in the air tanks and x_{i0}, $i = 1, 2$, are the initial positions of the air/liquid interface. From the initial conditions, we also have

$$p_{10} = p_{20} = p_0,$$
$$x_{10} = x_{20} = l/2,$$

where $l = L_1 = L_2$. Substituting the above equations into (2.5.8), we get to leading order

$$\ddot{x}_1 = \frac{\epsilon p_0 l}{2\rho}\left(\frac{1}{x_1} - \frac{1}{x_2}\right).$$

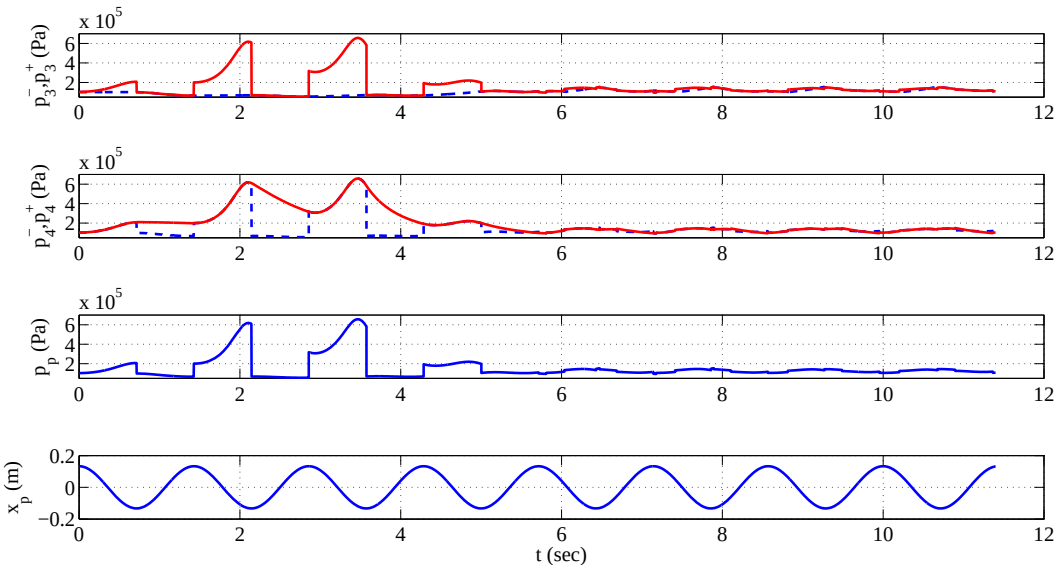

Figure 2.16: $p_3^{\pm}$, $p_4^{\pm}$, p_p when $L_5 = 3200$ m. The dashed line shows p_i^-, $i = 3, 4$, and the solid line indicates p_i^+, $i = 3, 4$.

We can carry out similar analysis for (2.5.2) and get, also to leading order,

$$\ddot{x}_2 = -\frac{\epsilon p_0 l}{2\rho}\left(\frac{1}{x_1} - \frac{1}{x_2}\right).$$

Collectively,

$$\ddot{x}_1 = \Gamma^2\left(\frac{1}{x_1} - \frac{1}{x_2}\right), \tag{2.5.9}$$

$$\ddot{x}_2 = -\Gamma^2\left(\frac{1}{x_1} - \frac{1}{x_2}\right) \tag{2.5.10}$$

where $\Gamma^2 = \epsilon p_0 l/2\rho$. By letting $y_1 = x_1$, $y_2 = x_2$, $y_3 = \dot{x}_1$, and $y_4 = \dot{x}_2$, we have

$$\dot{y}_1 = y_3, \quad \dot{y}_2 = y_4, \quad \dot{y}_3 = \Gamma^2\left(\frac{1}{y_1} - \frac{1}{y_2}\right), \quad \dot{y}_4 = -\Gamma^2\left(\frac{1}{y_1} - \frac{1}{y_2}\right). \tag{2.5.11}$$

The critical points of the system (2.5.11) are: $y_1 = y_2 = k$, $y_3 = 0$, $y_4 = 0$, where $0 < k < l$. If we choose $k = l/2$ (the choice of this k matches up the initial conditions in our previous simulations, however, k can be arbitrary and it will only change the frequency) then the critical point is $y^* = (l/2, l/2, 0, 0)$.

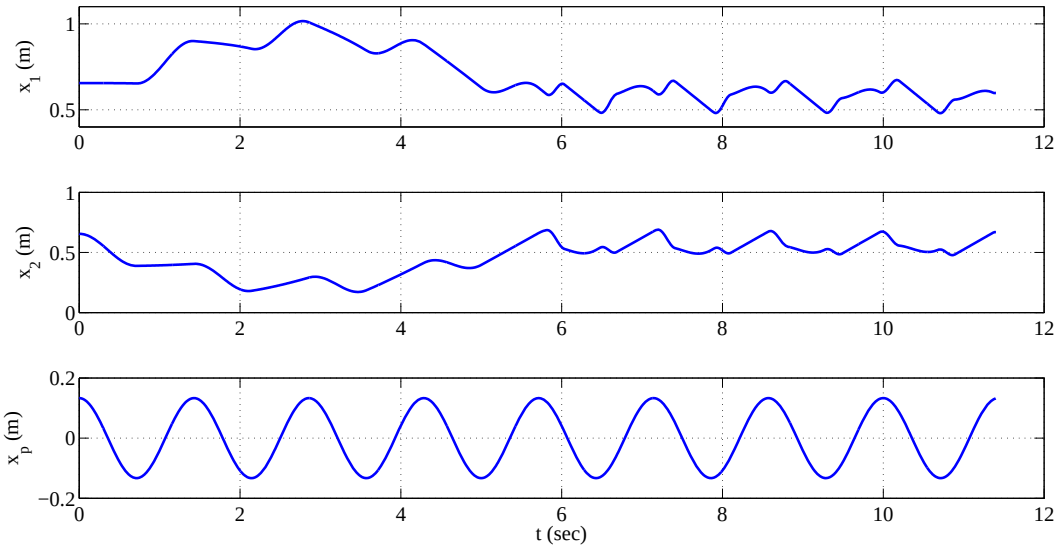

Figure 2.17: x_1, x_2 when $L_5 = 3200$ m.

The Jacobian matrix then becomes

$$J\big|_{y^*} = \begin{pmatrix} 0 & 0 & 1 & 0 \\ 0 & 0 & 0 & 1 \\ -\dfrac{4\Gamma^2}{l^2} & \dfrac{4\Gamma^2}{l^2} & 0 & 0 \\ \dfrac{4\Gamma^2}{l^2} & -\dfrac{4\Gamma^2}{l^2} & 0 & 0 \end{pmatrix} \tag{2.5.12}$$

where

$$\frac{4\Gamma^2}{l^2} = \frac{2\epsilon p_0}{\rho l}.$$

with eigenvalues of

$$\lambda_i = 0, 0, \pm 2i\sqrt{\frac{\epsilon p_0}{\rho l}}. \tag{2.5.13}$$

In the next part, we will verify that the angular frequency of natural oscillations corresponding to the geometry of the closed pumping loop can be approximated as $2\sqrt{\epsilon p_0/\rho l}$. This corresponds to our previous observation that the period of natural oscillation is proportional to $\sqrt{L_5}$.

2.5.2 Natural Frequency

In this section, we solve the equations in situations 1 and 2 separately, so that one of the valves is always open and the other valve is always closed. Figure 2.18 shows the numerical solution of (2.5.1)-(2.5.3) (valve 1 is always open, valve 2 is always closed) with the initial conditions in Table 2.3. Figure 2.19 shows the numerical solution of (2.5.4)-(2.5.6) (valve 1 is always closed, valve 2 is always open) with the same initial conditions. We can see the symmetry between both cases, i.e., the case where valve 1 is open and valve 2 is closed is a mirror image of the case where valve is 1 closed and valve is 2 open.

From (2.5.13), we know that the approximated angular frequency for natural oscillation is

$$\omega_{\text{approx}} = 2\sqrt{\frac{\epsilon p_0}{\rho l}} = 2\sqrt{\frac{1.013 \times 10^5}{200 \times 10^3 \times 1.31}} \text{ rad/sec} \approx 1.4236 \text{ rad/sec}.$$

And by measuring the distance between similar crests (or troughs) of x_2 for example, in Figure 2.18, we get the angular frequency is 1.4047 rad/sec.

If we change L_5 to 800 m, we can see from Figure 2.20 that the frequency is lowered by 1/2. The approximated angular frequency is

$$\omega_{\text{approx}} = 2\sqrt{\frac{\epsilon p_0}{\rho l}} = 2\sqrt{\frac{1.013 \times 10^5}{800 \times 10^3 \times 1.31}} \text{ rad/sec} \approx 0.7118 \text{ rad/sec}.$$

and the measured frequency is 0.7229 rad/sec.

2.5.3 Switching Valves

In the previous section, we solved (2.5.1)-(2.5.3) and (2.5.4)-(2.5.6) separately without switching valves and found out the natural frequency is close to our prediction with the linearized model. Now we present some results for switching between both cases.

Instead of using the conditions in Table 2.1 and 2.2, we only switch between situations 1 and 2 and do not allow both valves to be open or both to be closed.

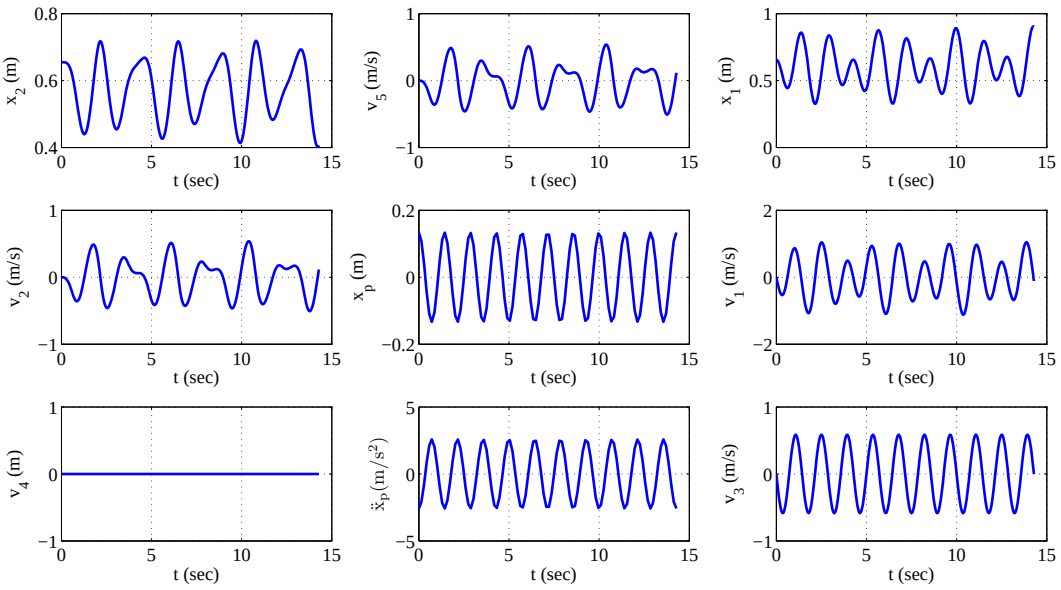

Figure 2.18: Solution for system (2.5.1)-(2.5.3), $L_5 = 200$ m. Valve 1 is always open and valve 2 is always closed.

Thus, we assume valve 1 is open and valve 2 is closed during the upward stroke and vice versa. Initial conditions are the same as in Table 2.3. We also assume $x_i \in C^1$, $i = 1, ..., 5$, i.e., the displacement and velocities are all continuous. So that we can use the last numerical value of the solution in the previous case as an initial condition to the next case.

Figure 2.21 shows the solution for $L_5 = 200$ m. The measured angular frequency in this case is 1.4380 rad/sec ($\omega_{\text{approx}} = 1.4236$ rad/sec). Figure 2.22 shows the solution for $L_5 = 800$ m and the observed angular frequency is 0.7649 rad/sec ($\omega_{\text{approx}} = 0.7118$ rad/sec).

Now we compare Figure 2.21 with Figure 2.10 and Figure 2.22 with Figure 2.14. We can see that the initial phase of x_1 and x_2 in 2.10 is resembled in Figure 2.21. Similarly, the initial phase of x_1 and x_2 in Figure 2.14 is resembled in Figure 2.22.

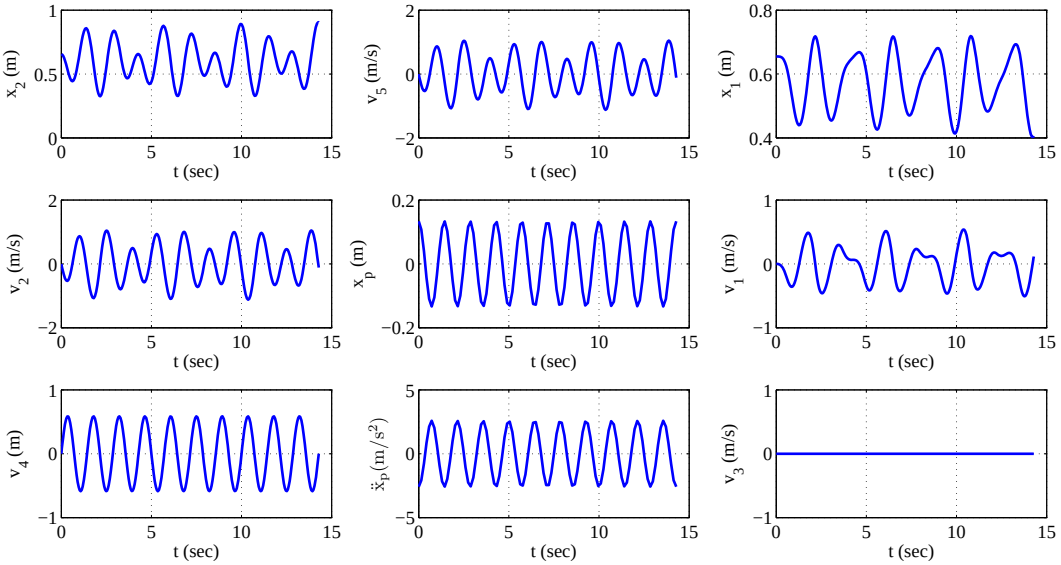

Figure 2.19: Solution for system (2.5.4)-(2.5.6), $L_5 = 200$ m. Valve 1 is always closed and valve 2 is always open.

Description	Symbol	Value	Units
Height of air tank 1	L_1	1.310	m
Height of air tank 2	L_2	1.310	m
Length of pipe L_3	L_3	0.338	m
Length of pipe L_4	L_4	0.338	m
Radius of the pipes	R_p	0.051	m
Angular frequency of the crank	ω	4.398	rad/sec
Maximum stroke length	x_0	0.133	m
Pressure needed to overcome the inertia of the valve	Δp	2.187×10^4	Pa
Initial pressure in air tank 1	p_{10}	1.013×10^5	Pa
Initial pressure in air tank 2	p_{20}	1.013×10^5	Pa
Initial position of the air/liquid interface in air tank 1	x_{10}	0.655	m
Initial position of the air/liquid interface in air tank 2	x_{20}	0.655	m
Initial flow velocity in air tank 1	v_{10}	0	m/s
Initial flow velocity in air tank 2	v_{20}	0	m/s
Initial flow velocity at valve 1	v_{30}	0	m/s
Initial flow velocity at valve 2	v_{40}	0	m/s
Initial flow velocity in L_5	v_{50}	0	m/s

Table 2.3: System Dimensions for Model PE-61A Plunger Pumps and initial conditions.

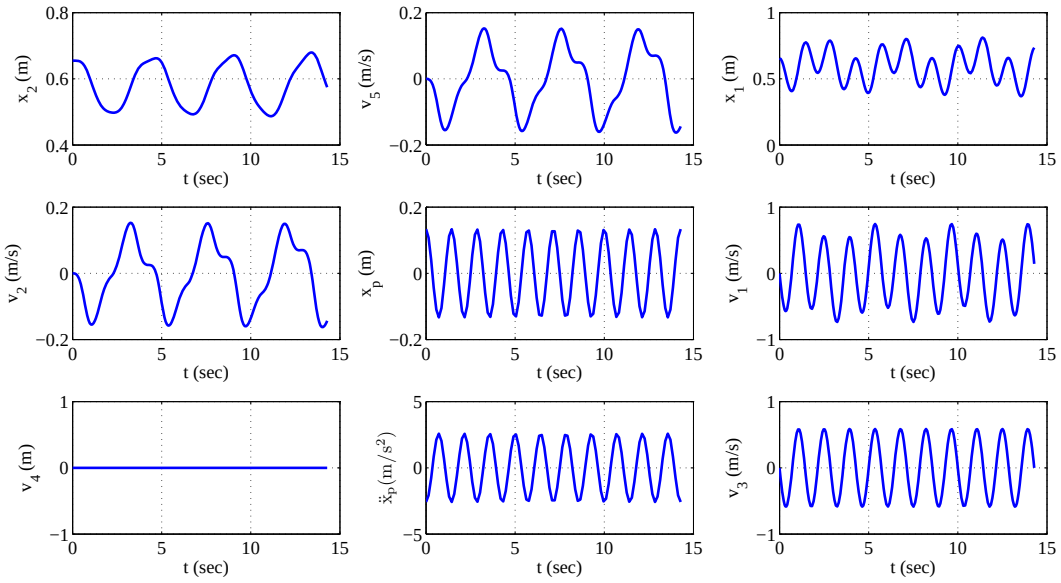

Figure 2.20: Solution for system (2.5.1)-(2.5.3), $L_5 = 800$ m. Valve 1 is always open and valve 2 is always closed.

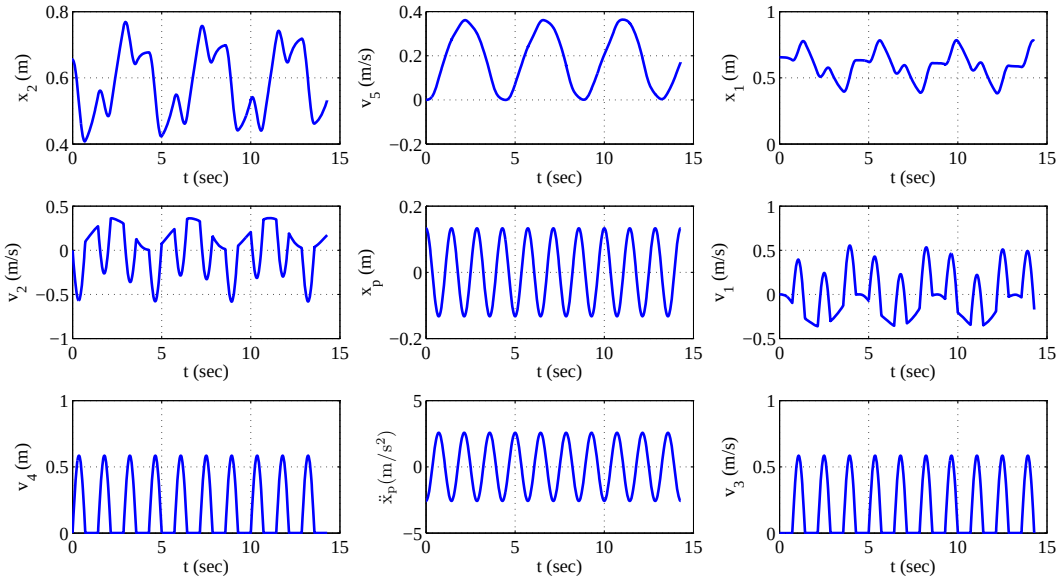

Figure 2.21: Solution for (2.5.1)-(2.5.3) and (2.5.4)-(2.5.6) with switching valves at the top and bottom of each stroke, $L_5 = 200$ m.

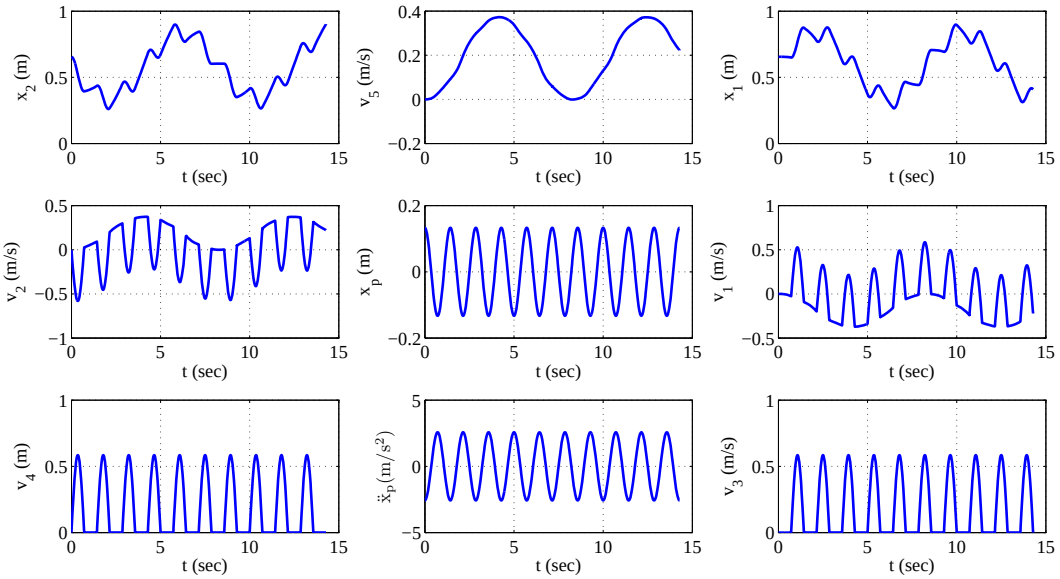

Figure 2.22: Solution for (2.5.1)-(2.5.3) and (2.5.4)-(2.5.6) with switching valves at the top and bottom of each stroke, $L_5 = 800$ m.

Chapter 3

Modelling the Valve Motion

The one-dimensional flow model from the previous chapter provides an overview of the flow under plunger motion within a closed circulation. However, the valves were assumed either fully open or completely closed and the motion of the valve are not resolved. In this chapter, we provide a refinement of the one-dimensional model by studying the motion of the valves. Instead of modeling with a closed loop, we use fixed pressure values at the discharge valve outlet (or suction valve inlet). Simulation results show that as we increase the frequency of the rotating crank (pump faster), the natural maximum displacement of the valve also increases. This explains the potential cause of the clicking noise as the valve hits the boundary.

3.1 How Do the Valves Move?

As mentioned in the introductory chapter, the valves are spherical and made of iron. While the valve is closed, it sits on a circular ring and seals the flow path, shown with a dashed circle in Figure 3.1. As the valve opens, fluid flows through the valve by going around the ball. Both suction and discharge valves have the same geometry.

To begin with modelling the valve motion, we first consider the simple case where the ball valve can only move vertically up or down. It is also assumed

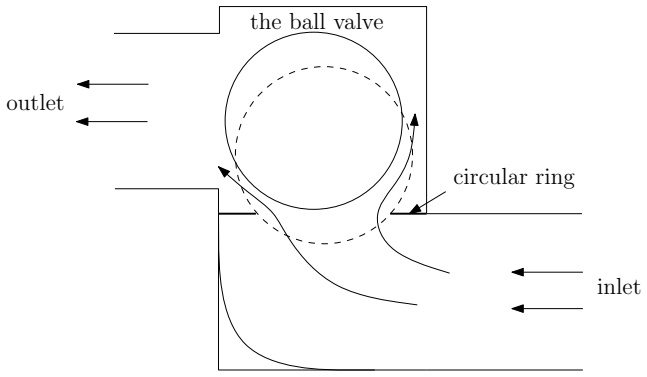

Figure 3.1: A cross-sectional view of the valve region.

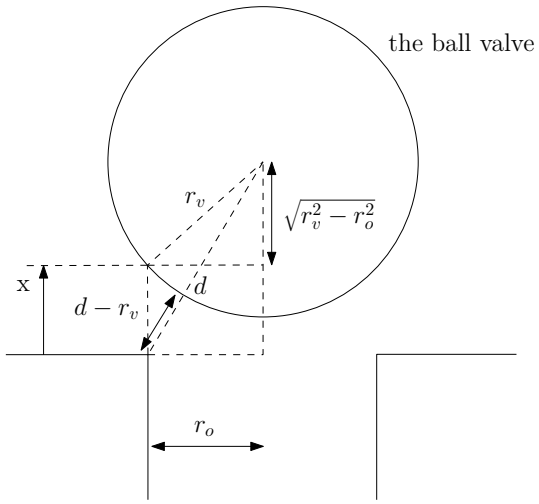

Figure 3.2: The geometry of the valve model.

that the circular ring of the valve seat has the same radius as the inlet pipe. Figure 3.2 shows the geometry of our valve model. The distance the valve travels from the original closed position is denoted by x, $0 \leq x \leq x_{\max}$, where $x_{\max}$ is the maximum distance that the valve is allowed to travel. The radius of the valve and the radius of the pipe are r_v and r_o respectively and d denotes the distance from the center of the valve to the corner of the pipe edge. A basic geometrical argument gives

$$d = \sqrt{\left(\sqrt{r_v^2 - r_o^2} + x\right)^2 + r_o^2}. \tag{3.1.1}$$

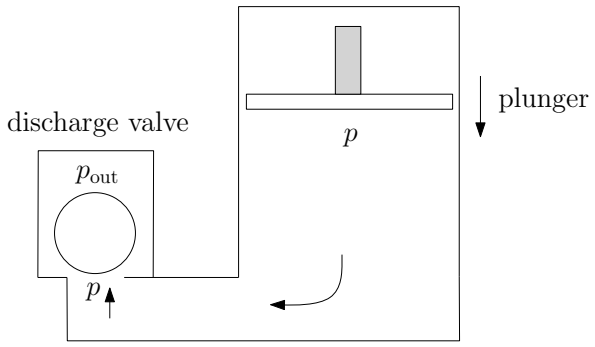

Figure 3.3: The case in which the suction valve is shut.

In order to understand how the valves are popped open and move up or down, let us begin with the case where the suction valve is shut and the plunger is pushing downwards from the top of the stroke. In this case, only the discharge valve is allowed to move. This situation is illustrated in Figure 3.3. The pressure underneath the plunger is denoted by p and it is assumed to be uniform everywhere in the plunger cylinder and below the ball valve. The pressure at the discharge valve outlet is denoted by p_{out} and it is assumed to be a fixed constant in our model.

3.2 The Equations of Motion

3.2.1 Forces Acting on the Valve

We will discuss the forces acting on the discharge valve to determine the equations of valve motion. We assume that the ball valve is always fully immersed in the fluid, thus it experiences both gravitational and buoyant forces, denoted F_g and F_b respectively and

$$\vec{F_g} = -m_v g \hat{e}_x,$$
$$\vec{F_b} = m_f g \hat{e}_x,$$

where m_v is the mass of the valve, m_f is the mass of the fluid occupied by the same volume as the valve, g is the acceleration due to gravity, and $\hat{e}_x$ is the

unit vector along the x-axis.

To simplify the effects of fluid pressure on the valve, we assume that the pressures underneath the valve is uniform everywhere and they act on a surface area of $\pi d_v^2/4$, where d_v is the diameter of the valve. Similarly for the pressures at the top of the valve. So,

$$\vec{F}_{\text{below}} = p\frac{\pi d_v^2}{4}\hat{e}_x,$$
$$\vec{F}_{\text{out}} = -p_{\text{out}}\frac{\pi d_v^2}{4}\hat{e}_x.$$

As the valve is in motion, there is also a drag force acting on it to oppose the motion. We assume that the motion of the valve is slow enough so that the drag force is linearly proportional to the relative velocity of the valve to the fluid. Thus,

$$\vec{F}_{\text{drag}} = -\gamma\left(\dot{x} - v_f\right)\hat{e}_x,$$

where γ is a constant drag coefficient and v_f is the velocity of the fluid at the valve.

We sum all the above forces with account of directions and use the Newton's second law to obtain

$$m_v\ddot{x} = \frac{\pi d_v^2}{4}\left(p - p_{\text{out}}\right) - \left(m_v - m_f\right)g - \gamma\left(\dot{x} - v_f\right),$$

for $0 \le x \le x_{\max}$. If we let $v = \dot{x}$, then

$$\frac{dx}{dt} = v, \tag{3.2.1}$$
$$\frac{dv}{dt} = \frac{\pi d_v^2}{4m_v}\left(p - p_{\text{out}}\right) - g\left(1 - \frac{m_f}{m_v}\right) - \frac{\gamma}{m_v}\left(v - v_f\right). \tag{3.2.2}$$

If p is constant, then (3.2.1) and (3.2.2) can be solved exactly with appropriate initial conditions. However, the pressure in the plunger cylinder is related to the motion of the plunger and it is time dependent. So next we will discuss how the pressure varies in the plunger cylinder.

3.2.2 Pressure Variations in the Plunger Cylinder

We assumed the fluid is incompressible in the previous chapter since liquid water is effectively incompressible. However, the liquid in the pump can contain air bubbles. So the fluid can be considered as compressible although the compression is very small. We can use this compressibility to derive a differential equation for the pressure.

The process of liquid discharge can be represented by the volumetric balance of the fluid (Lyashkov, 1972). The amount of liquid being pushed by the plunger minus the amount of liquid being compressed must be equal to the amount of liquid going out of the valve, if we assumed there is no leakage and the temperature prevents a change of phase. Thus we have

$$dV_p + dV_c = dV_v, \tag{3.2.3}$$

where dV_p is the change in volume of the liquid under the plunger during downward plunger movement for an element of time dt, dV_c is the change in volume due to liquid compressibility during the same dt, and dV_v is the volume of liquid flowing through the discharge valve during the time dt.

The first term in (3.2.3) is given by

$$dV_p = \frac{\pi d_p^2}{4} v_p dt, \tag{3.2.4}$$

where d_p is the diameter of the plunger cylinder, v_p is the velocity of the plunger and

$$v_p = -\omega x_0 \sin(\omega t),$$

where ω is the angular frequency of the rotating crank and x_0 is the maximum stroke length. The negative sign on the right-hand side of the above equation is to ensure that v_p is positive as the plunger is moving downwards.

The process of the downward stroke can be assumed adiabatic (no change

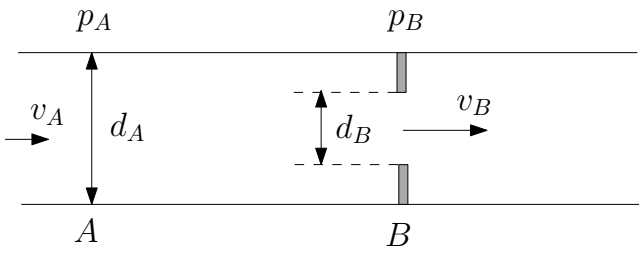

Figure 3.4: The flow in a pipe going through an orifice.

in heat in the liquid) so that

$$dV_c = -\beta_s V dp, \tag{3.2.5}$$

where β_s is the adiabatic compression coefficient, defined as the relative change of volume with pressure at constant entropy. The volume V can be calculated as

$$V = V_0 + \frac{\pi d_p^2}{4} x_0 \cos \omega t,$$

where V_0 is the fluid volume in the plunger cylinder when the plunger is at the center of the downward stroke.

In order to derive the last term in (3.2.3), let us first consider the pipe flow with an orifice (Çengel and Cimbala, 2006), shown in Figure 3.4. The orifice is located at B and point A is a location before the orifice. d_A and d_B denote the diameter of the cross-sectional area at point A and B respectively. The velocities at A and B are denoted by v_A and v_B. Similarly, p_A and p_B denote the pressures. From the conservation of mass, we have

$$\frac{\pi d_A^2}{4} v_A = \frac{\pi d_B^2}{4} v_B$$

so that

$$v_A = \frac{d_B^2}{d_A^2} v_B. \tag{3.2.6}$$

We assume that the flow in the pipe is steady, incompressible and frictionless.

Recalling the Bernoulli's Equation derived in the Appendix, we have

$$\frac{1}{2}v_A^2 + \frac{p_A}{\rho} = \frac{1}{2}v_B^2 + \frac{p_B}{\rho}. \tag{3.2.7}$$

Substituting (3.2.6) into (3.2.7) and rearranging, we get

$$v_B = \sqrt{\frac{2\,(p_A - p_B)}{\rho\,(1-\beta^4)}},$$

where $\beta = d_B/d_A$, provided $p_A \geq p_B$. If d_B/d_A is small, v_B can be approximated as

$$v_B = \sqrt{\frac{2}{\rho}\,(p_A - p_B)}.$$

So we see that the velocity at the orifice is proportional to the square root of the pressure difference between A and B. Taking account of the pressure losses due to frictional effects, we introduce a correction factor, called the *discharge coefficient*, denoted by μ. Thus,

$$v_B = \mu\sqrt{\frac{2}{\rho}\,(p_A - p_B)}$$

where $0 \leq \mu \leq 1$ and the volumetric flow rate is given by

$$\dot{V}_B = \frac{\pi d_B^2}{4}\mu\sqrt{\frac{2}{\rho}\,(p_A - p_B)}. \tag{3.2.8}$$

We can use the above idea to derive the expression for V_v, the volume of liquid flowing through the discharge valve. In reality, the flow is unlikely to be steady. However, as we solve the equations numerically, we can still assume the flow to be steady within each time interval so that Bernoulli's equation for steady flow can be applied. The compressibility is also very small and the frictional effect is negligible. Thus, we obtain an expression for dV_v which is

comparable to (3.2.8):

$$dV_v = f_v \mu \sqrt{\frac{2}{\rho}(p - p_{\text{out}})} dt, \tag{3.2.9}$$

where $f_v \simeq 2\pi r_o (d - r_v)$ is the cross-sectional area of the orifice for the valve and d is given by (3.1.1).

Substituting (3.2.4), (3.2.5) and (3.2.9) back into (3.2.3) and re-arranging, we get

$$\frac{dp}{dt} = \frac{1}{\beta_s V(t)} \left[\frac{\pi d_p^2}{4} v_p(t) - f_v(x) \mu \sqrt{\frac{2}{\rho}(p - p_{\text{out}})} \right], \tag{3.2.10}$$

where

$$V(t) = V_0 + \frac{\pi d_p^2}{4} x_0 \cos \omega t, \tag{3.2.11}$$

$$v_p(t) = -\omega x_0 \sin \omega t, \tag{3.2.12}$$

$$f_v(x) = 2\pi r_o \left(\sqrt{\left(\sqrt{r_v^2 - r_o^2} + x \right)^2 + r_o^2} - r_v \right). \tag{3.2.13}$$

Notice that while the valve is closed, the second term on the right-hand side of (3.2.10) is zero.

3.3 Numerical Simulation

From the previous section, we would like to solve the following system of equations numerically:

$$\frac{\mathrm{d}x}{\mathrm{d}t} = v, \tag{3.3.1}$$

$$\frac{dv}{dt} = \frac{\pi d_v^2}{4m_v}(p - p_{\text{out}}) - g\left(1 - \frac{m_f}{m_v}\right) - \frac{\gamma}{m_v}(v - v_f), \tag{3.3.2}$$

$$\frac{dp}{dt} = \frac{1}{\beta_s V(t)} \left[\frac{\pi d_p^2}{4} v_p(t) - f_v(x) \mu \sqrt{\frac{2}{\rho}(p - p_{\text{out}})} \right], \tag{3.3.3}$$

where $V(t)$, $v_p(t)$ and $f_v(x)$ are given in (3.2.11)-(3.2.13). By assuming the discharge valve is closed at the beginning, we also have the initial conditions:

$$x(0) = 0, \qquad v(0) = 0, \qquad p(0) = p_0, \tag{3.3.4}$$

where $p_0 < p_{\text{out}}$.

We also need more considerations about the position of x. While the valve is closed, $x = 0$. If the valve is accelerating downwards, then it stays at the zero position since it is stuck on the ring seat. If the valve hits the maximum position and it is accelerating upwards, it cannot go beyond $x_{\max}$ but bounces back from the boundary in the opposite direction.

With the above considerations, we will present below the algorithm to solve the system (3.3.1)-(3.3.3) with the initial conditions (3.3.4).

3.3.1 The Algorithm

Divide the time interval $[0, t_{\text{end}}]$ into N equal subintervals with the size Δt, i.e.,

$$t^{(i+1)} = t^{(i)} + \Delta t$$

where $i = 0, ..., N-1$. At $t = 0$, initial values are given for the pressure $p^{(0)} = p_0$, the position of the valve $x^{(0)} = 0$, and the velocity of the valve $v^{(0)} = 0$. For $t = t^{(0)}, ..., t^{(N-1)}$:

Step 1: Update x, v and p using a Euler's scheme, for example,

$$x^{(i+1)} = x^{(i)} + \Delta t\ v^{(i)}, \tag{3.3.5}$$

$$v^{(i+1)} = v^{(i)} + \Delta t \left[\frac{\pi d_v^2}{4m_v} \left(p^{(i)} - p_{\text{out}}\right) - g\left(1 - \frac{m_f}{m_v}\right) - \frac{\gamma}{m_v}(v^{(i)} - v_f) \right]. \tag{3.3.6}$$

$$p^{(i+1)} = p^{(i)} + \Delta t \frac{1}{\beta_s V(t^{(i)})} \left[\frac{\pi d_p^2}{4} v_p(t^{(i)}) - f_v(x^{(i)}) \mu \sqrt{\frac{2}{\rho}\left(p^{(i)} - p_{\text{out}}\right)} \right]. \tag{3.3.7}$$

Step 2: Re-calculate $x^{(i+1)}$ if it is out of range. We denote the terms in the square bracket in the right-hand side of (3.3.6) by $\dot{v}^{(i)}$ and re-calculate $x^{(i+1)}$ by the following conditions:

If $x^{(i+1)} < 0$:

Set $x^{(i+1)} = 0$, and if $\dot{v}^{(i)} < 0$, set $v^{(i+1)} = 0$.

If $x^{(i+1)} > x_{\max}$:

Find Δt_1 where $x^{(i)} + v^{(i)}\Delta t_1 = x_{\max}$. Next, set $v^{(i+1)} = -v^{(i)}$. Then $x^{(i+1)} = x_{\max} + v^{(i+1)}(\Delta t - \Delta t_1)$.

Step 3: Set $t^{(i+1)} = t^{(i)} + \Delta t$.

3.3.2 Parameters and Small Time Steps

The values of parameters and initial conditions are given in Table 3.1. The drag coefficient, discharge coefficient, and the fluid velocity at the valve are chosen to be fixed constants for simplicity.

The adiabatic compression coefficient of water at 20°C and 0.1MPa is $\beta_s = 4.5594 \times 10^{-10}$ ms^2/kg. This small number introduces difficulties for our numerical algorithm and small time steps are required to ensure stability.

3.4 Results

A program in Matlab is coded for our simulation. We give explanations for the numerical results, as well as examine the local behavior while the valve is opening. At the end, we show that as we increase the angular frequency ω of the crank, the natural maximum displacement of the valve also increases. As the natural maximum displacement exceeds the maximum displacement allowed, the ball valve hits the boundary. This explains potentially the clicking noise as the power of the plunger pump is increased.

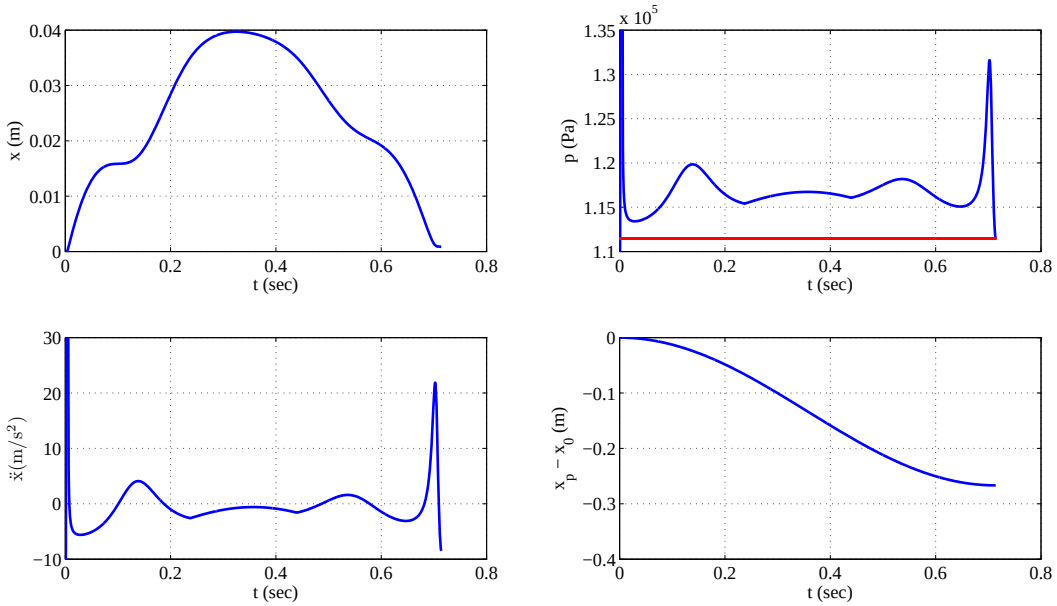

Figure 3.5: Solution of equations (3.3.1) to (3.3.3) with initial conditions (3.3.4), $\omega = \frac{7\pi}{5}$ rad/sec.

3.4.1 Pressure Peaks and Valve Opening

Figure 3.5 and 3.6 show a typical simulation for a complete downward stroke ($t_{\text{end}} = \pi$) with $\omega = 7\pi/5$ rad/sec (the maximum designed frequency of the pump). We can see in Figure 3.5, as the plunger is moving downwards, the valve is popped open, reaches a maximum displacement about 0.04 m and then comes back, as shown in the top left graph of x. Figure 3.6 shows the local behavior of the solution just after $t = 0$. The horizontal line in the pressure graph indicates the valve outlet pressure and the curve is the pressure inside the plunger cylinder. We can see that initially $p_0 < p_{\text{out}}$ and the valve is closed. As the plunger is pushing downwards, the pressure in the cylinder builds up and then pops the valve open as the acceleration of the valve changes from negative to positive.

There are two peaks in the pressure graph. The first pressure peak is at the beginning of the stroke and it is related to the opening of the valve as shown in Figure 3.6. The second peak is at the end of the downward stroke while the valve is trying to close.

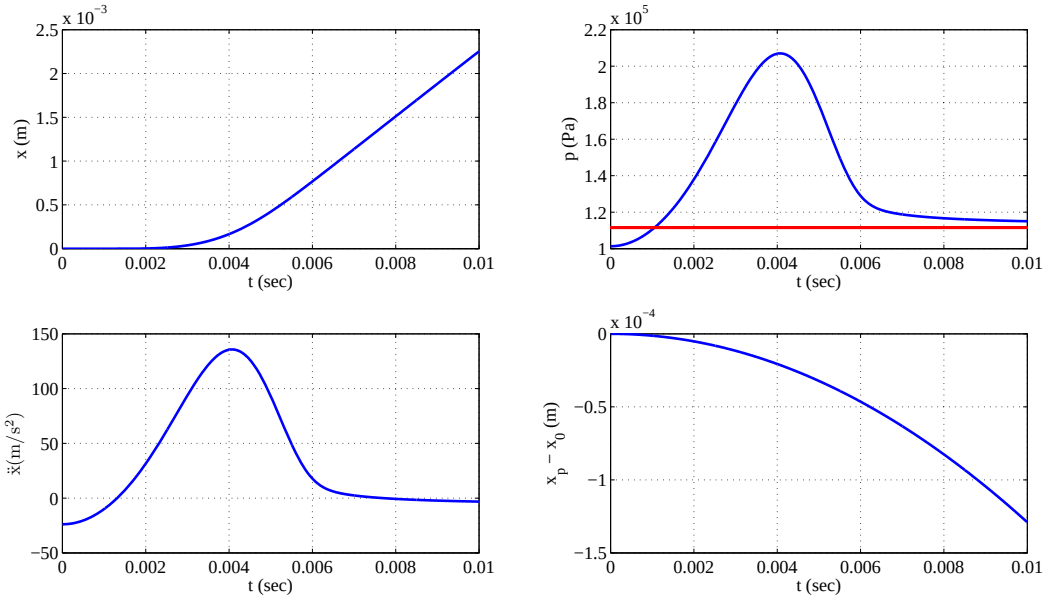

Figure 3.6: Local behavior of the solution just after $t = 0$, $\omega = \frac{7\pi}{5}$ rad/sec.

3.4.2 Variation of ω and Impact of the Valve

Numerical experiments show that the natural maximum displacement of the valve increases as the angular frequency of the crank ω increases. Figures 3.7 to 3.14 show the solutions for $\omega = 4\pi/5$, π, $6\pi/5$, and $8\pi/5$ rad/sec. We can see that the maximum value of x increases as ω increases. At $\omega = 8\pi/5$, the natural maximum displacement exceeds $x_{\max}$ and the valve hits the boundary and bounces back. This mechanism may explain the clicking noise when the pump is operated under higher resistance. By looking at the dominant effects in (3.3.1)-(3.3.3), we see that increasing ω and keeping γ constant is effectively the same as increasing γ and keeping ω constant. Thus, increasing the frequency of the pump gives a higher resistance in the system.

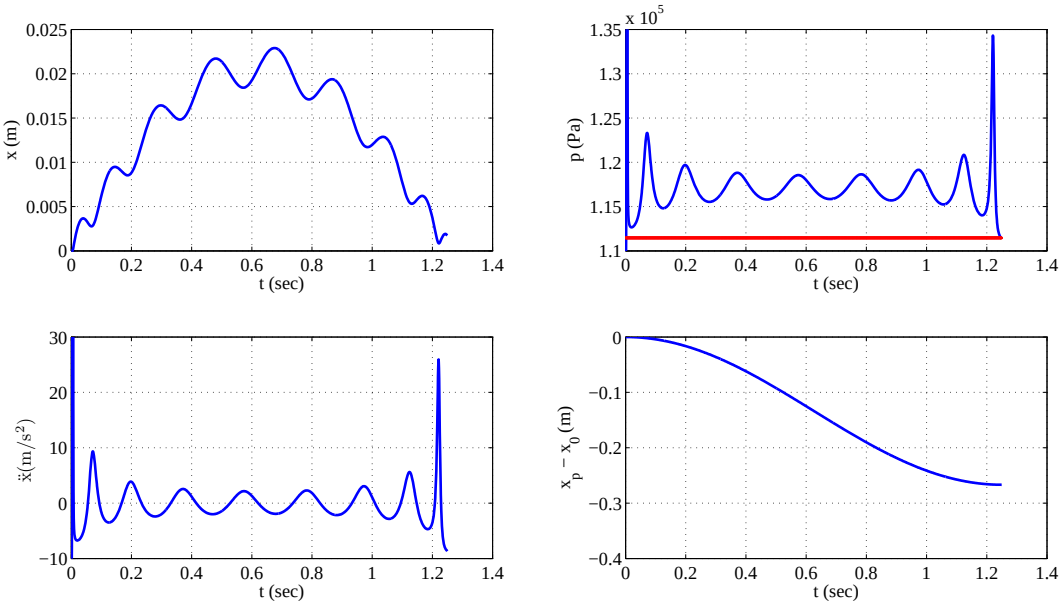

Figure 3.7: Solution of equations (3.3.1) to (3.3.3) with initial conditions (3.3.4), $\omega = \frac{4\pi}{5}$ rad/sec.

Description	Symbol	Value	Units
Average liquid volume in the plunger cylinder	V_0	0.0055	m^3
Maximum stroke length	x_0	0.1334	m
Diameter of the plunger cylinder	d_p	0.2000	m
Adiabatic compression coefficient	β_s	4.5594×10^{-10}	ms^2/kg
Radius of the pipes	r_o	0.0508	m
Radius of the valve	r_v	0.0631	m
Mass of the valve	m_v	8.2823	kg
Drag coefficient	γ	0.0100	kg/s
Discharge coefficient	μ	0.7000	dimensionless
Fluid velocity at the valve	v_f	0.2000	m/s
Maximum displacement of the valve	$x_{\max}$	0.0500	m
Pressure at the discharge valve outlet	p_{out}	1.1146×10^5	Pa
Initial pressure inside the plunger cylinder	p_0	1.0133×10^5	Pa
Initial valve position	x_0	0	m
Initial valve velocity	v_0	0	m/s

Table 3.1: Parameters and initial conditions for simulating the valve motion.

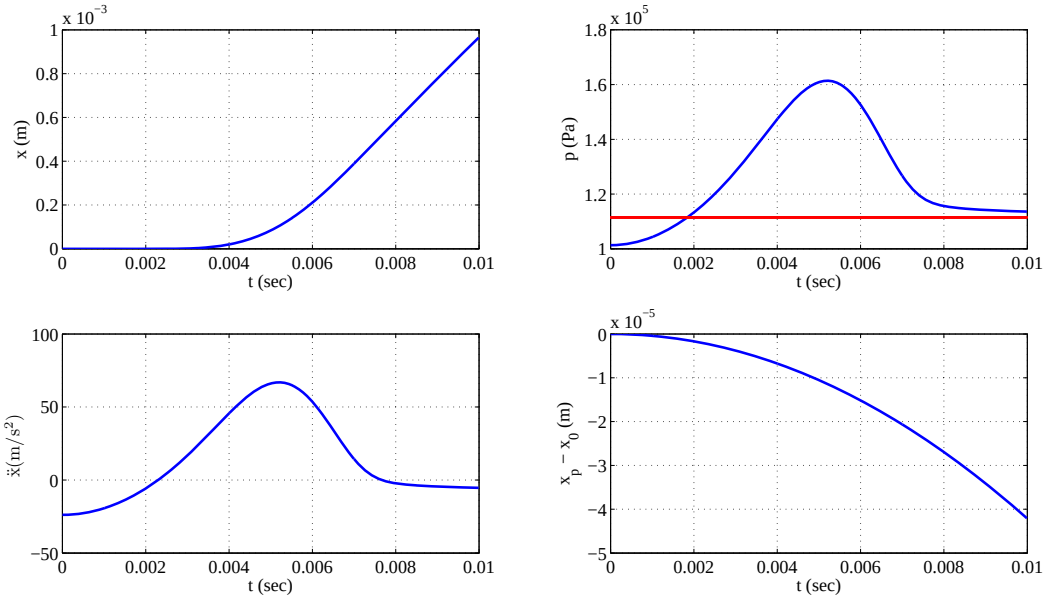

Figure 3.8: Local behavior of the solution just after $t = 0$, $\omega = \frac{4\pi}{5}$ rad/sec.

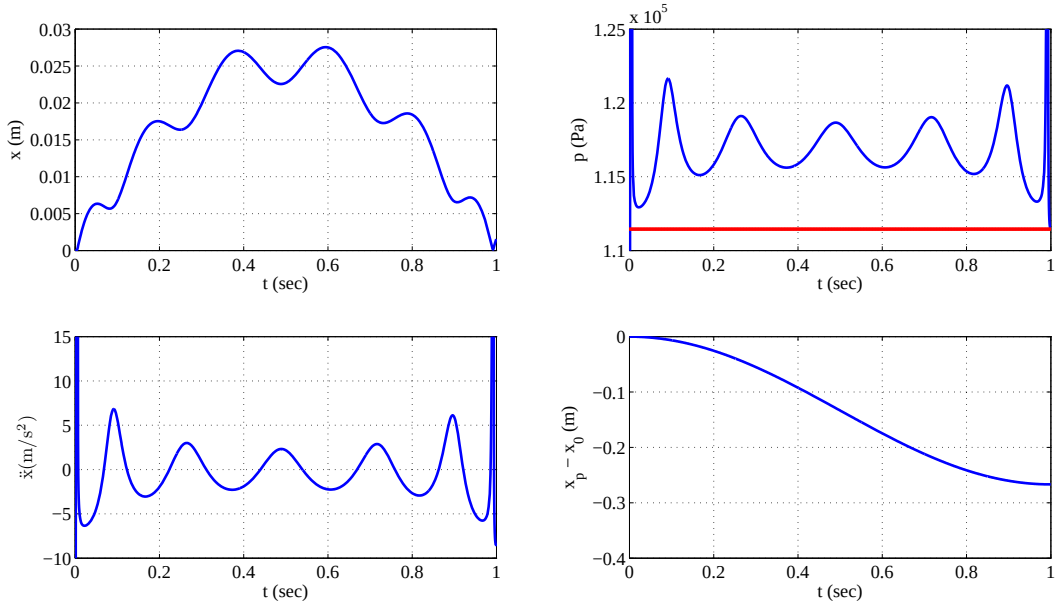

Figure 3.9: Solution of equations (3.3.1) to (3.3.3) with initial conditions (3.3.4), $\omega = \pi$ rad/sec.

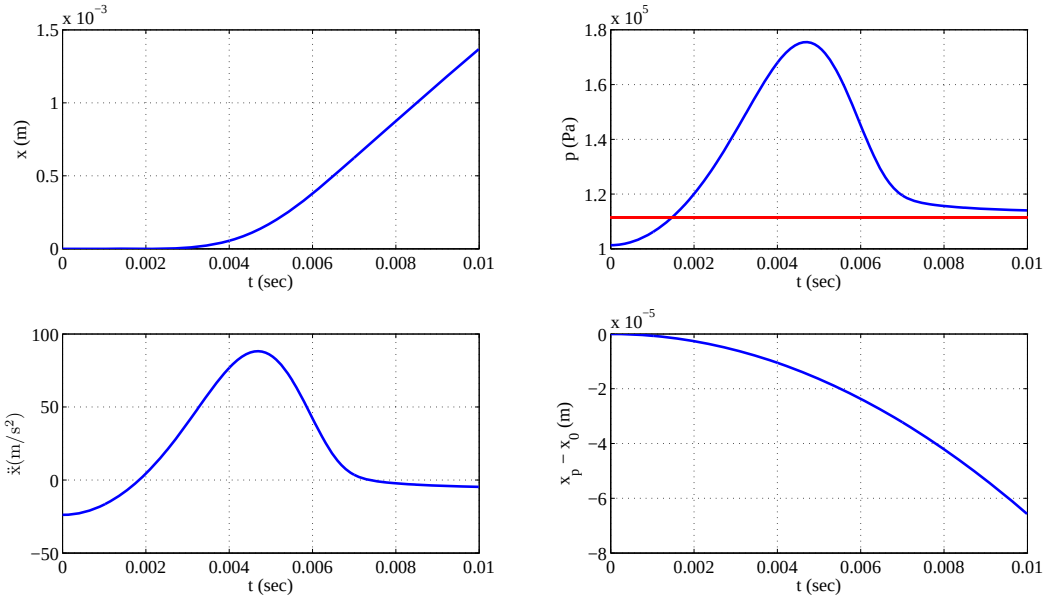

Figure 3.10: Local behavior of the solution just after $t = 0$, $\omega = \pi$ rad/sec.

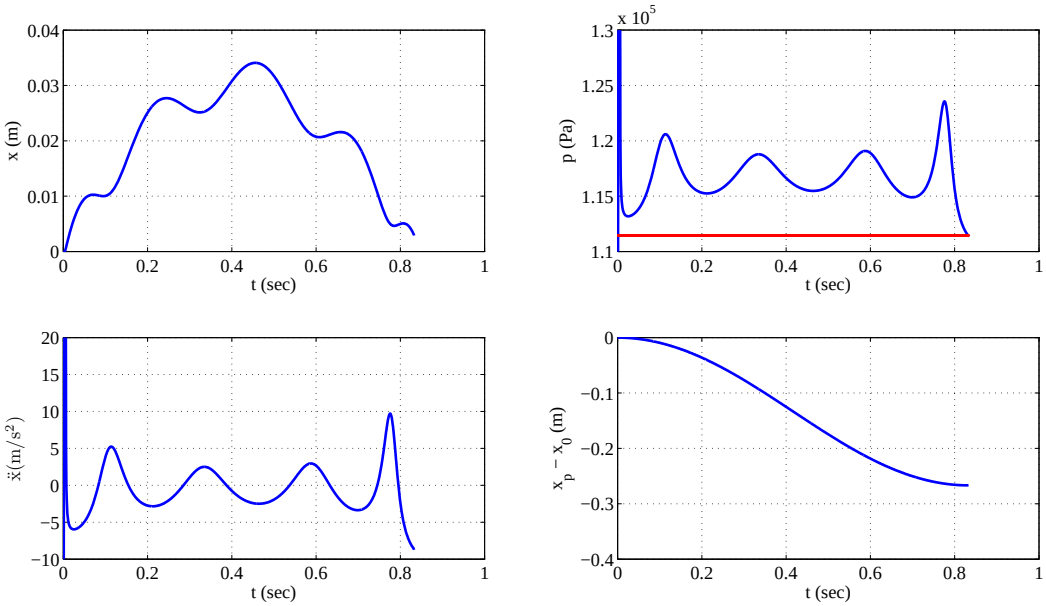

Figure 3.11: Solution of equations (3.3.1) to (3.3.3) with initial conditions (3.3.4), $\omega = \frac{6\pi}{5}$ rad/sec.

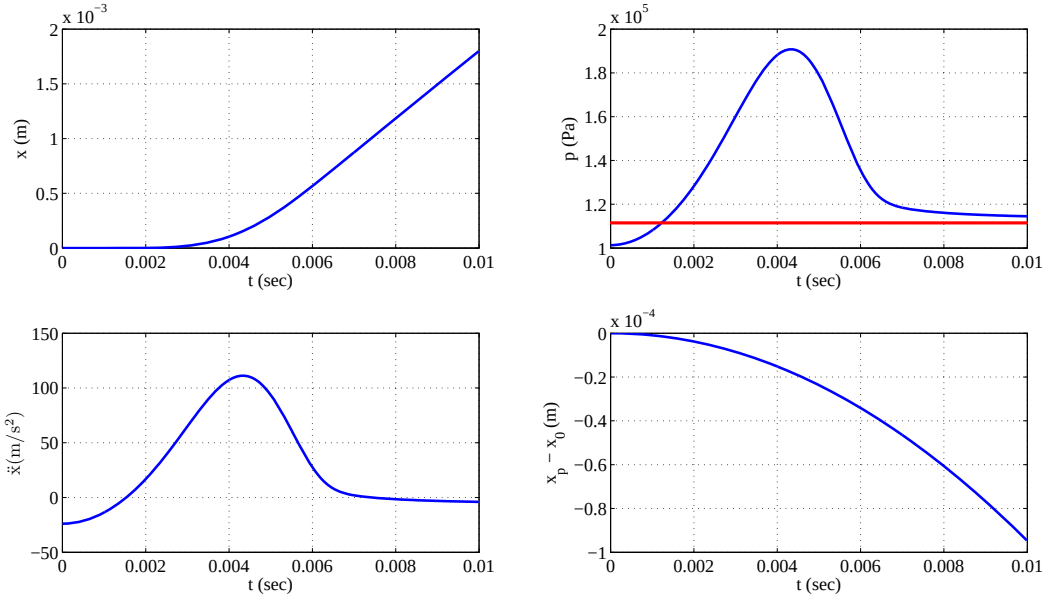

Figure 3.12: Local behavior of the solution just after $t = 0$, $\omega = \frac{6\pi}{5}$ rad/sec.

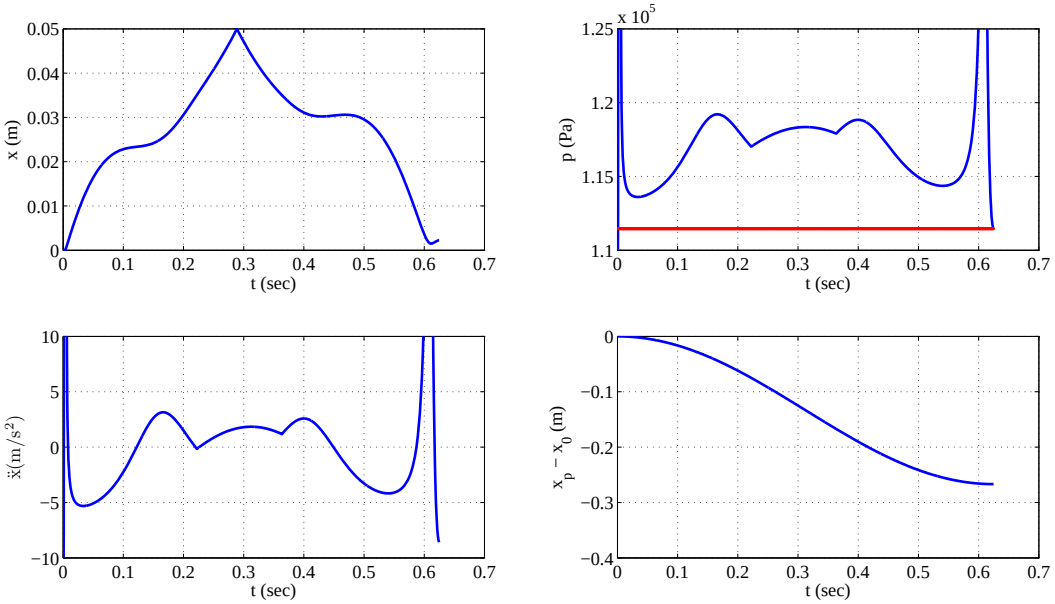

Figure 3.13: Solution of equations (3.3.1) to (3.3.3) with initial conditions (3.3.4), $\omega = \frac{8\pi}{5}$ rad/sec.

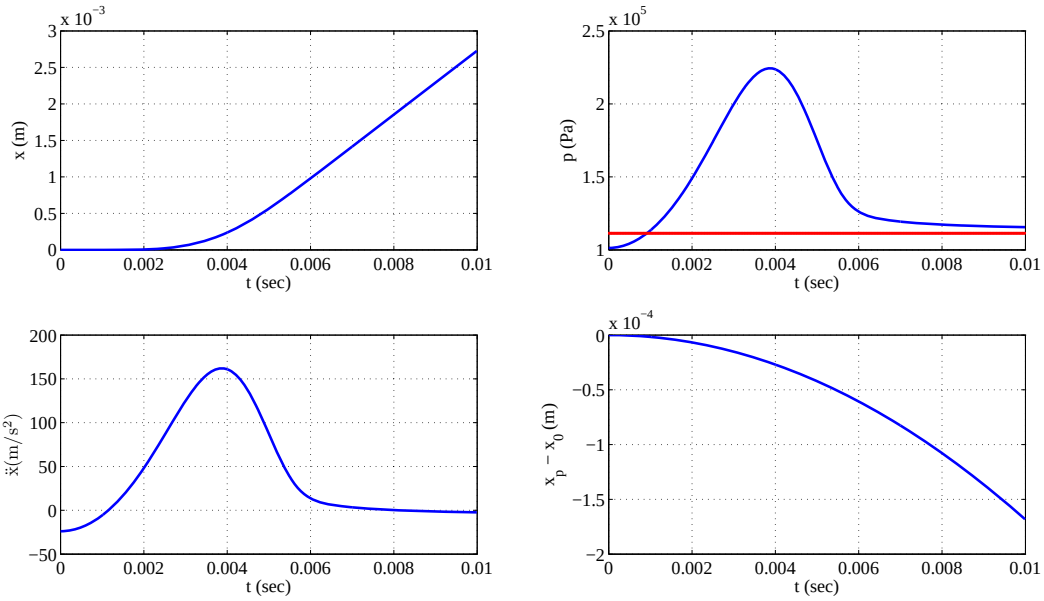

Figure 3.14: Local behavior of the solution just after $t = 0$, $\omega = \frac{8\pi}{5}$ rad/sec.

Chapter 4

Future Work and Conclusions

4.1 Future Work

In the future, we would like to study the valve dynamics in a higher resolution, especially by computer simulations. We can simulate the flow past the spherical valve in the valve region, shown in Figure 4.1. Navier-Stokes equations can be solved numerically for the fluid with appropriate boundary conditions to ensure the fluid-solid interactions.

In order to achieve the goal of simulating the moving valve with the fluid, we divide the work into two parts. First of all, we can study the flow across a fixed valve at various positions. This will provide us some indications about how the valve can be driven according to the flow. On the other hand, some novel numerical techniques can be used to simulate the moving valve together with the motion of the fluid. Immersed boundary method, for example, is suitable for such fluid-structure interaction problems.

4.1.1 Flow across a Fixed Valve at Various Positions

For studying the flow across a fixed valve, we divide the computational domain into the *fluid domain* and the *obstacle domain*. The Navier-Stokes equations are only solved in the fluid domain. The no-slip conditions are then applied

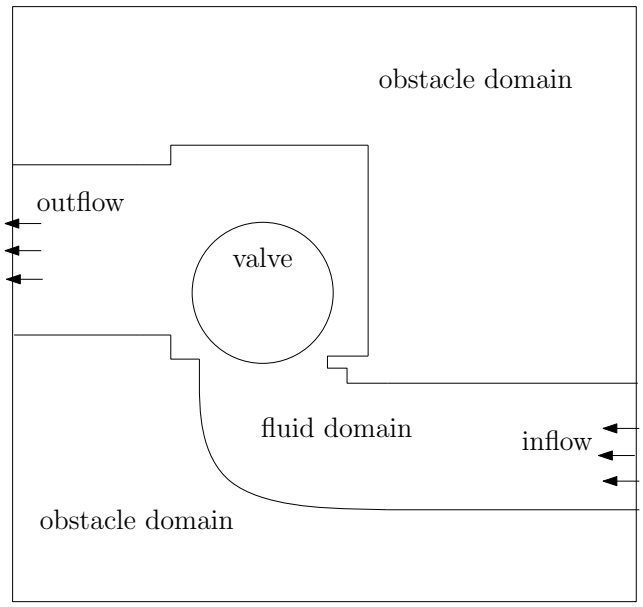

Figure 4.1: Geometry of the valve region for fluid simulation.

to the boundary of the obstacle. Details of the numerical treatment of the Navier-Stokes equations with complex geometries are presented in Appendix B.

Some example simulations are shown within a simple geometry. We assume a circular obstacle of radius 0.25 within a rectangular domain $[0, 8] \times [0, 1]$. The obstacle represents the valve and the rectangular domain a segment of the pipe with inflow at $x = 0$ and outflow at $x = 8$. The obstacle is located at $(0.5, 0.5)$ to be close to the inflow boundary. The boundary conditions are given by

$$\begin{aligned} u &= \frac{Re}{2} y(1-y), \qquad & v &= 0, \qquad & &\text{on the lines } x = 0 \text{ and } x = 8, \\ u &= 0, & v &= 0, & &\text{on the lines } y = 0 \text{ and } y = 1, \end{aligned}$$

and initial condition of $u = v = 0$ everywhere except at perhaps a boundary.

Figure 4.2 and Figure 4.3 show the velocity and pressure solution around the circular obstacle for $Re = 100$ at $t = 2.5$. The flow is divided into two streams at the obstacle and vortices can clearly be seen behind the circle. The flow is eventually settled down at some length after the obstacle. Higher

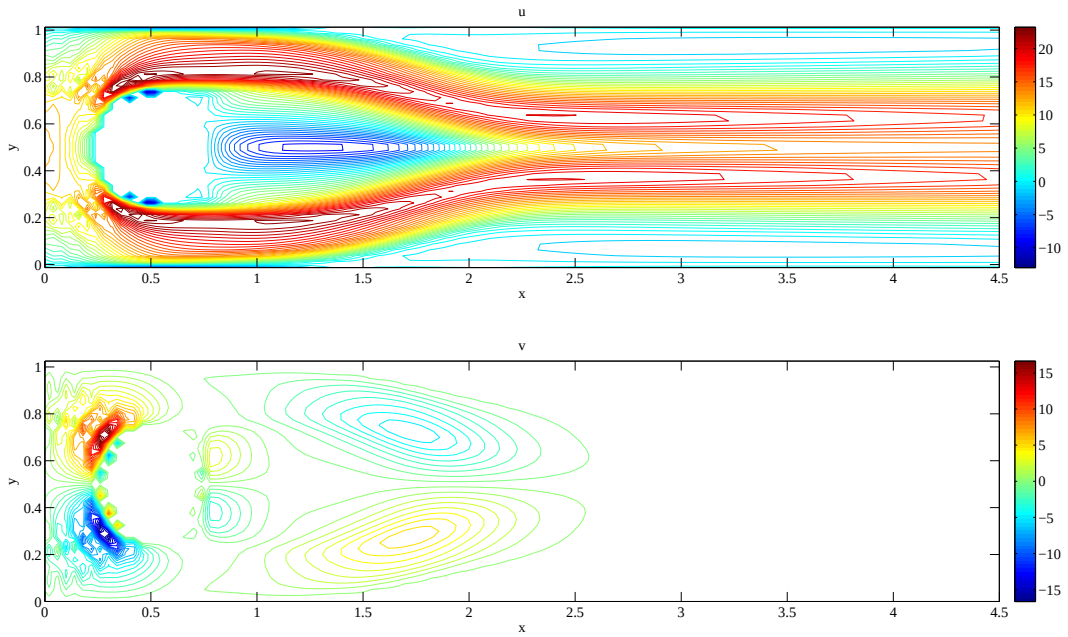

Figure 4.2: u and v-velocity around the obstacle for $Re = 100$ at $t = 2.5$ with obstacle centered at $(0.5, 0.5)$.

Reynolds number will create more disturbances downstream. In the real valve geometry, the symmetry observed in Figures 4.2 and 4.3 will break down sinc we will have a kinked pipe. We can simulate the flow patterns and obtain some hints of where the valve will hit. If the flow direction has suddenly changed, the ball valve may not be able to react as fast and be drifted to some non-preferred locations.

4.1.2 Towards the Moving Valve with the Immersed Boundary Method

The finite difference method that we described in Appendix B for simulating the flow around the solid will likely lead to loss of accuracy near the boundary, since the curved boundary is approximated onto the grid lines. Another conventional approach to simulate the flow past a curved solid boundary is to employ grids that conform to the body. However, body-fitted methods may require high computational cost, especially in the case of a moving body (Mit-

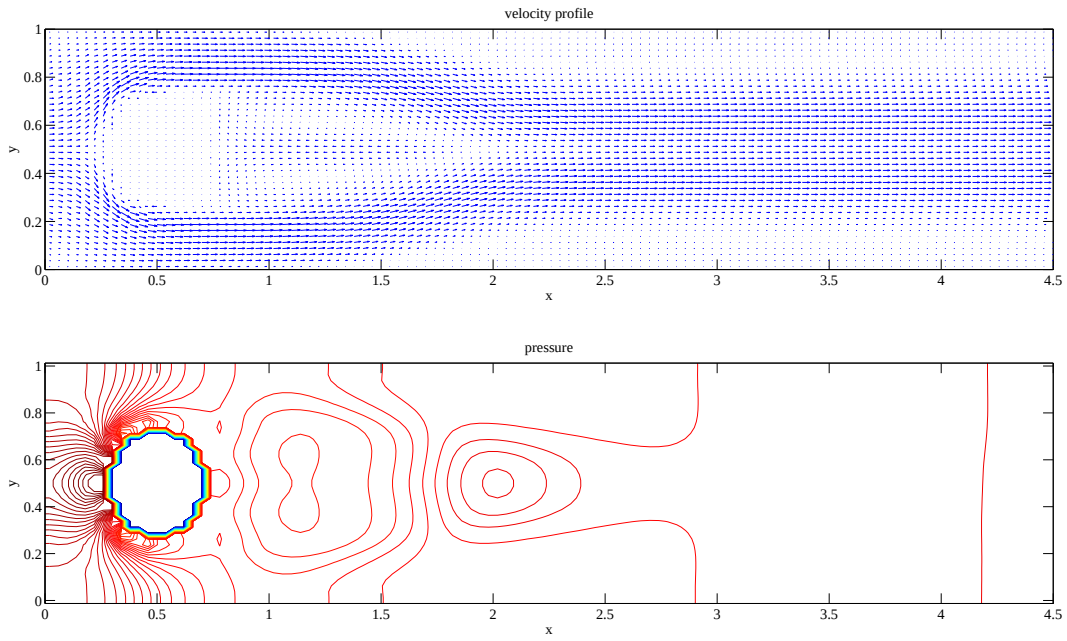

Figure 4.3: Velocity vector plot and pressure around the obstacle for $Re = 100$ at $t = 2.5$ with obstacle centered at $(0.5, 0.5)$.

tal and Iaccarino, 2005). Here we introduce the immersed boundary method, in order to handle simulations for a moving boundary with less computational cost.

For simplicity, consider a problem of viscous incompressible fluid in a two-dimensional square domain containing a massless immersed boundary in the form of a simple closed curve Γ, shown in Figure 4.4. The configuration of Γ is given in parametric form: $\vec{X}(s,t)$, where s is a variable that tracks a material point of the immersed boundary, and t is the variable of time. The equations

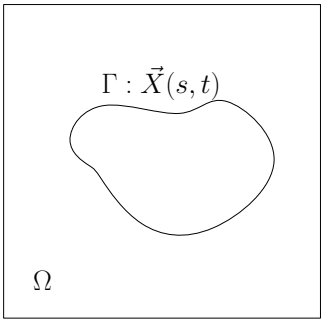

Figure 4.4: A two-dimensional square fluid domain Ω with a massless immersed boundary Γ.

of motion of the system are:

$$\rho\left(\frac{\partial \vec{v}}{\partial t} + \vec{v}\cdot\nabla\vec{v}\right) = -\nabla p + \mu\nabla^2\vec{v} + \rho\vec{g} + \vec{f}, \tag{4.1.1}$$

$$\nabla\cdot\vec{v} = 0, \tag{4.1.2}$$

$$\vec{f}(\vec{x},t) = \int_\Gamma \vec{F}(s,t)\delta(\vec{x} - \vec{X}(s,t))\,ds \tag{4.1.3}$$

$$\frac{\partial \vec{X}(s,t)}{\partial t} = \vec{v}(\vec{X}(s,t),t) = \int_\Omega \vec{v}(\vec{x},t)\delta(\vec{x} - \vec{X}(s,t))\,d\vec{x}, \tag{4.1.4}$$

$$\vec{F}(s,t) = \vec{S}(\vec{X}(\cdot,t),t). \tag{4.1.5}$$

Here $\vec{x} = (x,y)$, $\vec{v} = (u(\vec{x},t), v(\vec{x},t))$ is the fluid velocity, $p(\vec{x},t)$ is the fluid pressure, and $\vec{g}$ is the acceleration due to gravity. ρ and μ are constant fluid density and dynamic viscosity. $\vec{f}$ is the force density (with respect to $d\vec{x}$) acting on the fluid and $\vec{F}(s,t)$ is the boundary force density (with respect to ds).

Expressions (4.1.1) and (4.1.2) are the Navier-Stokes equations and the constraint for incompressibility whereas (4.1.3) and (4.1.4) describe the interaction between the immersed boundary and the fluid. In (4.1.3), the force density is applied to the fluid by the immersed boundary, while in (4.1.4), the immersed boundary is carried along with the fluid. Equation (4.1.5) states that the boundary force on the particular segment at time t is determined by the boundary configuration at time t. If the boundary is elastic, the function

$\vec{S}$ satisfies a generalized Hooke's law. Since the boundary force $\vec{F}(s,t)$ is integrated with a two-dimensional Dirac delta function over a one-dimensional curve Γ, the force density $\vec{f}(\vec{x},t)$ is a one-dimensional singular Dirac delta function.

For elastic boundaries, the forcing term (4.1.5) can be expressed explicitly. However, for flow over a rigid boundary, there are some difficulties since the boundary force $\vec{F}(s,t)$ is unknown. It must be applied to the fluid so that the boundary condition (e.g. the no-slip condition) is satisfied. The interactions between the fluid and the rigid body can be viewed as follows. When a fluid flows over a body it exerts a force on the surface. Conversely, the surface exerts a force of opposite sign on the fluid.

One straight forward method for the rigid boundaries is known as *feedback forcing*. The rigid body is still considered to be elastic but extremely stiff and the forcing term $\vec{F}$ is given as (Lai and Peskin, 2000)

$$\vec{F}(s,t) = \kappa(\vec{X}^e(s) - \vec{X}(s,t)), \tag{4.1.6}$$

where κ is a positive constant such that $\kappa \gg 1$. We can interpret (4.1.6) as if we connected the boundary points $\vec{X}$ to fixed equilibrium points $\vec{X}^e$ with a very stiff spring. The solid boundary is allowed to move a little. If the boundary points fall away from the desired places, the force on the spring will pull these boundary points back.

The major drawback of the feedback forcing approach is that large negative values of κ requires very small time steps to ensure stability and the flow simulations can be extremely expensive. Alternative forcing approaches, such as the *direct forcing* approach, have less limitations on the time steps (Mittal and Iaccarino, 2005). Another advantage of the direct forcing approach is that the calculation of the force field is viable when the interface is moving or deforming. The computation of the Lagrangian force field is directly from the momentum equation and all the Navier-Stoles terms are calculated over

the Lagrangian points. However, a complicated interpolation scheme must be employed (Lima E Silva et al., 2003).

Looking back to Figure 4.1, we are aiming to simulate the moving valve in a complex geometry. We can use the strategy described in Appendix B to deal with the curved boundaries of the pipe and the kinked domain. The valve inside the fluid domain can be treated with the immersed boundary method described above. As discussed above, the Navier-Stokes equations can be solved together with a singular force on the boundary to describe the fluid-solid interactions. The direct forcing approach, for example, can be used to calculate the forcing term for the solid valve. The motion of the valve is not known a prior, however, can be studied from the overall forces acting on the valve at each time step. This could lead us to the simulation of a moving valve driven by the fluid.

4.2 Conclusions

The one-dimensional flow model was designed and studied to understand the plunger pump operation in general. The valve motion was then modeled by taking care of the geometry of the valve. It has been found that the valve motion is related to the plunger speed and as the plunger speed is increased, the valve hits the boundary more violently. This observation is consistent with the clicking noise observed at high speed operation of the pump. For understanding the flow around the valve in higher resolution, we studied the numerical method for solving the Navier-Stokes equations. By introducing the immersed boundary method, a methodology of simulating solid-fluid interactions is presented.

The one-dimensional model calculates the flow velocities and pressures at the air tanks, the valves, and underneath the plunger. Since the model was designed with a closed loop, the natural frequencies of the solution are found to be dependent on the length of the outer circular pipe. Another important

observation is the pressure jumps at opening and closing the valves. The first model does not take into account the valve motion.

To understand the valve motion and the pressure jumps at opening and closing the valve, the geometry of the valve is considered in detail. Simulation results show that as the frequency of the rotating crank is increased, the natural displacement of the valve also increases. Since increasing frequency of the pump is effectively the same as increasing the resistance of the system, this means that as we increase the resistance, the valve is likely to hit the boundary and causing some noise, as observed by the manufacturers.

In the future, we would like to study the valve motion in a higher resolution. Flow patterns around a circular obstacle has been shown in a rectangular geometry. By extending this methodology to a complex geometry, we can simulate the flow across a fixed valve at various positions. This will allow us to predict how the valve can be driven with the fluid. Next, the immersed boundary method is introduced to provide a methodology for simulating the moving valve. The rigid boundary poses some difficulties at computing the forcing term at the boundary, however, forcing approaches such as the direct forcing method can be employed. At the end, we provide a plan for future simulation of the moving valve.

Appendix A

Derivation of the Navier-Stokes Equations

Since this thesis is based on the theory of fluid dynamics, we shall provide some background in this Appendix. We start from the continuity equation and deduce that the velocity field for incompressible flows is divergence free. Euler's equation then provides a tool for modelling inviscid flow which helps the development of the first one-dimensional model. Bernoulli's equation is used in Chapter 3. By extending to viscous fluids, we provide the constitutive equation (stress-strain rate relation) and hence derive the Navier-Stokes equations for an incompressible viscous fluid.

A.1 The Equation of Continuity

Fluid dynamics is the study of the motion of fluids (liquids and gasses). The phenomena considered in fluid dynamics are macroscopic, so a fluid is regarded as a *continuum*. This means that any small volume element in the fluid is always supposed so large that it contains a great number of molecules. The physical quantities associated with the fluid within a given small volume will be regarded as being spread uniformly over that volume (Batchelor, 1970).

The mathematical description of the state of a moving fluid is determined

by the fluid velocity $\vec{v}$, the pressure p and the density ρ. If we are in a three-dimensional cartesian coordinate system, these quantities are functions of the coordinates x, y, z and of the time t.

Let us derive some fundamental equations of fluid dynamics (Landau and Lifshitz, 1987). We begin with the equation which expresses the conservation of matter. Consider some volume V_0 of space. The mass of fluid in this volume is $\int \rho \, dV$, where the integral is taken over V_0 and ρ is the fluid density. The mass of fluid flowing in unit time through an area ds of the surface bounding this volume is $\rho(\vec{v} \cdot \hat{n})ds$, where $\hat{n}$ is the unit normal pointing outward from the volume (we put a hat on n instead of an arrow just to indicate it is a unit vector). Then $\rho(\vec{v} \cdot \hat{n})ds$ is positive if the fluid is flowing out of the volume, and negative if the flow is into the volume. The total mass of fluid flowing out of the volume V_0 in unit time is therefore

$$\oint_{\partial V_0} \rho \vec{v} \cdot \hat{n} \, ds$$

where the integration is taken over the whole of the closed surface ∂V_0 surrounding the volume V_0. On the other hand, the decrease per unit time in the mass of fluid in the volume V_0 is

$$-\frac{\partial}{\partial t} \int_{V_0} \rho \, dV.$$

Equating the above two expressions,

$$\frac{\partial}{\partial t} \int_{V_0} \rho \, dV = - \oint_{\partial V_0} \rho \vec{v} \cdot \hat{n} \, ds = - \int_{V_0} \nabla \cdot (\rho \vec{v}) \, dV \qquad \text{(A.1.1)}$$

by applying Green's theorem. Thus,

$$\int \left[\frac{\partial \rho}{\partial t} + \nabla \cdot (\rho \vec{v}) \right] dV = 0.$$

Since the above equation must hold for any volume, then provided the inte-

grand is sufficiently regular, the integrand must vanish, i.e.,

$$\frac{\partial \rho}{\partial t} + \nabla \cdot (\rho \vec{v}) = 0. \tag{A.1.2}$$

This is known as the *equation of continuity*.

A.1.1 Divergence Free for Incompressible Flow

Incompressible flow means that the density within an infinitesimal volume that moves with the velocity of the fluid is constant. We shall show that the continuity equation is equivalent to the divergence free of the velocity field. Since the vector identity

$$\nabla \cdot (\rho \vec{v}) = \rho \nabla \cdot \vec{v} + \vec{v} \cdot \nabla \rho,$$

the continuity equation (A.1.2) becomes

$$\frac{\partial \rho}{\partial t} + \rho \nabla \cdot \vec{v} + \vec{v} \cdot \nabla \rho = 0. \tag{A.1.3}$$

For incompressible flow,

$$\frac{d}{dt} \rho(x(t), y(t), z(t), t) = \frac{\partial \rho}{\partial t} + \vec{v} \cdot \nabla \rho = 0.$$

Therefore, the divergence of the fluid velocity must vanish for incompressible flow:

$$\nabla \cdot \vec{v} = 0. \tag{A.1.4}$$

A.2 Euler's Equation

Consider some volume V_0 in the fluid. The total force acting on this volume is

$$-\oint_{\partial V_0} p\hat{n}\, ds$$

where p is the fluid pressure and the integral is taken over the surface bounding the volume. Transforming it to a volume integral,

$$-\oint_{\partial V_0} p\hat{n}\, ds = -\int_{V_0} \nabla p\, dV.$$

Thus the fluid surrounding any volume element dV exerts on that element a force $-dV\nabla p$, i.e., a force $-\nabla p$ acts on unit volume of the fluid. The equation of motion of a volume element in the fluid neglecting any external forces can be written by equating the force $-\nabla p$ to the product of the mass per unit volume ρ and the acceleration $d\vec{v}/dt$:

$$\rho\frac{d\vec{v}}{dt} = -\nabla p. \tag{A.2.1}$$

$d\vec{v}/dt$ denotes the rate of change of the velocity of a given fluid particle as it moves in space. We notice that the change $d\vec{v}$ of the given fluid particle during the time dt consists of two parts (Landau and Lifshitz, 1987). The first part is the change during dt in the velocity at a point fixed in space, namely $(\partial\vec{v}/\partial t)\, dt$. The second part is the difference between the velocities at the same instance at two points $d\vec{r}$ apart, namely $d\vec{r}\cdot\nabla\vec{v}$, where $d\vec{r}$ is the distance moved by the given fluid particle during the time dt. Thus,

$$d\vec{v} = \left(\frac{\partial\vec{v}}{\partial t}\right) dt + d\vec{r}\cdot\nabla\vec{v}.$$

Dividing both sides by dt,

$$\frac{d\vec{v}}{dt} = \frac{\partial\vec{v}}{\partial t} + \vec{v}\cdot\nabla\vec{v}.$$

Substituting this in (A.2.1), we get

$$\frac{\partial \vec{v}}{\partial t} + \vec{v} \cdot \nabla \vec{v} = -\frac{1}{\rho} \nabla p. \tag{A.2.2}$$

This is the *Euler's equation* and is one of the fundamental equations of fluid dynamics.

If the fluid is in a gravitational field, an additional force $\rho \vec{g}$ acts on any unit volume, where $\vec{g}$ is the acceleration due to gravity. Thus (A.2.2) becomes

$$\frac{\partial \vec{v}}{\partial t} + \vec{v} \cdot \nabla \vec{v} = -\frac{1}{\rho} \nabla p + \vec{g}. \tag{A.2.3}$$

Note that in the above derivations, we have not taken into account of internal friction (viscosity) in the fluid. The motions of fluids in which viscosity are unimportant are said to be *ideal*. The one-dimensional model in Chapter 2 is derived based on the assumption of an ideal fluid.

A.3 Bernoulli's Equation

In the case of steady flow, the equations of fluid dynamics are greatly simplified. *Steady flow* means that the velocity is constant in time at any point in the fluid. So $\vec{v}$ is a function of spatial coordinates only and $\partial \vec{v}/\partial t = 0$. Thus (A.2.2) becomes

$$\vec{v} \cdot \nabla \vec{v} = -\frac{1}{\rho} \nabla p.$$

By using the vector identity

$$\frac{1}{2} \nabla \vec{v}^2 = \vec{v} \times (\nabla \times \vec{v}) + \vec{v} \cdot \nabla \vec{v},$$

we have

$$\frac{1}{2} \nabla \vec{v}^2 - \vec{v} \times (\nabla \times \vec{v}) = -\frac{1}{\rho} \nabla p. \tag{A.3.1}$$

Let us now introduce the concept of *streamlines*. Streamlines are lines such that the tangent to a streamline at any point gives the direction of the velocity at that point. In steady flow the streamlines do not vary with time and coincide with the paths of the fluid particles. We take the scalar product of (A.3.1) with the unit vector tangent to the streamline at each point (Landau and Lifshitz, 1987). We denote this unit vector by $\hat{l}$, so

$$\frac{1}{2}\nabla\vec{v}^2 \cdot \hat{l} - \vec{v} \times (\nabla \times \vec{v}) \cdot \hat{l} = -\frac{1}{\rho}\nabla p \cdot \hat{l}.$$

Since the vector $\vec{v} \times (\nabla \times \vec{v})$ is perpendicular to $\vec{v}$, the second term on the left-hand side is zero and thus, denoting the directional derivative in the direction of $\hat{l}$ as $\partial/\partial\hat{l}$,

$$\frac{\partial}{\partial\hat{l}}\left(\frac{1}{2}\vec{v}^2\right) + \frac{1}{\rho}\frac{\partial p}{\partial\hat{l}} = 0.$$

Since the flow is incompressible, ρ is constant, and

$$\frac{\partial}{\partial\hat{l}}\left(\frac{1}{2}\vec{v}^2 + \frac{p}{\rho}\right) = 0.$$

Therefore,

$$\frac{1}{2}\vec{v}^2 + \frac{p}{\rho} = \text{constant} \tag{A.3.2}$$

along a streamline. Equation (A.3.2) is the *Bernoulli's Equation*. In general the constant takes different values for different streamlines.

A.4 The Constitutive Equation

In any viscous flow, fluid layers move at different velocities and internal frictions arise from the shear stresses between the layers. As the need of studying viscous flow, we shall first derive the constitutive equation, which is a relationship between the stress tensor and the rate-of-strain tensor. The constitutive relation is then used to derive the Navier-Stokes equations in the next Section.

Before digging into the technical details, let us first clarify some notations for tensor calculus.

A.4.1 Notations (Heinbockel, 1996)

Index Notation

We can write vectors $\vec{A} = (A_1, A_2, A_3)$, for example, in the index notation. The quantities

$$A_i,\ i = 1, 2, 3$$

represents the components of the vector $\vec{A}$. The symbol A_i refers to all of the components of the vector $\vec{A}$ simultaneously.

The Kronecker Delta

The *Kronecker delta* δ_{ij} is defined as

$$\delta_{ij} = \begin{cases} 1, \text{ if } i = j, \\ 0, \text{ if } i \neq j. \end{cases} \tag{A.4.1}$$

With i, j ranging over the values $1, 2, 3$, it represents 9 quantities. It is a second rank identity tensor, as we shall use later.

The Levi-Civita Symbol

In three-dimensions, the *Levi-Civita* or *permutation* symbol ϵ_{ijk} is defined as

$$\epsilon_{ijk} = \begin{cases} 1, & \text{if } (i, j, k) \text{ is an even permutation of the integers } (1, 2, 3), \\ -1, & \text{if } (i, j, k) \text{ is an odd permutation of the integers } (1, 2, 3), \\ 0, & \text{otherwise.} \end{cases} \tag{A.4.2}$$

A permutation of $(1, 2, 3)$ is called even or odd depending on whether there is an even or odd number of transpositions of the digits.

The Summation Convention

The summation convention states that whenever there arises an expression where there is an index which occurs twice on the same side of any equation, it represents summation on these repeated indices. For example,

$$y_k = a_{ki}x_i, \ i,k = 1,2$$

represents the linear equations

$$y_1 = a_{11}x_1 + a_{12}x_2,$$
$$y_2 = a_{21}x_1 + a_{22}x_2.$$

With the notations above, we now continue our journey towards the constitutive equation.

A.4.2 The Stress Tensor

It is possible to distinguish two kinds of forces which act on a fluid (Batchelor, 1970). The first kind of forces are called *volume forces* or *body forces*. Such forces are capable of penetrating into the interior of the fluid, and act on all elements of the fluid. Gravity is an example. The second kind of forces, which only act on a thin layer adjacent to the boundary of the fluid element, are called *surface forces*.

We define *stress* as the surface force per unit area, denoted by $\boldsymbol{\sigma}$. We shall determine the dependence of $\boldsymbol{\sigma}$ on the direction of the normal to the surface element across which it acts. This will lead to the definition of stress tensor.

Let us consider a fluid element in the shape of a tetrahedron with volume ΔV, shown in Figure A.1 (Batchelor, 1970; Heinbockel, 1996). The three orthogonal faces have areas ΔA_x, ΔA_y, ΔA_z, and unit outward normals $-\hat{x}$, $-\hat{y}$, $-\hat{z}$. The inclined surface has area ΔA and unit outward normal $\hat{n}$. Surface

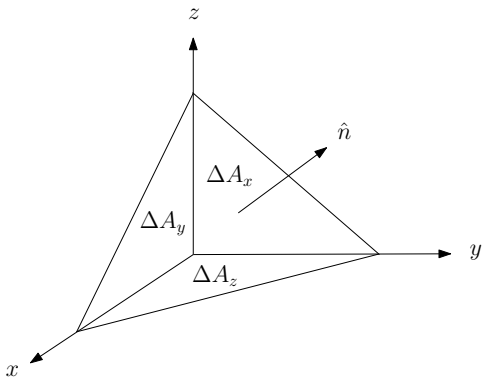

Figure A.1: A tetrahedral fluid element.

forces act on the fluid in the tetrahedron across each of the four faces and their sum is:

$$\boldsymbol{\sigma}_n \Delta A + \boldsymbol{\sigma}_{-x} \Delta A_x + \boldsymbol{\sigma}_{-y} \Delta A_y + \boldsymbol{\sigma}_{-z} \Delta A_z,$$

where the subscript of $\boldsymbol{\sigma}$ denotes the unit outward normal of the surface which the stress acts on. From the orthogonality of three of the faces, we have

$$\begin{aligned} \Delta A_x &= (\hat{n} \cdot \hat{x}) \Delta A = n_x \Delta A, \\ \Delta A_y &= (\hat{n} \cdot \hat{y}) \Delta A = n_y \Delta A, \\ \Delta A_z &= (\hat{n} \cdot \hat{z}) \Delta A = n_z \Delta A, \end{aligned}$$

where the subscript of n denotes the coordinate component of the vector $\hat{n}$. We also have from Newton's third law,

$$\boldsymbol{\sigma}_{-x} = -\boldsymbol{\sigma}_x,$$

and similarly for other stresses. Thus, the sum of the surface forces can be written as

$$\left[\boldsymbol{\sigma}_n - (n_x \boldsymbol{\sigma}_x + n_y \boldsymbol{\sigma}_y + n_z \boldsymbol{\sigma}_z)\right] \Delta A, \tag{A.4.3}$$

which is proportional to ΔA.

The total body force on the fluid within the tetrahedron is proportional to the volume ΔV. The mass of the fluid in the tetrahedron is also of order ΔV, provided the local density is finite. So the product of the mass and acceleration of the fluid is of order ΔV, provided the local acceleration is finite. Thus if the linear dimensions of the tetrahedron are approaching zero without change of its shape, the last term of the equation

$$\text{mass} \times \text{acceleration} \;=\; \text{total body forces} \;+\; \text{total surfaces forces}$$

approaches zero only as ΔA, whereas the first two terms approaches zero as ΔV, which is of smaller order than ΔA. The equation can only be satisfied if the coefficient of ΔA in (A.4.3) vanishes identically. Thus,

$$\boldsymbol{\sigma}_n = n_x \boldsymbol{\sigma}_x + n_y \boldsymbol{\sigma}_y + n_z \boldsymbol{\sigma}_z.$$

Writing the above equation in component form,

$$\begin{aligned} \sigma_{nx} &= n_x \sigma_{xx} + n_y \sigma_{yx} + n_z \sigma_{zx}, \\ \sigma_{ny} &= n_x \sigma_{xy} + n_y \sigma_{yy} + n_z \sigma_{zy}, \\ \sigma_{nz} &= n_x \sigma_{xz} + n_y \sigma_{yz} + n_z \sigma_{zz}. \end{aligned} \tag{A.4.4}$$

Instead of using x, y, z as subscripts, we can use digits 1, 2, 3 and the system (A.4.4) can be written as

$$\sigma_{nj} = n_i \sigma_{ij}, \;\; i, j = 1, 2, 3. \tag{A.4.5}$$

Equation (A.4.5) is known as the *Cauchy stress law* and σ_{ij} is the *stress tensor* and it can be shown that it is symmetric. σ_{ij} denotes the stress in the j-component of the force per unit area exerted across a plane surface element normal to the i-direction, shown in Figure A.2. The diagonal components σ_{ii} (no sum) are called the *normal stresses* and the other components are called

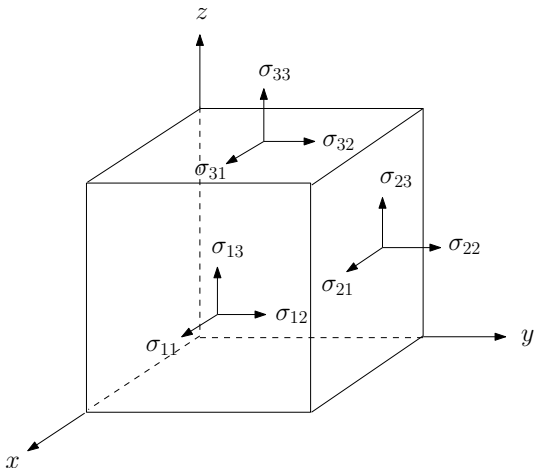

Figure A.2: The stress tensor.

the *tangential stresses*.

A.4.3 The Rate-of-Strain Tensor

In the theory of elasticity, strain represents the deformation of a material. In one-dimension, *strain* is defined as the change in length divided by the original length. When a force is applied to a solid, strains arise. If the deformation is small, stresses and strains are related by Hooke's law. However in the theory of fluid dynamics, the force exerted by one portion of fluid on a neighboring portion is related with the rate of deformation of the fluid. Thus, we will consider rate-of-strain instead of strain.

To introduce the rate-of-strain tensor, let us consider the differences of velocities in space (Zhou et al., 2000). Let the velocity of a fluid at position $\vec{x}$ and time t be $\vec{v}(\vec{x}, t)$, and a simultaneous velocity at a neighboring position $\vec{x} + \delta\vec{x}$ be $\vec{v}(\vec{x} + \delta\vec{x}) + \delta\vec{v}$, where $\delta\vec{x}$ is small. For rectangular coordinates,

$$\delta v_i = \delta x_j \frac{\partial v_i}{\partial x_j}.$$

To see the geometrical character of the relative velocity $\delta\vec{v}$, we split $\partial v_i/\partial x_j$ (a

second-rank tensor) into parts which are symmetric and anti-symmetric, i.e.,

$$\frac{\partial v_i}{\partial x_j} = e_{ij} + \xi_{ij}, \tag{A.4.6}$$

where

$$e_{ij} = \frac{1}{2}\left(\frac{\partial v_i}{\partial x_j} + \frac{\partial v_j}{\partial x_i}\right), \tag{A.4.7}$$

$$\xi_{ij} = \frac{1}{2}\left(\frac{\partial v_i}{\partial x_j} - \frac{\partial v_j}{\partial x_i}\right). \tag{A.4.8}$$

Then, we can write

$$\delta v_i = \delta v_i^{(s)} + \delta v_i^{(a)},$$

where

$$\delta v_i^{(s)} = \delta x_j e_{ij}, \qquad\qquad \delta v_i^{(a)} = \delta x_j \xi_{ij}.$$

The contribution $\delta v_i^{(s)}$ represents a pure straining motion. e_{ij} is a symmetric second rank tensor, known as the *rate-of-strain tensor*. Explicitly, if we let $\vec{v} = (u, v, w)$, then

$$e_{ij} = \begin{pmatrix} \dfrac{\partial u}{\partial x} & \dfrac{1}{2}\left(\dfrac{\partial u}{\partial y} + \dfrac{\partial v}{\partial x}\right) & \dfrac{1}{2}\left(\dfrac{\partial u}{\partial z} + \dfrac{\partial w}{\partial x}\right) \\ \dfrac{1}{2}\left(\dfrac{\partial v}{\partial x} + \dfrac{\partial u}{\partial y}\right) & \dfrac{\partial v}{\partial y} & \dfrac{1}{2}\left(\dfrac{\partial v}{\partial z} + \dfrac{\partial w}{\partial y}\right) \\ \dfrac{1}{2}\left(\dfrac{\partial w}{\partial x} + \dfrac{\partial u}{\partial z}\right) & \dfrac{1}{2}\left(\dfrac{\partial w}{\partial y} + \dfrac{\partial v}{\partial z}\right) & \dfrac{\partial w}{\partial z} \end{pmatrix}. \tag{A.4.9}$$

The diagonal components represent the rate of dilation in each direction and the off-diagonal components represent the rate of angle changes due to the deformation. To understand better the components of the rate-of-strain tensor, let us consider a two-dimensional (three-dimensional analysis is similar) rectangular element of fluid with dimensions Δx and Δy. Figure A.3 shows the velocities of the fluid at each point A, B, C and D.

First, we assume that the only non-zero component of the tensor is $\partial u/\partial x$.

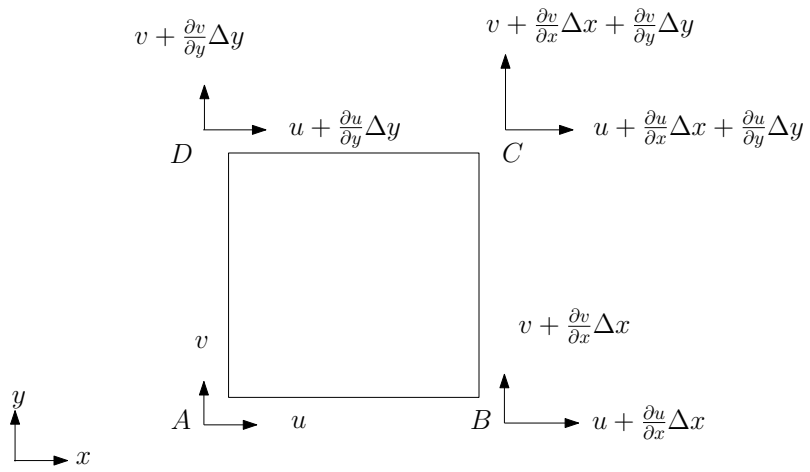

Figure A.3: An infinitesimal square element of fluid in 2D.

After some time Δt, $ABCD$ will become $A'B'C'D'$, shown in Figure A.4. The segment AB is stretched in the x-direction and its rate of strain per unit length is

$$\frac{\left(u + \dfrac{\partial u}{\partial x}\Delta x\right)\Delta t - u\Delta t}{\Delta x \Delta t} = \frac{\partial u}{\partial x} = e_{11}.$$

Similar arguments can be carried out for all the diagonal components of the tensor. Thus e_{ii} (no sum) represent the rates of dilation per unit length in the i-directions.

It is interesting to relate the volumetric change of a fluid element with the divergence of its velocity field. We extend the two-dimensional fluid element $ABCD$ to a cubic by adding a third dimension Δz and the velocity at A becomes $\vec{v} = (u, v, w)$. Then the rate of change of volume of the cubic element is

$$\frac{\left(\Delta x + \dfrac{\partial u}{\partial x}\Delta x \Delta t\right)\left(\Delta y + \dfrac{\partial v}{\partial y}\Delta y \Delta t\right)\left(\Delta z + \dfrac{\partial w}{\partial z}\Delta z \Delta t\right) - \Delta x \Delta y \Delta z}{\Delta x \Delta y \Delta z \Delta t}$$
$$\approx \frac{\partial u}{\partial x} + \frac{\partial v}{\partial y} + \frac{\partial v}{\partial z} = \nabla \cdot \vec{v}.$$

Therefore, a divergence free velocity field is equivalent to an incompressible fluid flow.

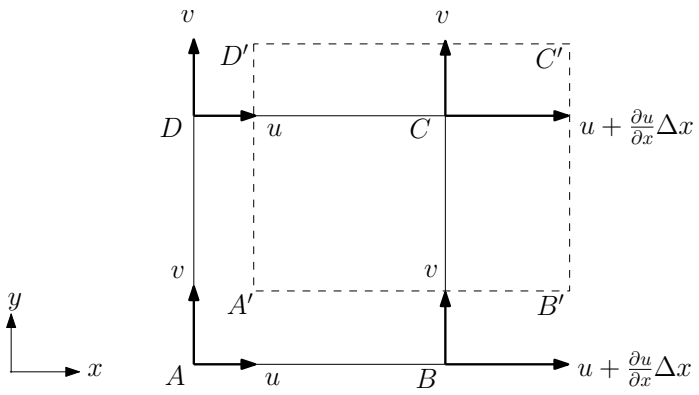

Figure A.4: Deformation of a fluid element due to dilation.

The geometrical meanings of the off-diagonal terms can be understood as follows. We assume now the only non-zero terms are $\partial u/\partial y$ and $\partial v/\partial x$. After some short time Δt, the rectangle $ABCD$ will become $A'B'C'D'$, shown in Figure A.5. Since

$$\alpha \approx \tan\alpha = \frac{\dfrac{\partial v}{\partial x}\Delta x \Delta t}{\Delta x} = \frac{\partial v}{\partial x}\Delta t,$$
$$\beta \approx \tan\beta = \frac{\dfrac{\partial u}{\partial y}\Delta y \Delta t}{\Delta y} = \frac{\partial u}{\partial y}\Delta t,$$

we see that the rate of change of angle BAD is approximately

$$\frac{\alpha+\beta}{\Delta t} = \left(\frac{\partial v}{\partial x} + \frac{\partial u}{\partial y}\right) = 2e_{12} = 2e_{21}.$$

Therefore, the quantity e_{12} or e_{21} (due to symmetry) represents the averaged rate of change from a 45° angle due to the deformation. The other off-diagonal components have similar representations.

For $\delta v_i^{(a)}$, we see that ξ_{ij} is an anti-symmetrical tensor and can be written as

$$\xi_{ij} = -\frac{1}{2}\epsilon_{ijk}\omega_k,$$

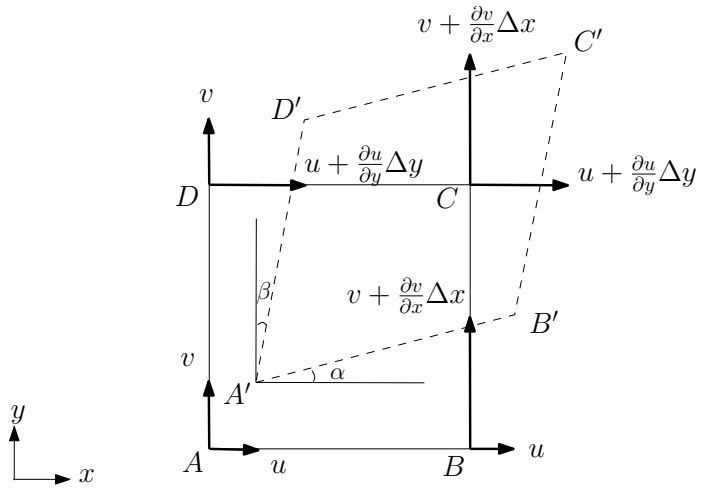

Figure A.5: Deformation of a fluid element due to angle change.

where

$$\omega_1 = \frac{\partial v_3}{\partial x_2} - \frac{\partial v_2}{\partial x_3}, \qquad \omega_2 = \frac{\partial v_1}{\partial x_3} - \frac{\partial v_3}{\partial x_1}, \qquad \omega_3 = \frac{\partial v_2}{\partial x_1} - \frac{\partial v_1}{\partial x_2}.$$

Thus,

$$\delta v_i^{(a)} = \delta x_j \xi_{ij} = -\frac{1}{2}\epsilon_{ijk}\delta x_j \omega_k,$$

which is the i-component of the vector $\frac{1}{2}\vec{\omega} \times \delta\vec{x}$. So, $\delta\vec{v}^{(a)}$ is the velocity produced at position $\delta\vec{x}$ relative to a point about which there is a rigid-body rotation with angular velocity $\frac{1}{2}\vec{\omega}$.

A.4.4 The Relation between Stress Tensor and Rate-of-Strain Tensor

If a fluid is at rest, only normal stresses are exerted, and the stress tensor has the form

$$\sigma_{ij} = -p\delta_{ij}, \ i, j = 1, 2, 3, \tag{A.4.10}$$

where p is the hydrostatic pressure. For a fluid in motion, experiments show that the shear stress components are not zero and so we assume a stress tensor

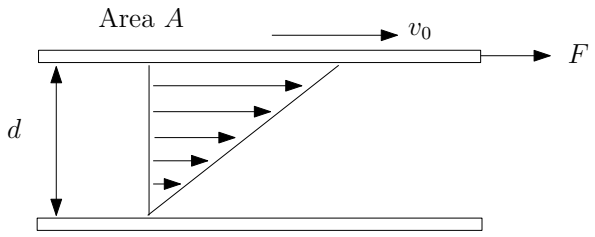

Figure A.6: The viscosity experiment.

having the form

$$\sigma_{ij} = -p\delta_{ij} + \tau_{ij}, \ i, j = 1, 2, 3, \tag{A.4.11}$$

where τ_{ij} is called the *viscous stress tensor*.

When a fluid at rest is sheared, it begins to flow. Consider the experiment involving a fluid moving between two parallel planes (Heinbockel, 1996), shown in Figure A.6. Let d denote the distance between the two planes. Now keep the lower surface fixed and move the upper surface with a constant velocity $\vec{v}_0$. It is shown by experiment that the force F required to maintain the constant velocity of the upper surface is related to the area of the upper surface A and the ratio v_0/d as

$$\frac{F}{A} = \mu \frac{v_0}{d}. \tag{A.4.12}$$

The constant μ is called the *coefficient of viscosity*. The result indicates that the stress is proportional to the gradient of the velocity.

The above experiment with viscosity suggests that the viscous stress tensor τ_{ij} is proportional to the velocity gradient $\partial v_i/\partial x_j$. So we write

$$\tau_{ij} = c_{ijmp} \frac{\partial v_m}{\partial x_p}, \tag{A.4.13}$$

where c_{ijmp} is a proportionality constant and it is a forth rank tensor. We shall restrict to fluids of isotropic structure, thus the viscous stress must be independent of any reference frame. Hence we assume that c_{ijmp} is an isotropic

tensor. From tensor analysis, an isotropic tensor has the basic form

$$c_{ijmp} = \lambda\delta_{ij}\delta_{mp} + \mu(\delta_{im}\delta_{jp} + \delta_{ip}\delta_{jm}) + \nu(\delta_{im}\delta_{jp} - \delta_{ip}\delta_{jm}) \tag{A.4.14}$$

where λ, μ, ν are constants. From (A.4.11) we find that the viscous stress tensor is symmetric since the stress tensor is symmetric, which means that c_{ijmp} needs to be symmetric in the indices i and j. This requires that ν be zero. Thus,

$$c_{ijmp} = \lambda\delta_{ij}\delta_{mp} + \mu(\delta_{im}\delta_{jp} + \delta_{ip}\delta_{jm})$$

and (A.4.13) reduces to

$$\tau_{ij} = \lambda\delta_{ij}\frac{\partial v_p}{\partial x_p} + \mu\left(\frac{\partial v_j}{\partial x_i} + \frac{\partial v_i}{\partial x_j}\right). \tag{A.4.15}$$

The coefficient μ is called the *first coefficient of viscosity* and λ is the *second coefficient of viscosity*. In terms of the rate-of-strain tensor defined in (A.4.7), equation (A.4.15) can be written as

$$\tau_{ij} = \lambda\delta_{ij}e_{kk} + 2\mu e_{ij}. \tag{A.4.16}$$

If we substitute (A.4.16) back into (A.4.11), we have

$$\sigma_{ij} = -p\delta_{ij} + \lambda\delta_{ij}e_{kk} + 2\mu e_{ij}. \tag{A.4.17}$$

This is the relationship between the stress tensor and the rate-of-strain tensor, known as the *constitutive equation*. For incompressible flow, $e_{kk} = 0$, thus

$$\sigma_{ij} = -p\delta_{ij} + 2\mu e_{ij}. \tag{A.4.18}$$

Note that the viscous stress tensor is a linear function of the rate-of-strain tensor. Such a fluid is called a *Newtonian fluid*. In cases where the viscous stress tensor is a nonlinear function of the rate-of-strain tensor, the fluid is

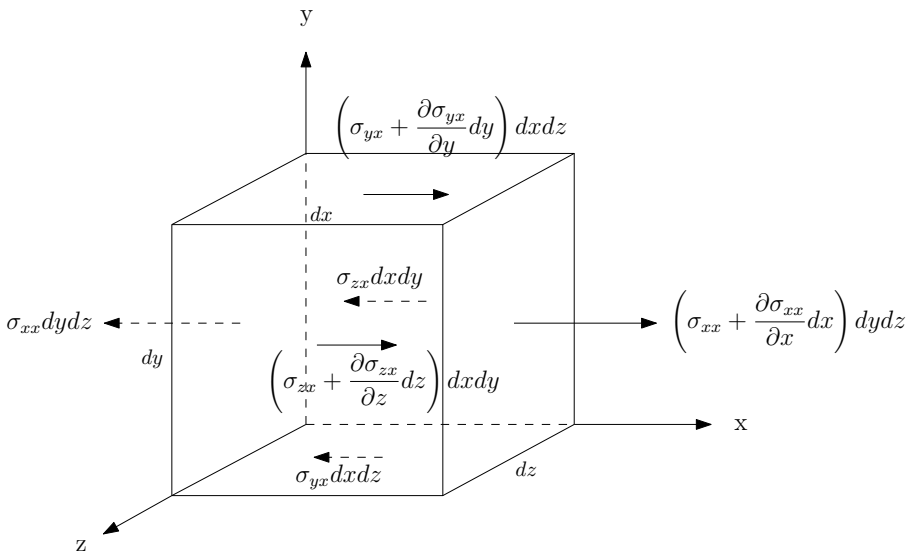

Figure A.7: An infinitesimal cubic fluid element with surface stresses shown in x-direction only.

called *non-Newtonian*.

A.5 The Navier-Stokes Equations

Let us now go back to the equations of motion of fluids. In order to obtain the equations of motion of a viscous fluid, we need to include the additional terms in the equation of motion of an ideal fluid as explained previously. The equation of continuity is valid for both ideal and viscous fluids. However, Euler's equation requires modification (Landau and Lifshitz, 1987). First, let us re-write the Euler's equation (A.2.2) in the index notation,

$$\rho \left(\frac{\partial v_i}{\partial t} + v_k \frac{\partial v_i}{\partial x_k} \right) = - \frac{\partial p}{\partial x_i}. \tag{A.5.1}$$

where v_i are components of the velocity of the fluid, x_i are components of the cartesian coordinates.

Let us now consider the effects of stresses on a fluid particle and hence derive the terms to be added to the Euler's equation. Figure A.7 shows an infinitesimal cubic fluid element in cartesian coordinates with surface forces

shown in the x-direction only (White, 1986). The net surface force in the x-direction is given by

$$dF_{x,\text{surf}} = \left[\frac{\partial}{\partial x}(\sigma_{xx}) + \frac{\partial}{\partial y}(\sigma_{yx}) + \frac{\partial}{\partial z}(\sigma_{zx})\right] dxdydz. \tag{A.5.2}$$

From (A.4.11), we notice that the stress tensor can be decomposed into two parts, namely the viscous stresses and the hydrostatic pressure. So we can rewrite (A.5.2) as

$$\frac{dF_{x,\text{surf}}}{dV} = -\frac{\partial p}{\partial x} + \frac{\partial}{\partial x}(\tau_{xx}) + \frac{\partial}{\partial y}(\tau_{yx}) + \frac{\partial}{\partial z}(\tau_{zx})$$

where $dV = dxdydz$. Similarly,

$$\begin{aligned}
\frac{dF_{y,\text{surf}}}{dV} &= -\frac{\partial p}{\partial y} + \frac{\partial}{\partial x}(\tau_{xy}) + \frac{\partial}{\partial y}(\tau_{yy}) + \frac{\partial}{\partial z}(\tau_{zy}), \\
\frac{dF_{z,\text{surf}}}{dV} &= -\frac{\partial p}{\partial z} + \frac{\partial}{\partial x}(\tau_{xz}) + \frac{\partial}{\partial y}(\tau_{yz}) + \frac{\partial}{\partial z}(\tau_{zz}).
\end{aligned}$$

Collectively, we have

$$\frac{d\vec{F}_{\text{surf}}}{dV} = -\nabla p + \nabla \cdot \tau_{ij} \tag{A.5.3}$$

where

$$\tau_{ij} = \begin{pmatrix} \tau_{xx} & \tau_{yx} & \tau_{zx} \\ \tau_{xy} & \tau_{yy} & \tau_{zy} \\ \tau_{xz} & \tau_{yz} & \tau_{zz} \end{pmatrix}.$$

The term $-\nabla p$ in (A.5.3) is already included in the Euler's equation, so the equations of motion of a viscous fluid can now be obtained by adding the expression $\partial\tau_{ij}/\partial x_j$ to the right-hand side of Euler's equation (A.5.1). By comparing (A.4.11) with (A.4.18) and using the definition of the rate-of-strain

tensor (A.4.7), we get

$$\tau_{ij} = \mu \left(\frac{\partial v_i}{\partial x_j} + \frac{\partial v_j}{\partial x_i} \right). \tag{A.5.4}$$

Thus,

$$\rho \left(\frac{\partial v_i}{\partial t} + v_k \frac{\partial v_i}{\partial x_k} \right) = -\frac{\partial p}{\partial x_i} + \frac{\partial}{\partial x_j} \left[\mu \left(\frac{\partial v_i}{\partial x_j} + \frac{\partial v_j}{\partial x_i} \right) \right]. \tag{A.5.5}$$

In general, the viscosity coefficients do not change much in the fluid, and they can be treated as a constant. By using the incompressibility constraint, we then have equation (A.5.5), in vector form, as

$$\rho \left(\frac{\partial \vec{v}}{\partial t} + \vec{v} \cdot \nabla \vec{v} \right) = -\nabla p + \mu \nabla^2 \vec{v} \tag{A.5.6}$$

where ρ is the density of fluid, $\vec{v}$ is the fluid velocity, p is the fluid pressure and μ is called the *dynamic viscosity*. Expression (A.5.6) is called the *Navier-Stokes equations*. Introducing the *kinematic viscosity* by the ratio

$$\nu = \frac{\mu}{\rho}, \tag{A.5.7}$$

we can also write the Navier-Stokes equations as

$$\frac{\partial \vec{v}}{\partial t} + \vec{v} \cdot \nabla \vec{v} = -\frac{1}{\rho} \nabla p + \nu \nabla^2 \vec{v}. \tag{A.5.8}$$

If the fluid is in a gravitational field and $\vec{g}$ is the acceleration due to gravity, then

$$\frac{\partial \vec{v}}{\partial t} + \vec{v} \cdot \nabla \vec{v} = -\frac{1}{\rho} \nabla p + \nu \nabla^2 \vec{v} + \vec{g}. \tag{A.5.9}$$

Appendix B

Numerical Treatment for the Navier-Stokes Equations

A finite-difference scheme is presented for solving the Navier-Stokes equations for incompressible flow in this appendix. The algorithm comes from the projection method (Chorin, 1968) which consists of two stages. First, for each time step, an intermediate velocity that does not satisfy the incompressibility constraint is computed. Then the pressure Poisson equation is solved to ensure the divergence-free condition is satisfied and used to update the velocity field for the next time step.

B.1 The Initial-Boundary Value Problem

B.1.1 The Two-dimensional Navier-Stokes Equations

Let us begin with the mathematical description of flows. Consider the flow of a fluid in a region $\Omega \subset \mathbb{R}^N$ (e.g. $N = 2, 3$) throughout time $t \in [0, t_{\text{end}}]$. The

flow is characterized by the following:

$$\vec{v} : \Omega \times [0, t_{\text{end}}] \to \mathbb{R}^N \text{ velocity field,}$$
$$p : \Omega \times [0, t_{\text{end}}] \to \mathbb{R} \text{ pressure,}$$
$$\rho : \Omega \times [0, t_{\text{end}}] \to \mathbb{R} \text{ density.}$$

The equations of motion of an incompressible fluid in their non-dimensional form are

$$\frac{\partial \vec{v}}{\partial t} + \vec{v} \cdot \nabla \vec{v} = -\nabla p + \frac{1}{Re} \nabla^2 \vec{v} + \vec{g}, \tag{B.1.1}$$
$$\nabla \cdot \vec{v} = 0, \tag{B.1.2}$$

where $Re = VL/\nu$ is the *Reynolds number*.

For clarity, we begin by considering variables in a two-dimensional space. Let $\vec{x} = (x, y)^\intercal$, $\vec{v} = (u, v)^\intercal$, $\vec{g} = (g_x, g_y)^\intercal$, where $\intercal$ denotes the transpose, the momentum equations (B.1.1) can be written as

$$\frac{\partial u}{\partial t} + \frac{\partial p}{\partial x} = \frac{1}{Re}\left(\frac{\partial^2 u}{\partial x^2} + \frac{\partial^2 u}{\partial y^2}\right) - \frac{\partial (u^2)}{\partial x} - \frac{\partial (uv)}{\partial y} + g_x, \tag{B.1.3}$$
$$\frac{\partial v}{\partial t} + \frac{\partial p}{\partial y} = \frac{1}{Re}\left(\frac{\partial^2 v}{\partial x^2} + \frac{\partial^2 v}{\partial y^2}\right) - \frac{\partial (v^2)}{\partial y} - \frac{\partial (uv)}{\partial x} + g_y, \tag{B.1.4}$$

and the continuity equation (B.1.2) becomes

$$\frac{\partial u}{\partial x} + \frac{\partial v}{\partial y} = 0. \tag{B.1.5}$$

Note that in (B.1.3) and (B.1.4), the term $\vec{v} \cdot \nabla \vec{v}$ in equation (B.1.1) has been rewritten using the continuity equation.

B.1.2 Initial Conditions

For initial conditions, we impose at $t = 0$

$$u = u_0(x, y) \text{ and } v = v_0(x, y) \tag{B.1.6}$$

such that the continuity equation (B.1.5) is satisfied.

B.1.3 Boundary Conditions

To formulate the boundary conditions for the velocities, let v_n denote the component of velocity orthogonal to the boundary, v_t the component of velocity parallel to the boundary, and $\partial v_n/\partial n$, $\partial v_t/\partial n$ their derivatives in the normal direction. If the boundary segments of the domain are parallel to the coordinate axes, then along the vertical boundary segments, we have

$$v_n = u, \qquad v_t = v, \qquad \frac{\partial v_n}{\partial n} = \frac{\partial u}{\partial x}, \qquad \frac{\partial v_t}{\partial n} = \frac{\partial v}{\partial x},$$

and along the horizontal boundary segments,

$$v_n = v, \qquad v_t = u, \qquad \frac{\partial v_n}{\partial n} = \frac{\partial v}{\partial y}, \qquad \frac{\partial v_t}{\partial n} = \frac{\partial u}{\partial y}.$$

For points along the fixed boundary $\partial\Omega$, we shall consider the following boundary conditions (Griebel et al., 1998):

1. **No-slip condition**: No fluid penetrates the boundary and the fluid is traveling at the same velocity as the boundary, for example, if the boundary is at rest,

$$v_n(x, y) = 0 \text{ and } v_t(x, y) = 0. \tag{B.1.7}$$

2. **Inflow condition**: Both velocity components are given, i.e.,

$$v_n(x, y) = v_n^0 \text{ and } v_t(x, y) = v_t^0 \tag{B.1.8}$$

where v_n^0 and v_t^0 are given data.

3. **Outflow condition**: Neither velocity component changes in the direction normal to the boundary, i.e.,

$$\frac{\partial v_n(x, y)}{\partial n} = 0 \text{ and } \frac{\partial v_t(x, y)}{\partial n} = 0. \tag{B.1.9}$$

B.2 Discretization in Two-dimensions

The two-dimensional Navier-Stokes equations on smooth domains with smooth Dirichlet boundary conditions (with the velocities rather than normal derivatives of velocities specified along the boundary) has a unique solution for all time (Ladyshenskaja, 1969). In general, the solution or solutions of the Navier-Stokes equations cannot be calculated analytically. Instead, we shall describe the numerical treatment of the unsteady incompressible Navier-Stokes equations, in particular the finite-difference method. We shall discuss the two-dimensional case below.

B.2.1 Spatial Discretization on Staggered Grids

When solving the Navier-Stokes equations, the computational domain is often discretized using a staggered grid (Harlow and Welch, 1965) to prevent possible pressure oscillations which could have occurred if we had evaluated all variables at the same grid points.

Suppose we have a rectangular region $\Omega = [a, b] \times [c, d] \subset \mathbb{R}^2$. Dividing this domain into M cells of equal size in the x-direction and N cells in the

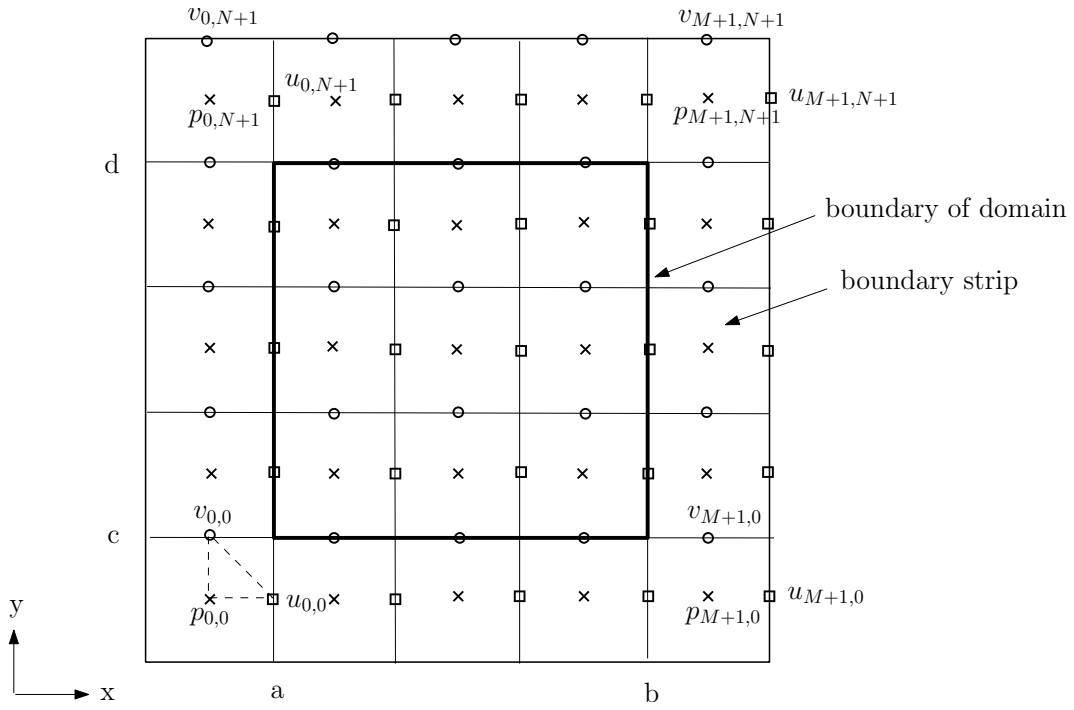

Figure B.1: Staggered grid arrangement with $M = N = 3$. The broad line is the boundary of the physical domain.

y-direction, the grid lines are spaced at a distance

$$\Delta x = \frac{b-a}{M} \text{ and } \Delta y = \frac{d-c}{N}.$$

The staggered grid arrangement is shown in Figure B.1. The pressure p is located at the cell centers, marked by the crosses; the velocity u is at the midpoint of the vertical cell edges, marked by the squares; and the velocity v is at the midpoints of the horizontal cell edges, marked by the circles. For this arrangement, not all grid points lie on the domain boundary. An extra boundary strip is needed, so that the boundary conditions can be applied by averaging the nearest grid points on either side (Griebel et al., 1998).

The continuity equation (B.1.5) is discretized at the center of each cell (i, j), $i = 1, ..., M$, $j = 1, ..., N$. We replace the partial derivatives $\partial u/\partial x$ and

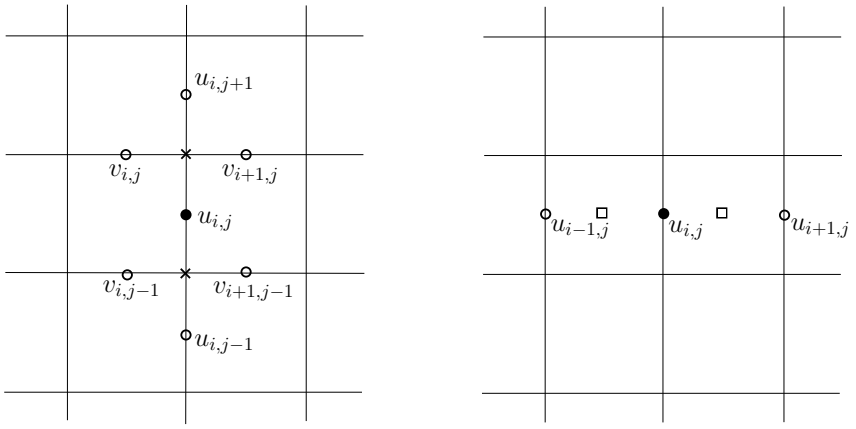

Figure B.2: Values required to discretize $\partial(uv)/\partial y$ (left) and $\partial(u^2)/\partial x$ (right) of cell (i, j).

$\partial v/\partial y$ by using the centered difference with half the mesh width:

$$\left[\frac{\partial u}{\partial x}\right]_{i,j} = \frac{u_{i,j} - u_{i-1,j}}{\Delta x}, \tag{B.2.1}$$

$$\left[\frac{\partial v}{\partial y}\right]_{i,j} = \frac{v_{i,j} - v_{i,j-1}}{\Delta y}. \tag{B.2.2}$$

The momentum equation (B.1.3) for u is discretized at the midpoints of the vertical cell edges, i.e., on the grid points where $u_{i,j}$'s are located while the momentum equation (B.1.4) for v is discretized at $v_{i,j}$ grid points. For the diffusive terms, we can use central differences with half the mesh width. However, for the convective terms $\partial(u^2)/\partial x$, $\partial(uv)/\partial y$, $\partial(v^2)/\partial y$, and $\partial(uv)/\partial x$, we need some special treatments. For instance, in order to discretize $\partial(uv)/\partial y$ at the midpoint of the right edge of cell (i, j) (black dot in Figure B.2), we need suitable values of the product uv lying on the same vertical line as $u_{i,j}$. One of the ways to tackle this difficulty is to take the average of u and v taken at the locations marked with an $\times$ in Figure B.2. Similarly, to discretize $\partial(u^2)/\partial x$, we use a central difference with half the mesh width of values averaged at the locations marked with a square in Figure B.2. Similarly for the convective terms in (B.1.4) for v.

Thus, in equation (B.1.3) for u at the midpoint of the right edge of cell

(i,j), $i = 1, ..., M-1$, $j = 1, ..., N$, we have

$$\left[\frac{\partial(u^2)}{\partial x}\right]_{i,j} = \frac{1}{\Delta x}\left(\left(\frac{u_{i,j}+u_{i+1,j}}{2}\right)^2 - \left(\frac{u_{i-1,j}+u_{i,j}}{2}\right)^2\right), \tag{B.2.3}$$

$$\left[\frac{\partial(uv)}{\partial y}\right]_{i,j} = \frac{1}{\Delta y}\frac{(v_{i,j}+v_{i+1,j})(u_{i,j}+u_{i,j+1})}{4} - \frac{1}{\Delta y}\frac{(v_{i,j-1}+v_{i+1,j-1})(u_{i,j-1}+u_{i,j})}{4}, \tag{B.2.4}$$

$$\left[\frac{\partial^2 u}{\partial x^2}\right]_{i,j} = \frac{u_{i+1,j}-2u_{i,j}+u_{i-1,j}}{\Delta x^2}, \tag{B.2.5}$$

$$\left[\frac{\partial^2 u}{\partial y^2}\right]_{i,j} = \frac{u_{i,j+1}-2u_{i,j}+u_{i,j-1}}{\Delta y^2}, \tag{B.2.6}$$

$$\left[\frac{\partial p}{\partial x}\right]_{i,j} = \frac{p_{i+1,j}-p_{i,j}}{\Delta x}. \tag{B.2.7}$$

Similarly in equation (B.1.4) for v at the midpoint of the upper edge of cell (i,j), $i = 1, ..., M$, $j = 1, ..., N-1$, we have

$$\left[\frac{\partial(v^2)}{\partial y}\right]_{i,j} = \frac{1}{\Delta y}\left(\left(\frac{v_{i,j}+v_{i,j+1}}{2}\right)^2 - \left(\frac{v_{i,j-1}+v_{i,j}}{2}\right)^2\right), \tag{B.2.8}$$

$$\left[\frac{\partial(uv)}{\partial x}\right]_{i,j} = \frac{1}{\Delta x}\frac{(u_{i,j}+u_{i,j+1})(v_{i,j}+v_{i+1,j})}{4} - \frac{1}{\Delta x}\frac{(u_{i-1,j}+u_{i-1,j+1})(v_{i-1,j}+v_{i,j})}{4}, \tag{B.2.9}$$

$$\left[\frac{\partial^2 v}{\partial x^2}\right]_{i,j} = \frac{v_{i+1,j}-2v_{i,j}+v_{i-1,j}}{\Delta x^2}, \tag{B.2.10}$$

$$\left[\frac{\partial^2 v}{\partial y^2}\right]_{i,j} = \frac{v_{i,j+1}-2v_{i,j}+v_{i,j-1}}{\Delta y^2}, \tag{B.2.11}$$

$$\left[\frac{\partial p}{\partial y}\right]_{i,j} = \frac{p_{i,j+1}-p_{i,j}}{\Delta y}. \tag{B.2.12}$$

B.2.2 Boundary Conditions

Due to the staggered arrangement, not all the values lie on the boundary. Thus for the boundary conditions of velocity components, we need (Griebel et al.,

1998)

$$u_{0,j},\ u_{M,j}, \qquad j = 1, ..., N, \tag{B.2.13}$$

$$v_{i,0},\ v_{i,N}, \qquad i = 1, ..., M, \tag{B.2.14}$$

on the boundary and also the values

$$u_{i,0},\ u_{i,N+1}, \qquad i = 1, ..., M, \tag{B.2.15}$$

$$v_{0,j},\ v_{M+1,j}, \qquad j = 1, ..., N, \tag{B.2.16}$$

outside the domain Ω. We shall discuss the following type of boundary conditions:

1. **No-slip Condition**

   For a no-slip boundary condition with the boundary at rest, the continuous velocities vanish at the boundary. For the values lying directly on the boundary, we set

   $$u_{0,j} = 0,\ u_{M,j} = 0, \qquad j = 1, ..., N, \tag{B.2.17}$$

   $$v_{i,0} = 0,\ v_{i,N} = 0, \qquad i = 1, ..., M. \tag{B.2.18}$$

   Since the horizontal boundary contains no u-values and the vertical boundary contains no v-values, the zero boundary condition is enforced in these cases by averaging the values on either side of the boundary:

   $$v_{0,j} = -v_{1,j},\ v_{M+1,j} = -v_{M,j}, \qquad j = 1, ..., N, \tag{B.2.19}$$

   $$u_{i,0} = -u_{i,1},\ u_{i,N+1} = -u_{i,N}, \qquad i = 1, ..., M. \tag{B.2.20}$$

2. **Inflow Conditions**

   On an inflow boundary, the velocities are explicitly given. We impose this for the velocities normal to the boundary by directly fixing the values

on the boundary line. For the velocity components tangential to the boundary, we average the values on either side of the boundary such that the average has the desired value on the boundary.

3. **Outflow Conditions**

   For an outflow boundary condition, the normal derivatives of both velocity components are set to zero at the boundary. This means that the total velocity does not change in the direction normal to the boundary. This can be achieved by setting velocity values at the boundary equal to their neighboring velocities inside the domain, i.e., for $j = 1, ..., N$,

$$u_{0,j} = u_{1,j}, \qquad u_{M,j} = u_{M-1,j}, \tag{B.2.21}$$

$$v_{0,j} = v_{1,j}, \qquad v_{M+1,j} = v_{M,j}, \tag{B.2.22}$$

   and for $i = 1, ..., M$,

$$u_{i,0} = u_{i,1}, \qquad u_{i,N+1} = u_{i,N}, \tag{B.2.23}$$

$$v_{i,0} = v_{i,1}, \qquad v_{i,N} = v_{i,N-1}, \tag{B.2.24}$$

B.2.3 Temporal Discretization

To discretize the time derivatives $\partial u/\partial t$ and $\partial v/\partial t$, we divide the time interval into equal subintervals with size Δt and use an Euler scheme to update the time:

$$\left[\frac{\partial u}{\partial t}\right]^{(n+1)} = \frac{u^{(n+1)} - u^{(n)}}{\Delta t}, \tag{B.2.25}$$

$$\left[\frac{\partial v}{\partial t}\right]^{(n+1)} = \frac{v^{(n+1)} - v^{(n)}}{\Delta t}, \tag{B.2.26}$$

where the superscripts denote the time level.

B.3 The Time-Stepping Algorithm

We begin at the initial time $t = 0$, with given initial velocities u and v, time is incremented by Δt at each step until the final time t_{end} is reached. At time step n, the values of all variables are known and they are used to compute the variables for step $n + 1$.

The idea of this time-stepping algorithm comes from Chorin's projection method (Chorin, 1968). The projection method is based on the Helmholtz decomposition of any vector field into a curl-free part and a divergence-free part. To understand the algorithm, let us first re-write the momentum equation (B.1.1) as

$$\frac{\partial \vec{v}}{\partial t} + \nabla p = \frac{1}{Re}\nabla^2 \vec{v} - \vec{v} \cdot \nabla \vec{v} + \vec{g} \equiv \mathcal{R}. \tag{B.3.1}$$

Taking the divergence on both sides of the above equation,

$$\nabla \cdot \left(\frac{\partial \vec{v}}{\partial t} \right) + \nabla^2 p = \nabla \cdot \mathcal{R}. \tag{B.3.2}$$

Since the velocity field is divergence free, the first term on the left hand side vanishes, so we get

$$\nabla^2 p = \nabla \cdot \mathcal{R} \equiv \nabla \cdot \left(\frac{1}{Re}\nabla^2 \vec{v} - \vec{v} \cdot \nabla \vec{v} + \vec{g} \right). \tag{B.3.3}$$

If we use the explicit Euler's method to first update the velocity field to an intermediate velocity $\vec{v}^*$ such that it does not involve the pressure term, i.e.,

$$\vec{v}^* = \vec{v}^{(n)} + \Delta t \mathcal{R},$$

then

$$\mathcal{R} = \frac{\vec{v}^* - \vec{v}^{(n)}}{\Delta t}. \tag{B.3.4}$$

Substituting (B.3.4) back to equation (B.3.3), we get

$$\nabla^2 p = \frac{1}{\Delta t}\nabla \cdot \vec{v}^* - \frac{1}{\Delta t}\nabla \cdot \vec{v}^{(n)}.$$

It is obvious that the second term of the right-hand side vanishes since $\vec{v}^{(n)}$ is divergence free. We are left with

$$\nabla^2 p = \frac{1}{\Delta t}\nabla \cdot \vec{v}^* \tag{B.3.5}$$

known as the *Pressure Poisson Equation* that we need to solve with (B.3.3) and (B.3.4). Once we have solved p, it is then used to update the velocity field to the next time step by projecting $\vec{v}^*$ back to the divergence free field, i.e.,

$$\vec{v}^{(n+1)} = \vec{v}^* - \Delta t \nabla p. \tag{B.3.6}$$

In (B.3.6), we used the Helmholtz decomposition of the vector field $\vec{v}^*$, where $\vec{v}^{(n+1)}$ is divergence free and ∇p is curl free since the curl of a gradient is always zero.

B.3.1 The Algorithm

Using the spatial discretization in the previous section, the time-stepping loop can be summarized as follows (Griebel et al., 1998; Chorin, 1968):

Step 1: Compute the intermediate velocities $F^{(n)}$ and $G^{(n)}$ (the right-hand side of (B.3.3)), where

$$F^{(n)} = u^{(n)} + \Delta t \left[\frac{1}{Re}\left(\frac{\partial^2 u}{\partial x^2} + \frac{\partial^2 u}{\partial y^2}\right) - \frac{\partial (u^2)}{\partial x} - \frac{\partial (uv)}{\partial y} + g_x\right], \tag{B.3.7}$$

$$G^{(n)} = v^{(n)} + \Delta t \left[\frac{1}{Re}\left(\frac{\partial^2 v}{\partial x^2} + \frac{\partial^2 v}{\partial y^2}\right) - \frac{\partial (v^2)}{\partial y} - \frac{\partial (uv)}{\partial x} + g_y\right]. \tag{B.3.8}$$

Step 2: Solve the Poisson equation for $p^{(n+1)}$ (the left-hand side of (B.3.3)):

$$\frac{\partial^2 p^{(n+1)}}{\partial x^2} + \frac{\partial^2 p^{(n+1)}}{\partial y^2} = \frac{1}{\Delta t}\left(\frac{\partial F^{(n)}}{\partial x} + \frac{\partial G^{(n)}}{\partial y}\right). \tag{B.3.9}$$

Step 3: Compute the new velocity field with the pressure values $p^{(n+1)}$ computed in step 2 (discrete version of (B.3.6)):

$$u^{(n+1)} = F^{(n)} - \Delta t \frac{\partial p^{(n+1)}}{\partial x}, \tag{B.3.10}$$

$$v^{(n+1)} = G^{(n)} - \Delta t \frac{\partial p^{(n+1)}}{\partial y}. \tag{B.3.11}$$

B.3.2 The Stability Conditions

In order to ensure stability of the numerical algorithm, we must impose the following conditions on the stepsizes Δx, Δy, and Δt (Tome and McKee, 1994):

$$\frac{2\Delta t}{Re} < \left(\frac{1}{\Delta x^2} + \frac{1}{\Delta y^2}\right)^{-1}, \quad |u_{\max}|\,\Delta t < \Delta x, \quad |v_{\max}|\,\Delta t < \Delta y, \tag{B.3.12}$$

where $u_{\max}$ and $v_{\max}$ are the maximal absolute values of the velocities occurring on the grid. The latter two are known as the Courant-Friedrichs-Lewy (CFL) conditions. They impose that no fluid particle may travel a distance greater than the mesh spacing Δx or Δy in time Δt.

B.4 The Pressure Poisson Equation

In Step 2 of the time-stepping algorithm above, the pressure $p^{(n+1)}$ is computed implicitly by solving a linear system of equations. The discrete Poisson equation is given by

$$\begin{aligned}\frac{p_{i+1,j}^{(n+1)} - 2p_{i,j}^{(n+1)} + p_{i-1,j}^{(n+1)}}{\Delta x^2} + \frac{p_{i,j+1}^{(n+1)} - 2p_{i,j}^{(n+1)} + p_{i,j-1}^{(n+1)}}{\Delta y^2} \\ = \frac{1}{\Delta t}\left(\frac{F_{i,j}^{(n)} - F_{i-1,j}^{(n)}}{\Delta x} + \frac{G_{i,j}^{(n)} - G_{i,j-1}^{(n)}}{\Delta y}\right),\end{aligned} \tag{B.4.1}$$

for $i = 1, ..., M$, $j = 1, ..., N$.

B.4.1 Pressure Boundary Conditions

In (B.4.1), the following pressure boundary values are required:

$$\begin{aligned} &p_{0,j},\ p_{M+1,j}, && j = 1, ..., N, \\ &p_{i,0},\ p_{i,N+1}, && i = 1, ..., M. \end{aligned}$$

Determining the pressure boundary conditions for open boundaries (e.g. inflow and outflow) is still an open question. Many treatments can be found in literature and they are problem dependent (Sani and Gresho, 1994). For closed boundaries, Neumann pressure boundary conditions are often used (Gresho and Sani, 1987). In particular, if no-slip condition is imposed for velocities at the boundary, then the normal derivatives of the pressure also vanish at the boundary. In this case,

$$p_{0,j} = p_{1,j},\ p_{M+1,j} = p_{M,j}, \qquad j = 1, ..., N, \tag{B.4.2}$$

$$p_{i,0} = p_{i,1},\ p_{i,N+1} = p_{i,N}, \qquad i = 1, ..., M. \tag{B.4.3}$$

B.4.2 Iterative Methods

From the pressure conditions (B.4.2) and (B.4.3), the discrete Poisson equation for the pressure (B.4.1) may become (Griebel et al., 1998)

$$\begin{aligned} &\frac{\epsilon_i^E \left(p_{i+1,j}^{(n+1)} - p_{i,j}^{(n+1)}\right) - \epsilon_i^W \left(p_{i,j}^{(n+1)} - p_{i-1,j}^{(n+1)}\right)}{\Delta x^2} \\ &+ \frac{\epsilon_j^N \left(p_{i,j+1}^{(n+1)} - p_{i,j}^{(n+1)}\right) - \epsilon_j^S \left(p_{i,j}^{(n+1)} - p_{i,j-1}^{(n+1)}\right)}{\Delta y^2} \\ =&\frac{1}{\Delta t}\left(\frac{F_{i,j}^{(n)} - F_{i-1,j}^{(n)}}{\Delta x} + \frac{G_{i,j}^{(n)} - G_{i,j-1}^{(n)}}{\Delta y}\right), i = 1, ..., M, j = 1, ..., N, \end{aligned} \tag{B.4.4}$$

where the ϵ's ((W)est, (E)ast, (S)outh, (N)orth) are defined as

$$\epsilon_i^W = \begin{cases} 0, & \text{if } i = 1, \\ 1, & \text{if } i > 1, \end{cases} \qquad \epsilon_i^E = \begin{cases} 1, & \text{if } i < M, \\ 0, & \text{if } i = M, \end{cases}$$

$$\epsilon_j^S = \begin{cases} 0, & \text{if } j = 1, \\ 1, & \text{if } j > 1, \end{cases} \qquad \epsilon_j^N = \begin{cases} 1, & \text{if } j < N, \\ 0, & \text{if } j = N. \end{cases}$$

Equation (B.4.4) is a linear system of equations containing MN equations and MN unknown p_{ij}'s to be solved numerically. Since the linear system above is large and sparse, we would choose iterative methods rather than direct methods which would be too costly for computations. A few classical iterative methods to solve a $n \times n$ linear system $\mathbf{A}\vec{z} = \vec{b}$ are summarized as follows (Burden and Faires, 2005):

The Jacobi Iterative Method

Given an initial guess of the solution $z_i^{(0)}$, where z_i are components of the vector $\vec{z}$ and the superscript denotes the iteration number. We calculate each $z_i^{(k)}$ from the components of $\vec{z}^{(k-1)}$ for $k \geq 1$ by

$$z_i^{(k)} = \frac{1}{a_{ii}} \left(\sum_{j=1, j \neq i}^{n} \left(-a_{ij} z_j^{(k-1)} \right) + b_i \right), \qquad i = 1, ..., n. \tag{B.4.5}$$

The Gauss-Seidel Iterative Method

A possible improvement of the Jacobi iterative method is the Gauss-Seidel method, given as

$$z_i^{(k)} = \frac{1}{a_{ii}} \left(-\sum_{j=1}^{i-1} \left(a_{ij} z_j^{(k)} \right) - \sum_{j=i+1}^{n} \left(a_{ij} z_j^{(k-1)} \right) + b_i \right), \quad i = 1, ..., n. \tag{B.4.6}$$

The Successive Over-Relaxation (SOR) Method

The convergence of both the Jacobi and Gauss-Seidel methods are guaranteed for any choice of the initial guess $\vec{z}^{(0)}$ for strictly diagonally dominant matrix $\mathbf{A}$. To accelerate the convergence for systems that are convergent by the Gauss-Seidel, we introduce the SOR method as:

$$z_i^{(k)} = (1-\omega)z_j^{(k-1)} + \frac{\omega}{a_{ii}}\left(-\sum_{j=1}^{i-1}\left(a_{ij}z_j^{(k)}\right) - \sum_{j=i+1}^{n}\left(a_{ij}z_j^{(k-1)}\right) + b_i\right), \tag{B.4.7}$$

$i = 1, ..., n$, where ω is a parameter such that $1 < \omega < 2$. Note that when $\omega = 1$, one recovers the Gauss-Seidel method.

Due to the sparsity of our pressure Poisson equation, any of the above methods provides us a simple formula to update the pressure. For example, the SOR method gives: for $\mathrm{it} = 1, ..., \mathrm{it}_{\max}$, $i = 1, ..., M$, $j = 1, ..., N$,

$$\begin{aligned} p_{i,j}^{\mathrm{it}+1} =& (1-\omega)p_{i,j}^{\mathrm{it}} + \frac{\omega}{\left(\frac{\epsilon_i^E+\epsilon_i^W}{\Delta x^2} + \frac{\epsilon_j^N+\epsilon_j^S}{\Delta y^2}\right)}\times \\ & \left(\frac{\epsilon_i^E p_{i+1,j}^{\mathrm{it}} + \epsilon_i^W p_{i-1,j}^{\mathrm{it}+1}}{\Delta x^2} + \frac{\epsilon_j^N p_{i,j+1}^{\mathrm{it}} + \epsilon_j^S p_{i,j-1}^{\mathrm{it}+1}}{\Delta y^2} - \mathrm{rhs}_{i,j}\right) \end{aligned} \tag{B.4.8}$$

where $\mathrm{rhs}_{i,j}$ denotes the right-hand side of the equation (B.4.4). The iteration terminates once a maximal number of iterations $\mathrm{it}_{\max}$ has been achieved or when the norm $\|p^{\mathrm{it}+1} - p^{\mathrm{it}}\|$ has fallen within a given tolerance. The norm can be chosen either as the discrete L^2-norm

$$\|r\|_2 = \left(\frac{1}{MN}\sum_{i=1}^{M}\sum_{j=1}^{N} r_{i,j}^2\right)^{1/2} \tag{B.4.9}$$

or the maximum norm

$$\|r\|_\infty = \max\left\{|r_{i,j}| \,\middle|\, i = 2, ..., M+1,\ j = 2, ..., N+1\right\} \tag{B.4.10}$$

where $r = p^{\mathrm{it}+1} - p^{\mathrm{it}}$.

A final remark is to note that the linear system for the pressure equation (B.4.4) is singular, since the boundary values for the pressure have only Neumann conditions. In our case for simulating the incompressible flow, we do not need the actual pressure values, but rather the gradient of the pressure. Thus one way to resolve this singularity is to assign the pressure values along the boundary to their corresponding neighboring cells in the boundary strip prior to each iteration. The ϵ's in equation (B.4.4) become identical 1's.

B.5 Flow in Complex Geometries

Below we present the treatment for flows in obstacle domains by extending the ideas of rectangular domains explained above.

B.5.1 The Obstacle Domains

First we imbed the fluid domain Ω in a rectangular domain Φ. The cells of Φ are then divided into *fluid cells* and *obstacle cells*. The Navier-Stokes equations are solved only in the fluid cells. The artificial boundary strips are also considered as obstacle cells. Furthermore, we denote those obstacle cells which share an edge with at least one fluid cell as *boundary cells*. A domain Ω that has an arbitrary curved boundary is approximated by a domain $\bar{\Omega}$ whose boundary is specified by the set of boundary edges lying on grid lines. Figure B.3 illustrates the fluid cells, obstacle cells and boundary cells in a rectangular domain.

The set of boundary cells are further classified to determine the boundary values. We classify the boundary cells into 8 different types by determining which of the four adjacent cells are fluid cells. For example, we use the notation B_E to denote a boundary cell whose right (eastern) neighbor cell belongs to $\bar{\Omega}$, or B_{NW} to denote a boundary cell whose north and west cells belong to $\bar{\Omega}$. Thus, B_E, B_W, B_N and B_S are *edge cells* whereas B_{NE}, B_{NW}, B_{SW} and B_{SE} are *corner cells*. Boundary cells with two opposite or more than two

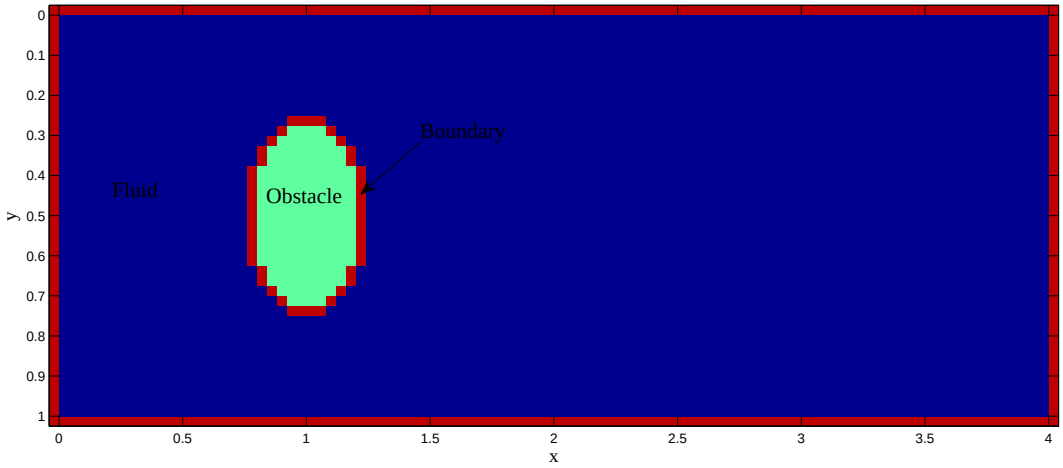

Figure B.3: Fluid cells are shown in blue and boundary cells are shown in red. Obstacle cells include red and green blocks.

neighboring fluid cells are not admissible.

B.5.2 Boundary Conditions for Obstacle Cells

For simplicity, we present the implementation of the boundary conditions using the no-slip condition. Depending on the cell types, we use different formulas for the boundary values. For an edge cell, for example a B_E cell (i, j) (see Figure B.4), we set

$$u_{i,j} = 0, \qquad v_{i,j} = -v_{i+1,j}, \qquad v_{i,j-1} = -v_{i+1,j-1} \tag{B.5.1}$$

for the velocity boundary values and the pressure condition is

$$p_{i,j} = p_{i+1,j}. \tag{B.5.2}$$

For a corner cell B_{NE} for instance (see Figure B.4), we have

$$v_{i,j} = 0, \qquad u_{i,j} = 0 \tag{B.5.3}$$

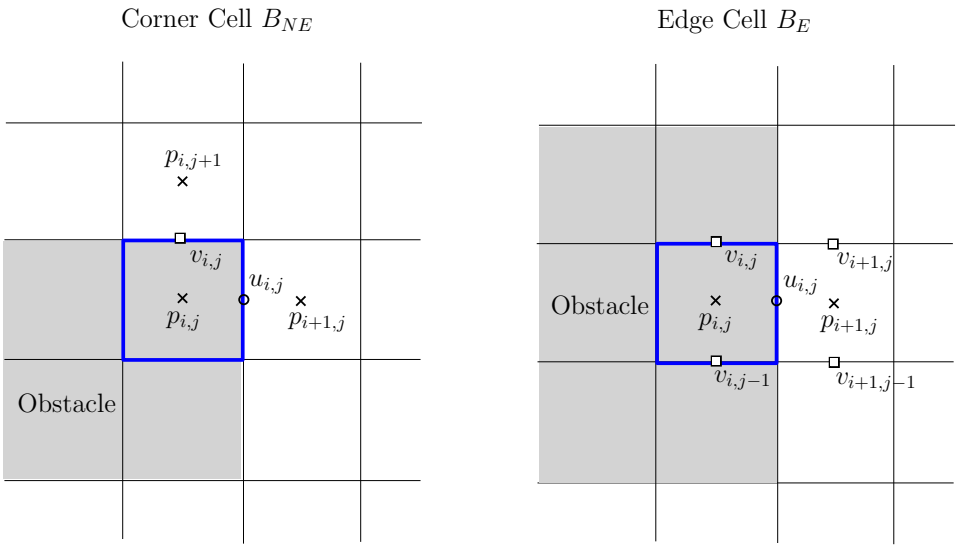

Figure B.4: Boundary conditions at obstacle boundary cells.

for velocities. For pressure, we use an average of the two adjacent values, i.e.,

$$p_{i,j} = \frac{1}{2}(p_{i+1,j} + p_{i,j+1}). \tag{B.5.4}$$

Appendix C

The Numerical Scheme of the Immersed Boundary Method

The immersed boundary (IB) method was originally developed by Peskin to model blood flow in a human heart (Peskin, 1972). A regular Eulerian grid is used for the fluid and a Lagrangian grid is used for the immersed boundary. The boundary condition at the immersed boundary is modeled as forces exerted by the immersed structure onto the fluid in the domain. Mathematically, it is a force distribution along the immersed boundary and the boundary moves with the local fluid velocity. Thus the Navier-Stokes equations with a complicated boundary condition are converted into a problem on a rectangular region with singular forces. The essential idea of the IB method is that the interaction between the fluid and the immersed boundary is connected through the spreading of the singular force from the Lagrangian grid to the Eulerian grid by using a discrete delta function (Lai and Peskin, 2000).

The immersed boundary method employs a mixture of Eulerian and Lagrangian variables so we need two distinct discretized grids. For instance, we choose a fixed Cartesian mesh for the whole fluid domain and a curvilinear mesh for the immersed boundary. Let the fluid domain $\Omega = [0, L] \times [0, L]$. For the Cartesian mesh, a staggered grid discretization can be used, as described in Chapter 4. If we divide the domain into N cells in both directions,

$h = \Delta x = \Delta y = L/N$ is the mesh width. For the curvilinear mesh, we use another set of K Lagrangian points $\vec{X} = (X_k, Y_k)$ for $k = 0, 1, ..., K-1$ to discretize the immersed boundary with initial mesh width Δs. Notice that the Cartesian points are fixed and the boundary points are moving, and those two sets of points generally do not coincide with each other.

A simple explicit version of the immersed boundary method is presented below (Peskin and Printz, 1993; Lai and Peskin, 2000). At the beginning of the time step, $(\vec{X}^{(n)}(s), \vec{v}^{(n)}(\vec{x}))$ are given, and we need to update to $(\vec{X}^{(n+1)}(s), \vec{v}^{(n+1)}(\vec{x}))$. The superscript is to denote the time step index.

Step 1: Compute the boundary force $\vec{F}^{(n)}(s)$ and apply the force to the fluid:

$$\vec{F}^{(n)}(s) = \vec{S}^{(n)}(\vec{X}^{(n)}), \tag{C.0.1}$$

$$\vec{f}^{(n)}(\vec{x}) = \sum_s \vec{F}^{(n)} \delta_h(\vec{x} - \vec{X}^{(n)}(s)) \Delta s, \tag{C.0.2}$$

where the two-dimensional discrete delta function is defined as

$$\delta_h(\vec{x}) = \phi_h(x)\phi_h(y) \tag{C.0.3}$$

and ϕ_h can be chosen as

$$\phi_h(r) = \begin{cases} \dfrac{1}{4h}\left(1 + \cos\dfrac{\pi r}{2h}\right) & |r| \le 2h, \\ 0 & \text{otherwise.} \end{cases} \tag{C.0.4}$$

Step 2: Use the finite-difference scheme described in Chapter 4, for example, to solve the Navier-Stokes equations with the force term $\vec{f}^{(n)}(\vec{x})$ to update the velocity field $\vec{v}^{(n+1)}(\vec{x})$.

Step 3: Interpolate the new velocity from the Cartesian grid to the bound-

ary points, and move the boundary points to new positions $\vec{X}^{(n+1)}(s)$:

$$\vec{V}^{(n+1)}(s) = \sum_{\vec{x}} \vec{v}^{(n+1)}(\vec{x})\delta_h(\vec{x} - \vec{X}^{(n)}(s))h^2, \tag{C.0.5}$$

$$\vec{X}^{(n+1)}(s) = \vec{X}^{(n)}(s) + \Delta t\vec{V}^{(n+1)}(s), \tag{C.0.6}$$

where δ_h is the discrete delta function defined above.

Expression (C.0.4) is to ensure δ_h is a smooth approximation to the Dirac delta function. There are other choices of ϕ_h (Peskin, 2002). Notice that ϕ is continuous and has a compact support. Continuity of ϕ is to avoid sudden jumps in the velocity and force as the immersed boundary moves through the computational grid of the fluid. Bounded support of ϕ is to keep down the computational cost of the algorithm.

Bibliography

Batchelor, G. K. (1970). *An Introduction to Fluid Dynamics*. Cambridge Univeristy Press.

Brenan, K. E., Campbell, S. L., Campbell, S. L. V., and Petzold, L. R. (1996). *Numerical Solution of Initial-Value Problems in Differential-Algebraic Equations*. SIAM.

Burden, R. L. and Faires, J. D. (2005). *Numerical Analysis, 8th edition*. Thomson Brooks/Cole.

Çengel, Y. A. and Cimbala, J. M. (2006). *Fluid Mechanics: fundamentals and applications*. McGraw-Hill Higher Education.

Chorin, A. J. (1968). Numerical simulation of the Navier-Stokes equations. *Math. Comp.*, 22:745–762.

Gresho, P. M. and Sani, R. L. (1987). On pressure boundary conditions for the incompressible navier-stokes equations. *Int. J. Numer. Methods Fluids*, 7:1111–1145.

Griebel, M., Dornseifer, T., and Neunhoeffer, T. (1998). *Numerical Simulation in Fluid Dynamics - A Practical Introduction*. SIAM.

Harlow, F. H. and Welch, J. E. (1965). Numerical calculation of time dependent viscous incompressible flow of fluid with free surface. *Phys. Fluids*, 8:2182.

Heinbockel, J. H. (1996). *Introduction to Tensor Calculus and Continuum Mechanics*.

Henshaw, T. (2009). Power pump valve dynamics - a study of the velocity and pressure distribution in outward-flow bevel-face and flat-face power pump valves. *Proc. 25th Int. Conf. Pump Users Symposium*.

Illner, R., Bohun, C. S., McCollum, S., and van Roode, T. (2000). *Mathematical Modelling - A Case Studies Approach*. American Mathematical Society.

Johnston, D. N. (1991). Numerical modelling of reciprocating pumps with self-acting valves. *Proceedings of the Institution of Mechanical Engineers, Part I*, 205:87–96.

Ladyshenskaja, O. (1969). *The Mathematical Theory of Viscous Incompressible Flow*. New York: Gordon and Breach.

Lai, M. and Peskin, C. S. (2000). Flow pattern around heart valves: A numerical method. *J. Comput. Phys.*, 160:705–719.

Landau, L. D. and Lifshitz, E. M. (1987). *Course of Theoretical Physics - Fluid Mechanics, 2nd edition*. Elsevier Science and Technology Books.

Lima E Silva, A. L. F., Silveira-Neto, A., and Damasceno, J. J. R. (2003). Numerical simulation of two-dimensional flows over a circular cylinder using the immersed boundary method. *J. Comput. Phys.*, 189:351–370.

Lyashkov, V. I. (1972). Digital computer simulation of the operation of the high pressure cryogenic pumps. *Chemical and Petroleum Engineering*, 8:897–900.

Mittal, R. and Iaccarino, G. (2005). Immersed boundary methods. *Ann. Rev. Fluid Mech.*, 37:239–261.

Peskin, C. S. (1972). Flow pattern around heart valves: A numerical method. *J. Comput. Phys.*, 10:252–271.

Peskin, C. S. (2002). The immersed boundary method. *Acta Numerica*, 11:479–517.

Peskin, C. S. and Printz, B. F. (1993). Improved volume conservation in the computation of flows with immersed elastic boundaries. *J. Comput. Phys.*, 105:33–46.

Price, S. M., Smith, D. R., and Tison, J. D. (1995). The effects of valve dynamics on reciprocating pump reliability. *Proc. 12th Int. Conf. Pump Users Symposium*, pages 221–230.

Rabier, P. J. and Rheinboldt, W. C. (1991). A generalized existence and uniqueness theorem for implicit differential-algebraic equations. *J. Diff. and Integral Equations*, 4:681–694.

Sani, R. L. and Gresho, P. M. (1994). Résumé and remarks on the open boundary condition minisymposium. *Int. J. Numer. Methods Fluids*, 18:983–1008.

Shu, J., Burrows, C. R., and Edge, K. A. (1997). Pressure pulsations in reciprocating pump piping systems, part 1: modelling. *Proceedings of the Institution of Mechanical Engineers, Part I*, 211.

Slatter, P. T. (1997). The rheological characterisation of sludges. *Wat. Sci. Tech*, 36:9–18.

Tome, M. and McKee, S. (1994). Gensmac: A computational marker and cell method for free surface flows in general domains. *J. Comput. Phys.*, 110:171–186.

White, F. M. (1986). *Fluid Mechanics, 2nd edition.* McGraw-Hill Higher Education.

Zhou, G., Yan, Z., Xu, S., and Zhang, K. (2000). *Fluid Dynamics, 2nd edition.* Higher Education Press.